

**Radiation Properties of a Slotted Elliptic Cylinder
Coated by Nonconfocal Chiral and Other Materials**

Biglar Najjar-Khatirkolaei

A Thesis

in

The Department

of

Electrical and Computer Engineering

Presented in Partial Fulfillment of the Requirements

For the Degree of Doctor of Philosophy at

Concordia University

Montreal, Quebec, Canada

August 2009

© Biglar Najjar-Khatirkolaei, 2009



Library and Archives
Canada

Published Heritage
Branch

395 Wellington Street
Ottawa ON K1A 0N4
Canada

Bibliothèque et
Archives Canada

Direction du
Patrimoine de l'édition

395, rue Wellington
Ottawa ON K1A 0N4
Canada

Your file *Votre référence*
ISBN: 978-0-494-63378-6
Our file *Notre référence*
ISBN: 978-0-494-63378-6

NOTICE:

The author has granted a non-exclusive license allowing Library and Archives Canada to reproduce, publish, archive, preserve, conserve, communicate to the public by telecommunication or on the Internet, loan, distribute and sell theses worldwide, for commercial or non-commercial purposes, in microform, paper, electronic and/or any other formats.

The author retains copyright ownership and moral rights in this thesis. Neither the thesis nor substantial extracts from it may be printed or otherwise reproduced without the author's permission.

In compliance with the Canadian Privacy Act some supporting forms may have been removed from this thesis.

While these forms may be included in the document page count, their removal does not represent any loss of content from the thesis.

AVIS:

L'auteur a accordé une licence non exclusive permettant à la Bibliothèque et Archives Canada de reproduire, publier, archiver, sauvegarder, conserver, transmettre au public par télécommunication ou par l'Internet, prêter, distribuer et vendre des thèses partout dans le monde, à des fins commerciales ou autres, sur support microforme, papier, électronique et/ou autres formats.

L'auteur conserve la propriété du droit d'auteur et des droits moraux qui protègent cette thèse. Ni la thèse ni des extraits substantiels de celle-ci ne doivent être imprimés ou autrement reproduits sans son autorisation.

Conformément à la loi canadienne sur la protection de la vie privée, quelques formulaires secondaires ont été enlevés de cette thèse.

Bien que ces formulaires aient inclus dans la pagination, il n'y aura aucun contenu manquant.


Canada

Abstract

Radiation Properties of a Slotted Elliptic Cylinder Coated by Nonconfocal Chiral and Other Materials

Biglar Najjar-Khatirkolaei, Ph.D.
Concordia University, 2009

Wireless communications technology is one of the most rapidly growing fields. An antenna is a key element that makes wireless communications possible. One of the most popular antennas is the slot antenna which is widely used in many wireless systems. The characteristics of a slot antenna on a perfectly conducting elliptic cylinder coated by nonconfocal materials are investigated theoretically and experimentally. Fields interior and exterior to the slot antenna are found rigorously using the separation of variable technique. The analysis is carried out by expressing the fields in and around the cylinder in terms of Mathieu and modified Mathieu functions. The structure is fed with a line source or a plane wave. The unknown aperture fields on the slot are expressed in terms of Fourier series with unknown expansion coefficients. The expansion coefficients of the interior, aperture and exterior fields are found by enforcing the boundary conditions and employing the addition theorem and orthogonality properties of the Mathieu functions. The general formulations are expressed for the TM case. However, expressions of the eigenfunction expansions for the TE case are given, as well. Furthermore, efficient algorithms for calculating the Mathieu functions are developed using the software package MATLAB. The algorithm developed here for calculating the Mathieu function is compact, fast, and efficient, and compared well with other results in the literature.

The exact analytical formulation is used to generate accurate numerical results and studying the effects of different geometrical and materials parameters. Numerical results of the antenna gain, aperture conductance, and aperture voltage (in a receiving mode) are presented and discussed for different design parameters and for both the TM and TE cases. For verification of accuracy and validation of formulations and software program, numerical results for special cases are generated and very good agreement between theory and available data is obtained. The antenna radiation patterns and directivities are computed for different design parameters. The accuracy of the solution is also attested by comparing with HFSS, a commercial CAD package, simulation results. Prototypes of non-coated and dielectric-coated elliptic slot antennas are designed, fabricated, and tested.

To My Great Parents;

My Mother

and in Loving Memory of

My Father

To My Lovely Family;

My Wife and her Parents,

My Daughter, and My Son

And to all those who supported me throughout these years

Contents

List of Figures	ix
List of Tables	xiii
List of Symbols	xiv
List of Abbreviations	xvii
1. Introduction	1
1.1 Motivations and Problem Statement	1
1.2 Objectives	4
1.3 Basic Assumptions	5
1.4 Overview of the Thesis	6
2. Literature Review	8
2.1 Slot Antennas	8
2.2 Electromagnetic Behaviours of Materials	12
2.2.1 Artificial Materials	13
2.2.2 Dielectric Materials	15
2.2.3 Isorefractive Media	17
2.2.4 Metamaterials	19
2.2.4.1 Basic Types of Metamaterials with Inclusions	21
2.2.4.2 Negative Refractive Index	24

2.2.5	Chiral Media	27
2.2.5.1	Electromagnetic Behaviours of Chiral Media	29
2.2.5.2	Artificial Chiral Media	30
2.2.6	Soft and Flexible Host Media	32
3.	Formulations for Elliptic Slot Antenna Coated by Nonconfocal Materials	33
3.1	Elliptic Cylindrical Coordinate System	33
3.2	Wave Equations	35
3.2.1	Wave Equations in Chiral Media	36
3.3	The Eigenfunction Expansions	39
3.3.1	Incident Wave	40
3.3.2	Fields in Region 1 ($\xi_c < \xi_1$)	42
3.3.3	Aperture Fields ($\xi_c = \xi_1$)	44
3.3.4	Fields in Region 2 ($\xi_c > \xi_1$ and $\xi \leq \xi_2$)	44
3.3.5	Fields in Region 3 ($\xi > \xi_2$)	46
3.4	Boundary Conditions	47
3.5	Finding the Coefficients	50
3.6	Far Zone Fields	55
3.7	Formulation for TE Case	58
4.	Transmitting and Receiving Characteristics of Elliptic Slot Antennas	63
4.1	Validation	64
4.1.1	Validation: Analytical Closed Form Solutions	64

4.1.2	Validation: Simulation	67
4.2	Effect of Geometrical and Material Parameters	69
4.2.1	Antenna Gain	69
4.2.2	Aperture Conductance	77
4.2.3	Aperture Voltage	81
5.	Fabrication and Testing of Elliptic Slot Antenna	88
5.1	Feeding of Cylindrical Slot Antenna	88
5.2	Analytical and Experimental Solutions	91
5.3	Simulation and Design	92
5.4	Fabrication and Measurement	101
6.	Conclusions and Future Works	110
6.1	Conclusions	110
6.2	Contributions	114
6.3	Future Works	116
	References	117
	Appendix <i>A</i> : Addition Theorem for Mathieu Functions	136
	Appendix <i>B</i> : G 's Matrices for TM Case	138
	Appendix <i>C</i> : T 's Matrices for TM Case	143
	Appendix <i>D</i> : G 's Matrices for TE Case	152
	Appendix <i>E</i> : T 's Matrices for TE Case	155

List of Figures

Figure 1.1 – Slotted elliptic cylinder coated by nonconfocal materials	3
Figure 1.2 – The HFSS model of a line source and a slotted elliptic cylinder	5
Figure 2.1 – Some shapes of slot antenna	10
Figure 2.2 – Conducting cylinder with loaded and coated materials	11
Figure 2.3 – Material classifications	13
Figure 2.4 – General sketch of a volumetric artificial material	14
Figure 2.5 – ENG Metamaterial	22
Figure 2.6 – MNG Metamaterial	23
Figure 2.7 – DNG Metamaterial	23
Figure 2.8 – Conventional material and LHM	25
Figure 2.9 – LHM flat lens consisting of an array of 3 by 20 by 20 unit cells	26
Figure 2.10 – Hands and chiral molecules	28
Figure 2.11 – Double helix	28
Figure 2.12 – Artificial chiral media (waveguide) using helices and foam	31
Figure 3.1 – Elliptic cylindrical coordinate system	34
Figure 3.2 – Geometry of slotted elliptic cylinder	40
Figure 4.1 – General Geometry of slotted elliptic cylinder	65

Figure 4.2 – Scattering by a chiral cylinder	66
Figure 4.3 – Scattering by a very narrow slotted elliptic cylinder	66
Figure 4.4 – The HFSS model of a slotted conducting elliptic cylinder	67
Figure 4.5 – Radiation patterns from a slotted cylinder coated by a dielectric	68
Figure 4.6 – Radiation patterns from a slotted cylinder coated by an isorefractive	69
Figure 4.7 – Effect of chirality on antenna gain in TM_z co-polarized	73
Figure 4.8 – Effect of chirality on antenna gain in TM_z cross-polarized	73
Figure 4.9 – Effect of chirality on antenna gain in TE_z co-polarized	74
Figure 4.10 – Effect of chirality on antenna gain in TE_z cross-polarized	74
Figure 4.11 – Effect of chirality on antenna gain in TM_z co-polarized	75
Figure 4.12 – Effect of material parameters on antenna gain in TM_z co-polarized	75
Figure 4.13 – Effect of material parameters on antenna gain in TE_z co-polarized	76
Figure 4.14 – Effect of coating thickness on antenna gain in TE_z co-polarized	76
Figure 4.15 – Effect of coating thickness on antenna gain in TM_z co-polarized	77
Figure 4.16 – Effect of coating thickness on aperture conductance	78
Figure 4.17 – Effect of coating thickness on aperture conductance	79
Figure 4.18 – Effect of coating thickness on aperture conductance	80
Figure 4.19 – Effect of coating thickness on aperture conductance	80
Figure 4.20 – Effect of chirality on aperture voltage	83
Figure 4.21 – Effect of chirality on aperture voltage	84
Figure 4.22 – Effect of chirality on aperture voltage	84
Figure 4.23 – Effect of chirality on aperture voltage	85
Figure 4.24 – Effect of material parameters on aperture voltage	85

Figure 4.25 – Effect of material parameters on aperture voltage	86
Figure 4.26 – Effect of material parameters on aperture voltage	86
Figure 4.27 – Effect of material parameters on aperture voltage	87
Figure 5.1 – Slotted rectangular waveguide antenna	89
Figure 5.2 – Evolution of slotted cylinder from slotted sheet	89
Figure 5.3 – Photograph of a circular slot antenna	90
Figure 5.4 – Geometry of an elliptic cylinder slot antenna	94
Figure 5.5 – Geometry of an electric line source parallel with a flat conductor	94
Figure 5.6 – Geometry of an elliptic cylinder slot antenna	95
Figure 5.7 – Geometry of a circular cylinder slot antenna	95
Figure 5.8 – Comparison of S11 for three different geometries	96
Figure 5.9 – Comparison of radiation patterns for three different geometries	96
Figure 5.10 – Geometry of an elliptic cylinder slot antenna coated by a dielectric	99
Figure 5.11 – Radiation patterns of an elliptic slot antenna coated by dielectric	99
Figure 5.12 – Geometry of an elliptic slot antenna partial coated by dielectric	100
Figure 5.13 – Radiation patterns of a slot antenna partial coated dielectric	100
Figure 5.14 – The materials which may be used to make cylindrical slot antenna	101
Figure 5.15 – Photographs to show how the slotted elliptic cylinder is made	102
Figure 5.16 – Photographs of fabricated non-coated elliptic slot antenna	104
Figure 5.17 – The simulation and measurement results of elliptic slot antenna	104
Figure 5.18 – Photograph of non-coated elliptic slot antenna under measurement	105
Figure 5.19 – Radiation patterns of non-coated elliptic slot antenna	105

Figure 5.20 – Photograph of fabricated elliptic slot antenna coated by dielectric	107
Figure 5.21 – The simulation and measurement results of coated slot antenna	107
Figure 5.22 – Photograph of partial coated slot antenna under measurement	108
Figure 5.23 – Radiation patterns of partial coated elliptic slot antenna	108

List of Tables

Table 5.1 – Design parameters for a non-coated elliptic slot antenna	97
--	----

List of Symbols

α	alpha	Angle between the x axes of the local and global coordinates
β	beta	Angular Distance (in Polar Coordinates)
∇	del	Del Operator
ϵ	epsilon	Electric Permittivity
ϵ_0	epsilon zero	Permittivity of Vacuum, $\epsilon_0 = 8.854 \times 10^{-12}$ F/m
ϵ_c	epsilon c	Effective Permittivity of the Chiral Medium
ϵ_r	epsilon r	Relative Permittivity
η	eta	Angular Distance (in Elliptic Cylindrical Coordinates, $0 \leq \eta \leq 2\pi$)
γ	gamma	Chiral Admittance of the Medium
μ	mu	Magnetic Permeability
μ_0	mu zero	Permeability of Vacuum, $\mu_0 = 4\pi \times 10^{-7}$ N/A ²
μ_r	mu r	Relative Permeability
ν	nu	Wave Velocity
ω	omega	Angular Velocity
ϕ^i	phi i	Incident Angle with respect to the x -axis
π	pi	Angular Distance in Radian, $\pi = 180$ degrees
ρ	rho	Electric Charge Density
ρ_0	rho zero	Radial Distance (in Circular Cylindrical Coordinates, $0 \leq \rho_0 \leq \infty$)
Σ	sigma	Summation

θ_1	theta 1	Incident Angle
θ_2	theta 2	Refraction Angle
ξ	xi	Radial Distance (in Elliptic Cylindrical Coordinates, $0 \leq \xi \leq \infty$)
\vec{B}		Magnetic Flux Density
\vec{D}		Electric Flux Density
\vec{E}		Electric Field
G_a		Aperture Conductance
\vec{H}		Magnetic field
\vec{J}		Electric Volume Current Density
\vec{M}_m		Vector Wave Function
\vec{N}_m		Vector Wave Function
$R^{(l)}()$		The l^{th} kind of Radial Mathieu Function
$S()$		Angular Mathieu Function
V		Aperture Voltage
a		Semi-major Axis (in Elliptic Cylindrical Coordinate System)
b		Semi-minor Axis (in Elliptic Cylindrical Coordinate System)
d		Radial Distance (in Polar Coordinates)
f		Semi-focal Length (in Elliptic Cylindrical Coordinate System)
h		Scale Factor (in Elliptic Cylindrical Coordinate System)

k	Propagation Constant (Wave Number)
k_L	Left-Hand Propagation Constant in Chiral Media
k_R	Right-Hand Propagation Constant in Chiral Media

List of Abbreviations

1D	One Dimension	
2D	Two Dimensions	
3D	Three Dimensions	
BW	Backward-Wave	
DNA	Deoxyribonucleic Acid	(DNA is a nucleic acid that contains the genetic instructions used in the development and functioning of all known living organisms.)
DPS	Double Positive	
E-Fields	Electric Fields	
ENG	epsilon-Negative	
FEM	Finite Element Method	
H-Fields	Magnetic Fields	
HFSS	High Frequency Structure Simulator	
LHM	Left-Handed Metamaterial	
MNG	mu-Negative	
NASA	National Aeronautics and Space Administration	
RNA	Ribonucleic Acid	(RNA is a nucleic acid made from a long chain of nucleotide units.)
SNG	Single-Negative	

SRR	Split-Ring Resonator
TE	Transverse Electric
TM	Transverse Magnetic

1. Introduction

1.1 Motivations and Problem Statement

Wireless communications technology is one of the most rapidly growing fields and is experiencing unprecedented market growth. The continuous demands of new services and technology challenge day by day scientists and engineers working in this field. The propagation of electromagnetic energy is the key physical phenomenon that makes wireless communications possible. An antenna can convert a guided electromagnetic wave on a transmission line to a plane wave propagating in free space and vice versa. Depending on the applications, there are many kinds of antennas. One of the most popular antennas is the slot antenna.

A slot antenna consists of a metal surface and a slot cut out. Slot antennas are widely used in many practical applications such as radar and satellite communications, space vehicles, aircrafts, missiles, and in standard desktop microwave sources for research purposes. The main advantages of slot antennas are adaptability, lightweight, design simplicity, ease of fabrication, high power capability, greater control of the radiation pattern compared to line antennas, and wider bandwidth compared to microstrip patch antennas.

Depending on the application, slot antennas are mounted on bodies which have different shapes. The shape and size of the slot, its loading and/or coating materials, and the driving source determine the radiation distribution pattern. Some known 2D mounting geometries include rectangular, circular and elliptic cylinders. The slotted circular

cylinder is one of the most investigated geometries in the area of scattering and radiation. However, because of some advantages of elliptic cylinder, i.e., extra design degree of freedom and some applications for this geometry, research in this area has increased, as well. In certain cases the elliptic cylinder provides a useful model for the body of an aircraft. Furthermore, as a limiting case, solutions of the slotted elliptic cylinder can be used for slotted circular cylinder.

Generally, slot antennas in some applications, i.e., aircrafts, space shuttles, and missiles are coated by materials for different purposes. For example, the slot antenna on the space shuttle is covered by heat-shielding tiles. In some applications, the coated materials can protect the slot antennas from the oxidations or damages. Even the plasma surrounding a re-entry vehicle can be considered as a coated material. Also, the electromagnetic properties of (loaded and coated) materials can be used for more control of the radiated power and increase the number of design parameters. Therefore, extensive investigations are reported about the characteristics of slotted antennas on conducting circular [1]-[8] and elliptic [9]-[14] cylinders loaded and/or coated by confocal or nonconfocal materials (i.e., dielectric and plasma). The number of design parameters increases when the coating is nonconfocal. Also, there are some applications which need nonconfocal coating. Examples include a slotted elliptic cylinder with more coating material in front of slot, and a slotted elliptic cylinder covered by a uniform thickness of material.

Dielectric is one of the most used materials for loading and coating. However, other kinds of materials which are made artificially and have special electromagnetic properties have recently become the subject of extensive studies. For examples, in the

studies for the characteristics of the elliptic slot antennas, the nonconfocal dielectric coating [12], and confocal metamaterial coating [15], [16] are considered. This work provides a general solution for the slotted elliptic cylinder coated by a nonconfocal chiral media. However, it can be used for circular cylinder and many other kinds of non-chiral materials (i.e. dielectric, isorefractive, and metamaterial), as well.

In this investigation, a general geometry of slotted conducting elliptic cylinder loaded and coated with nonconfocal materials is considered. A cross section of this geometry is shown in Figure 1.1 and its details are given in Chapter 3. Two elliptic cylindrical coordinate systems (local and global) are used. The analysis is carried out by expressing the fields in and around the cylinder in terms of Mathieu and modified Mathieu functions using the separation of variables and exact boundary value technique. The structure is fed with a line source or a plane wave. The unknown aperture fields are expressed in terms of Fourier series expansion with unknown coefficients. The expansion coefficients of the interior, aperture and exterior fields are found by enforcing the boundary conditions and employing the addition theorem and orthogonality properties of the Mathieu functions.

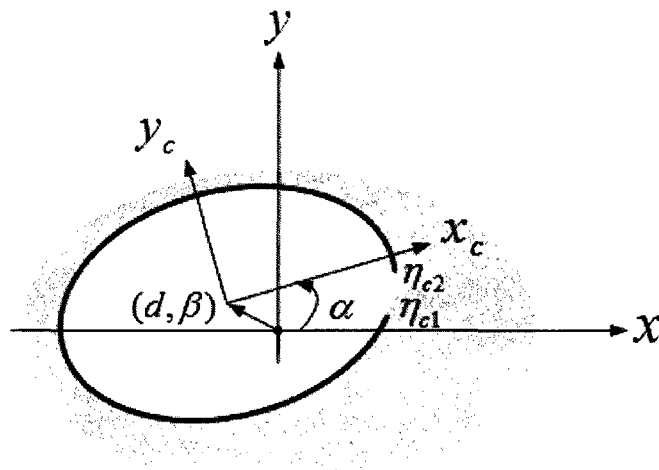


Figure 1.1 – Slotted elliptic cylinder loaded and coated with nonconfocal materials.

The exact analytical formulation is used to generate accurate numerical results and studying the effects of different geometrical and materials parameters. Prototypes of non-coated and dielectric-coated elliptic slot antennas are designed, fabricated, and tested.

1.2 Objectives

The main objective of this thesis is to develop an exact solution to finding the characteristics of a slot antenna on a conducting elliptic cylinder coated by nonconfocal materials (i.e. dielectric, isorefractive, metamaterial, and chiral media). To achieve such objective, a general solution for the slotted elliptic cylinder coated by a nonconfocal chiral media is considered. This solution can be used for circular cylinder and non-chiral materials, as well. Two elliptic cylindrical coordinate systems (local and global) are used. The expressions of the wave equations are derived for different regions (inside and outside) of the slotted elliptic cylinder in terms of an infinite series of wave functions and the addition theorem for Mathieu functions. The unknown expansion coefficients are found by applying the boundary conditions and employing the orthogonality properties of the Mathieu functions.

Other objectives of this work is to investigate the dependence of the antenna gain, aperture conductance, and aperture voltage (in receiving mode) on the slot and elliptic cylinder dimensions and properties as well on different kinds of loaded and coated materials. In addition, formulations and numerical results are presented for both the TM and TE cases. We also present prototypes of non-coated and dielectric-coated elliptic slot antennas for demonstration purposes.

1.3 Basic Assumptions

Figure 1.2 shows the 3D model of a line source and a slotted conducting elliptic cylinder coated by a nonconfocal material. The slot on conducting elliptic cylinder is an axial slot along the z -axis with angular width $\eta_{c2} - \eta_{c1}$. The unknown aperture fields are uniform in z direction but they are dependent on η and expressed in terms of Fourier series expansion with unknown coefficients. In practice, the line source and conducting elliptic cylinder have limited length in z direction. However, they are much greater than the applied wavelength, so that, they can be assumed as infinitely long.

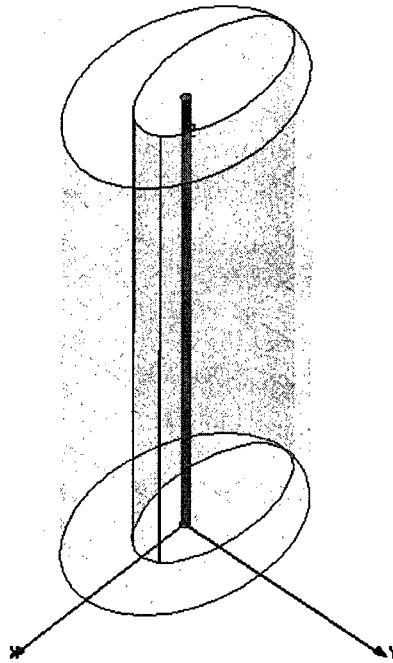


Figure 1.2 – The HFSS model of a line source and a slotted conducting elliptic cylinder coated by a nonconfocal material.

1.4 Overview of the Thesis

Background of slot antennas and properties of different materials (i.e., dielectric, isorefractive, metamaterials, and chiral media) together with related applications are presented in Chapter 2. Electromagnetic behavior of materials, natural and artificial materials, construction of artificial materials and experimental works of artificial materials are discussed. Also, an idea on how to produce an artificial material in general form with soft and flexible host media is presented in this chapter.

Formulations for radiation by an elliptic slot antenna coated by nonconfocal materials are given in Chapter 3. This chapter starts with elliptic cylindrical coordinate system and defines the confocal and nonconfocal cylinders. Wave equations, in particular wave equation in chiral media, and eigenfunction expansions are expressed for the TM case. Using two elliptic cylindrical coordinate systems (local and global), the expressions are derived for different regions. The boundary conditions are applied after transformation of the field components (inside the coating area) in terms of the global coordinate system. The unknown expansion coefficients and other required quantities are determined. Also in this chapter, expression of the eigenfunction expansions for the TE case is given and the unknown expansion coefficients are determined.

In Chapter 4, the accuracy and validation of formulations and associated software program are verified in two ways. Some numerical results for special cases are generated and compared to the numerical results which are analytically generated by other researchers, and some numerical results compared to results which are simulated by Ansoft's HFSS software [17]. The numerical results for characteristics of elliptic slot antenna are generated in transmitting and receiving modes. Results for antenna gain and

aperture conductance (in transmitting mode), and for aperture voltage (in receiving mode) are presented and discussed in this chapter.

Details of the simulation, design, fabrication, and measurement of the non-coated and dielectric-coated elliptic slot antennas are given in Chapter 5. In this chapter, the feeding of cylindrical slot antenna and the analytical and experimental solutions of elliptic slot antenna are discussed.

In Chapter 6, conclusions, the main research contributions of these theoretical and experimental works, and suggested future works are presented. Details of the addition theorem for Mathieu functions and details of some matrices involved in the developed solution are given in appendices.

2. Literature Review

A slot antenna consists of a metal surface and a hole or slot cut out. It radiates electromagnetic waves when the metal surface is driven as an antenna by a driving frequency sources. The radiated power of slot antenna can be more controlled if they are covered by materials. There are many kinds of materials which can be used for this purpose. Some kinds of materials are artificial materials with recent extensive investigations. Thus, the literature review covers both slot antennas and different kinds of materials.

2.1 Slot Antennas

Slot antennas are simple antennas which are analyzed in terms of the field on their associated aperture. The aperture field is dependent on the shape of the aperture and the body geometry on which the aperture is located. For a hollow conducting cylinder which acts the same as a waveguide, an aperture is the only pathway to transfer electromagnetic fields from inside to outside of the cylinder and vice versa.

The main advantages of slot antennas are adaptability, lightweight, design simplicity, ease of fabrication, high power capability, greater control of the radiation pattern compared to line source antennas, and wider bandwidth compared to microstrip patch antennas. They are widely used in many practical applications such as radar and satellite communications, space vehicles, aircrafts, missiles, and in standard desktop microwave devices for research purposes.

The basic problem of communicating to and from high-speed aircraft has stimulated research work into the theory and application of slotted cylinder antennas [18]-[20]. Silver and Saunders [21] have developed general expressions for the external field produced by a slot of arbitrary shape in the wall of an infinite circular cylinder. Wait [22] has published a comprehensive theoretical treatment of slots on cylindrical surfaces, i.e., circular and elliptic cylinders. Many kinds of slot antennas such as the short and long slots, the thin slot, cavity-backed slot, annular slot, waveguide slot, slotted cylinder, slot-dipole, open waveguide, rectangular and circular waveguide horn, and biconical horn are theoretically analyzed by Wolff [23].

Depending on the applications, the slot antennas are mounted on bodies which have different shapes (Figure 2.1). The pattern and other radiation characteristics of these antennas are profoundly influenced by the shape and the size of the body on which they are mounted. Because of mathematical difficulties, an exact theoretical analysis is not possible for some actual shapes, unless they have a known geometry shape. Some known geometry forms which are used as body of slot antennas have cylindrical shapes, i.e., rectangular, circular and elliptic cylinder. The slotted circular cylinder is one of the most investigated geometries in the area of scattering and radiation. However, because of some advantages of elliptic cylinder, i.e., extra design degree of freedom and some applications for this geometry, research in this area has increased, as well. Furthermore, as a limiting case, solutions of the slotted elliptic cylinder can be used for slotted circular cylinder.

Figure 2.1-(a) shows a short slot in an infinite ground plane which is the complement to a dipole in free space. This slot has the same radiation pattern as a dipole antenna with the same dimensions as the slot, except that the E- and H-fields are

swapped. As a result, the polarization rotates 90° , so that radiation from a horizontal slot is polarized vertically. For instance, a vertical slot has the same pattern as a horizontal dipole of the same dimensions and vice versa. Figure 2.1-(b) shows an annular slot antenna which can easily be constructed by terminating a coaxial line connected to the conducting ground plane. Figures 2.1-(c) and 2.1-(d) are slot antennas on circular and elliptic cylinders, respectively. They are also named as waveguide slot antennas. Waveguide slot antennas are simple, rugged, and fairly easy to build.

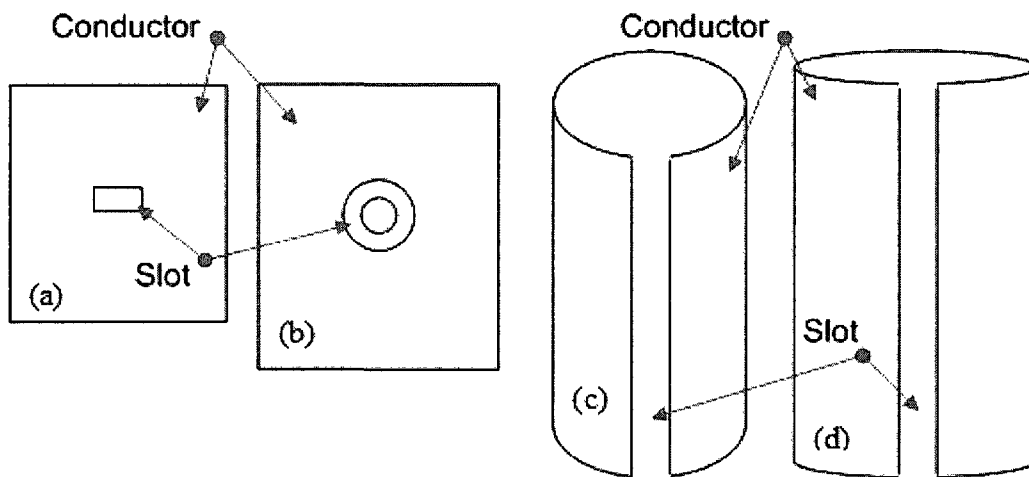


Figure 2.1 – Some shapes of slot antenna; (a) Short slot antenna. (b) Annular slot antenna. (c) Circular cylinder slot antenna. (d) Elliptic cylinder slot antenna.

Because of the electromagnetic properties of materials, a slotted cylinder loaded and coated with materials offers more control of the radiation power (Figure 2.2). Dielectric is one of the most used materials for this purpose. However, the other kinds of materials which are made artificially and have special electromagnetic properties have recently become the subject of widely studies.

Extensive investigations are reported [1]-[8] about the characteristics of slotted antenna on conducting circular cylinder loaded or coated by materials (i.e., dielectric and plasma). Many investigations are reported about the slotted antenna on conducting elliptic cylinder, as well. For instances; scattering and coupling properties of a slotted elliptic cylinder [9], [10] and the characteristics of slotted elliptic cylinder coated by materials [11]-[16].

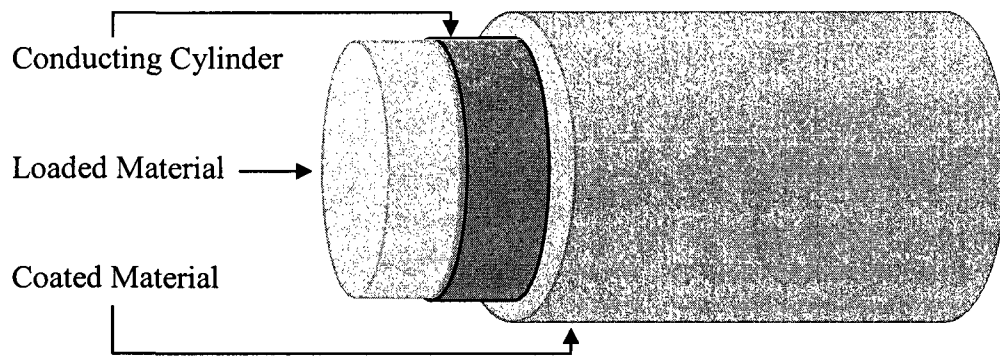


Figure 2.2 – Conducting cylinder with loaded and coated materials.

Definition of the aperture field is very significant. It is generally an unknown field. In most of the investigations about slotted cylinder, the aperture field is assumed as the known field and constant value. However, some works about non coated [9] and dielectric/metamaterial coated [16] slotted elliptic cylinders with unknown aperture field are reported, as well.

In this thesis, the characteristics of slot antenna on a conducting elliptic cylinder coated by nonconfocal materials (i.e., dielectric, isorefractive, metamaterial, and chiral media) are investigated. The numerical results are generated for both TM and TE cases. Prototypes of elliptic slot antennas are designed, fabricated, and tested.

2.2 Electromagnetic Behaviours of Materials

The response of materials to the presence of an electromagnetic field is determined by the properties of these materials. These properties are described by defining the macroscopic parameters, permittivity ϵ and permeability μ of these materials. This allows for the classification of a medium as follows [24].

A medium with both permittivity and permeability greater than zero ($\epsilon > 0, \mu > 0$) will be designated a double positive (DPS) medium. Most naturally occurring media (i.e., dielectrics) fall under this designation. A medium with permittivity less than zero and permeability greater than zero ($\epsilon < 0, \mu > 0$) will be designated an epsilon-negative (ENG) medium. In certain frequency regimes many plasmas exhibit this characteristic. For example, noble metals (i.e., silver, gold) behave in this manner in the infrared and visible frequency domains. A medium with the permittivity greater than zero and permeability less than zero ($\epsilon > 0, \mu < 0$) will be designated a mu-negative (MNG) medium. In certain frequency regimes some gyrotropic materials exhibit this characteristic. Artificial materials have been constructed that also have DPS, ENG, and MNG properties. A medium with the permittivity and permeability less than zero ($\epsilon < 0, \mu < 0$) will be designated a DNG medium. This medium classification can be graphically illustrated as shown in Figure 2.3.

The macroscopic interactions of electromagnetic fields with materials are also described by Maxwell's equations. Solution of Maxwell's equations requires knowledge of three constitutive properties of the material: the electric permittivity, the magnetic permeability, and the conductivity. In general, these parameters are dependent upon material temperature and frequency of the applied field. The electric permittivity and

magnetic permeability of a medium together determine the phase velocity of electromagnetic radiation through that medium.

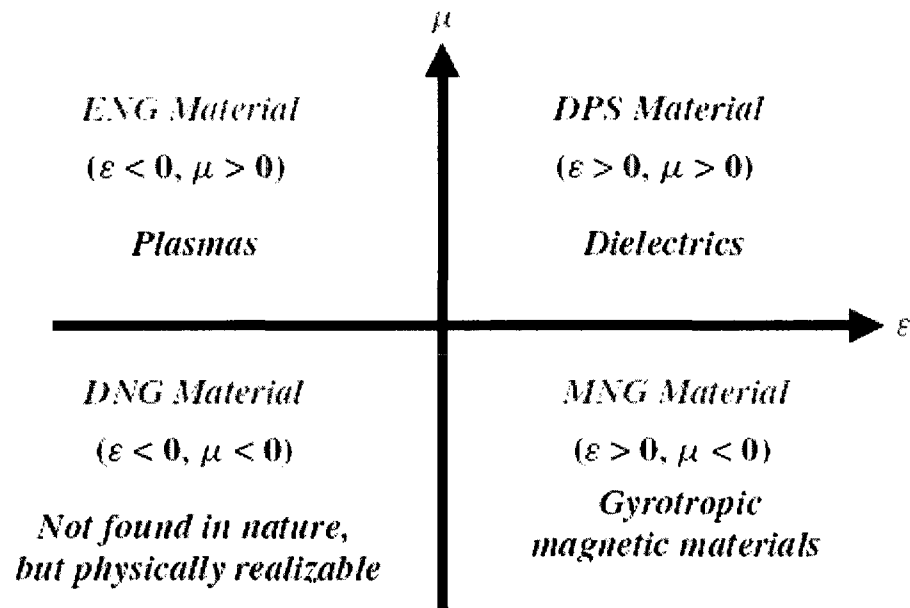


Figure 2.3 – Materials classifications [24].

2.2.1 Artificial Materials

Artificial materials are the materials which may not be available in nature. They are made by embedding various pieces of inclusions with novel geometry shapes in some host media (Figure 2.4). The cell size of the embedded pieces must be smaller than the wavelength of the incident wave.

The first attempt to explore the concept of artificial materials appears when in 1898 Jagadis Chunder Bose conducted the first microwave experiment on twisted structures-geometries that were essentially artificial chiral elements by today's terminology [25]. In 1914, Lindman worked on artificial chiral media by embedding

many randomly oriented small wire helices in a host medium [26]. In 1948, Kock [27] made lightweight microwave lenses by arranging conducting spheres, disks, and strips periodically and effectively tailoring the effective refractive index of the artificial media.

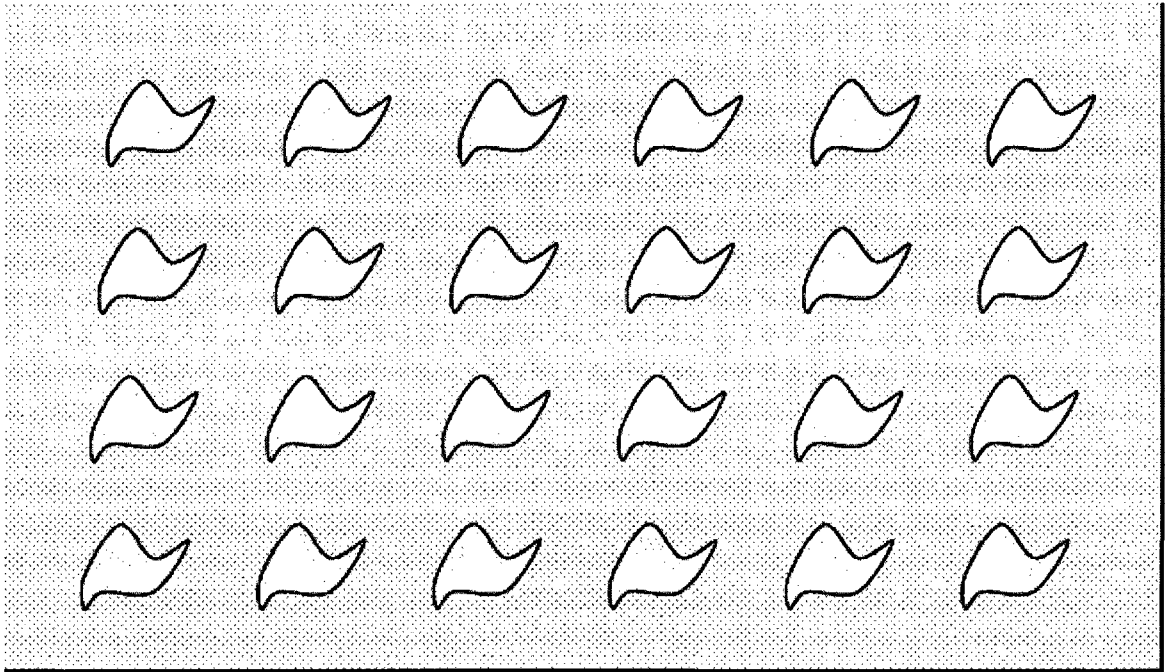


Figure 2.4 – General sketch of a volumetric artificial material synthesized by embedding various inclusions in a host medium [24].

In recent years new concepts in synthesis and novel fabrication techniques have allowed the construction of structures and composite materials that mimic known material responses or that qualitatively have new, physically realizable response functions that do not occur or may not be readily available in nature. These artificial materials can in principle be synthesized by embedding various constituents/inclusions with novel geometric shapes and forms in some host media. Various types of electromagnetic composite media, such as single-negative materials (SNG), double-

negative (DNG) materials, and chiral materials are interesting area for study by various research groups worldwide.

In particulate composite media, electromagnetic waves interact with the inclusions, inducing electric and magnetic moments, which in turn affect the macroscopic effective permittivity and permeability of the bulk composite medium. Since artificial materials can be synthesized by embedding artificially fabricated inclusions in a specified host medium or on a host surface, this provides the designer with a large collection of independent parameters (or degrees of freedom) - such as the properties of the host materials; the size, shape, and composition of the inclusions; and the density arrangement and alignment of these inclusions - to work with in order to engineer an artificial material with specific electromagnetic response functions not found in each of the individual constituents. All of these design parameters can play a key role in the final outcome of the synthesis process. Among these, the geometry of the inclusions is one that can provide a variety of new possibilities for artificial materials processing [24].

In addition, as the new idea, the host media can be chosen so that, it be soft and flexible to change the shape, and can easily be used for load to (and/or cover on) other electromagnetic devices. In the following sections some materials which exist in nature (i.e., dielectrics), and some of them which are made artificially (i.e., metamaterials and chiral media) are reviewed.

2.2.2 Dielectric Materials

A dielectric material is a substance that is a poor conductor of electricity, but an efficient supporter of electrostatic fields. The term was coined by Whewell [28] in

response to a request from Faraday. Since an electric field passes through the material, Whewell considered Greek's term "dia" (which means "through") and named dielectric, but felt that dielectric was easier to pronounce. While the nouns dielectric and insulator are generally considered synonymous, the term dielectric is more often used when considering the effect of alternating electric fields on the substance, and insulator is more often used when the material is being used to withstand a high electric field.

Von Hippel, in his seminal book [29] takes this definition further. He states, "Dielectrics are not a narrow class of so-called insulators, but the broad expanse of non metals considered from the standpoint of their interaction with electric, magnetic, of electromagnetic fields. Thus we are concerned with gases as well as with liquids and solids, and with the storage of electric and magnetic energy as well as its dissipation."

"Dielectrics" is the study of dielectric materials and involves physical models to describe how an electric field behaves inside a material. It is characterised by how an electric field interacts with an atom. It is possible to approach dielectrics from either a classical interpretation or a quantum one. However, the classical is much more intuitive.

Many phenomena in electronics, solid state and optical physics can be described using the underlying assumptions of the dielectric model. This can mean that the same mathematical objects can go by many different names. An important property of a dielectric is its ability to support an electrostatic field while dissipating minimal energy in the form of heat.

In practice, most dielectric materials are solid. Examples include porcelain (ceramic), mica, glass, plastics, and the oxides of various metals. Materials with moderate

dielectric constants include ceramics, distilled water, paper, mica, polyethylene, and glass. Metal oxides, in general, have high dielectric constants.

2.2.3 Isorefractive Media

Refraction is the change in direction of a wave due to a change in its speed. This is most commonly seen when a wave passes from one medium to another. Refraction is described by Snell's law, which states that the angle of incidence is related to the angle of refraction by

$$\frac{\sin \theta_1}{\sin \theta_2} = \frac{v_1}{v_2}, \quad (2.1)$$

where the wave velocities v_1 and v_2 through these media can be written,

$$v_1 = \frac{1}{\sqrt{\mu_1 \epsilon_1}} = \frac{1}{\sqrt{\mu_0 \epsilon_0} \sqrt{\mu_{r1} \epsilon_{r1}}}, \quad (2.2)$$

$$v_2 = \frac{1}{\sqrt{\mu_2 \epsilon_2}} = \frac{1}{\sqrt{\mu_0 \epsilon_0} \sqrt{\mu_{r2} \epsilon_{r2}}}. \quad (2.3)$$

From (2.1) – (2.3) we have

$$\sqrt{\mu_{r1} \epsilon_{r1}} \sin \theta_1 = \sqrt{\mu_{r2} \epsilon_{r2}} \sin \theta_2, \quad (2.4)$$

which means the refraction is related to the macroscopic properties permeability and permittivity of the media.

If $\mu_{r1} \epsilon_{r1} = \mu_{r2} \epsilon_{r2}$, Equation (2.4) is only valid if $\theta_1 = \theta_2$. That means there is no refraction (isorefractive). It is not possible unless two media are the same media, or two media have the same wave number and different intrinsic impedances. On the other words the isorefractive media is made by two different materials (i.e., dielectrics) which have the following conditions

$$\mu_{r1}\epsilon_{r1} = \mu_{r2}\epsilon_{r2}, \quad (2.5)$$

$$\mu_{r1} / \epsilon_{r1} \neq \mu_{r2} / \epsilon_{r2}. \quad (2.6)$$

It is almost not possible to find two natural materials so that they make isorefractive media. Therefore, isorefractive media must be constructed artificially. For example, by imbedding small spherical particles of diamagnetic material in a dielectric with a low dielectric constant, so that the product of the permittivity and the permeability of the material equals the product of the permittivity and permeability of the surrounding medium [30].

Isorefractive materials exhibit several interesting properties [30]. For example, when an electromagnetic wave is incident on the interface between two isorefractive media, the incident and transmitted wave numbers are parallel to each other. Also, the reflection and transmission coefficients at any regular point of the interface between two isorefractive media are independent of both angle of incidence and polarization of the incident wave.

The transfer of the electromagnetic waves from the first media to the second one without changing its direction (isorefractive) is an interesting phenomenon which has become the subject of study for researchers in recent years. Extensive studies with various subjects are reported by Uslenghi and his group in which isorefractive materials are considered. For instances; radiation and scattering waves by various geometries [31]-[38], waveguiding structures containing isorefractive materials [30], and currents on conducting surfaces of a semielliptical-channel-backed slotted screen in an isorefractive environment [39]. Many investigations about isorefractive media are reported by other research groups, as well. Subjects include scattering by elliptic cylinder [40], [41]

formulation of dyadic green's functions for a dielectric/isorefractive elliptic cylinder [42], and a class of artificial materials isorefractive with free space [43].

Among these, the reports [33], [35], and [39]-[42] are about the radiation and scattering with elliptic cylinder geometry.

2.2.4 Metamaterials

A metamaterial (or meta material) is a material that gains its properties from its structure rather than directly from its composition. To distinguish metamaterials from other composite materials, the metamaterial label is usually used for a material that has unusual properties. The term was coined in 1999 by Rodger M. Walser of the University of Texas at Austin [44]. He defined metamaterials as; "Macroscopic composites having a manmade, three-dimensional, periodic cellular architecture designed to produce an optimized combination, not available in nature, of two or more responses to specific excitation."

Among electromagnetic researchers, the term is often used, quite narrowly, for materials which exhibit negative refraction. Because of the special properties of metamaterials, they have become a subject of study by many research groups in worldwide. Hundreds investigations are rapidly reported about metamaterials with theoretical and experimental discussions. Most of these studies are reported after year 2002. Some of them are reviewed here.

In 1948, Kock [27] made lightweight microwave lenses by arranging conducting spheres, disks, and strips periodically and effectively tailoring the effective refractive index of the artificial media. The idea of complex materials in which both the permittivity

and the permeability possess negative real values at certain frequencies has received considerable attention. In 1967, Veselago [45] theoretically investigated plane-wave propagation in a material whose permittivity and permeability were assumed to be simultaneously negative. In recent years, Smith, Schultz, and their group constructed such a composite medium for the microwave regime and demonstrated experimentally the presence of anomalous refraction in this medium [46]-[48].

Extensive investigations with various subjects are reported by Engheta, Ziolkowski, and their groups in which about the response of metamaterials and methods for their fabrication are discussed in theoretically and experimentally [49]-[59]. Also, many theoretical and experimental works are reported [60]-[77], by other groups in various subjects such as radiations, scattering, transmissions, reflections, propagations, refractions, and waveguiding.

Some of the reported investigations are about the propagation in the waveguides, radiation from slot antennas, and electromagnetic wave scattering by cylindrical (rectangular, circular, and elliptic cylinder) objects coated by metamaterials, i.e., [15], [16], [56], [60], [62], [67]-[69], and [73]-[77].

Metamaterials are of particular importance in electromagnetism (especially optics and photonics). They show promise for a variety of optical and microwave applications such as new types of beam steerers, modulators, band-pass filters, lenses, microwave couplers, and antenna radomes. In order for its structure to affect electromagnetic waves, a metamaterial must have structural features smaller than the wavelength of the electromagnetic radiation it interacts with.

2.2.4.1 Basic Types of Metamaterials with Inclusions

Almost all bulk metamaterials used at the present state of the art are based on only two structures. These structures are a dense array of thin wires and an array of split-ring resonators (SRRs) [24]. They are embedded in the host media. The host media can be chosen so that they are soft and flexible to change the shape, and can easily be used for any electromagnetic devices.

2.2.4.1.1 Epsilon-Negative (ENG) Metamaterial

An array of parallel thin wires exhibits a high-pass behaviour for an incoming plane wave whose electric field is parallel to the wires. Below a special frequency (a cutoff frequency of the array) there is no propagation and an electromagnetic wave will experience total reflection. This behaviour is similar to the propagation of the electromagnetic waves in plasma [24].

Figure 2.5 shows an array of thin conducting wires with unit cell size a . If unit cell size a , is much smaller than a wavelength, the wire can be thought of as a continuous plasma. Since the epsilon value of this metamaterial is negative, it is named epsilon-negative (ENG) or single-negative (SNG) metamaterial. This is a way that an epsilon-negative (or single-negative) metamaterial can be fabricated.

2.2.4.1.2 Mu-Negative (MNG) Metamaterial

An array of split-ring resonator (SRR) inclusions can be used for the synthesis of mu-negative (MNG) metamaterials which is another single-negative metamaterial (Figure 2.6). A single SRR can be thought of as a small, capacitively loaded loop antenna. If this

antenna operates slightly above the resonant frequency, the local scattered magnetic field will be almost out of phase with the incident field. Thus, the resultant local magnetic field will be lower than that of the incident field. It leads to the negative magnetic polarization and negative effective permeability of the resulting metamaterial [24].

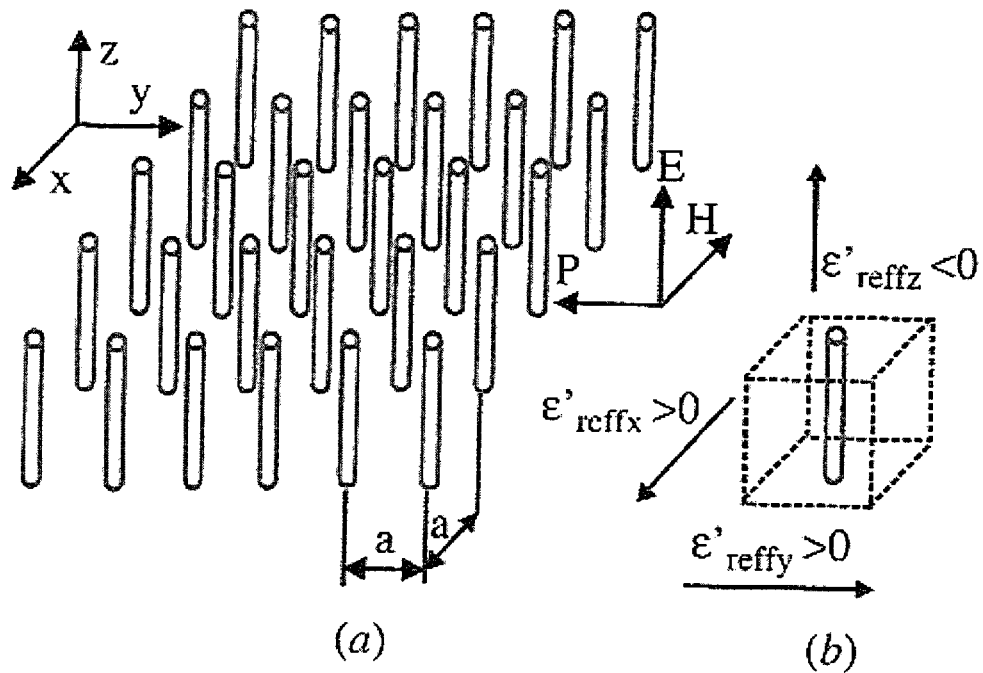


Figure 2.5 – ENG Metamaterial [24]; (a) Array of thin conducting wires. (b) Unit cell.

If the magnetic field vector of the incident plane wave is perpendicular to the SRR, it will give rise to the induced currents that eventually will yield the negative permeability. On the contrary, if the magnetic field vector is parallel to the SRR, it can not give rise to the induced currents and the presence of the SRR does not affect the effective permeability.

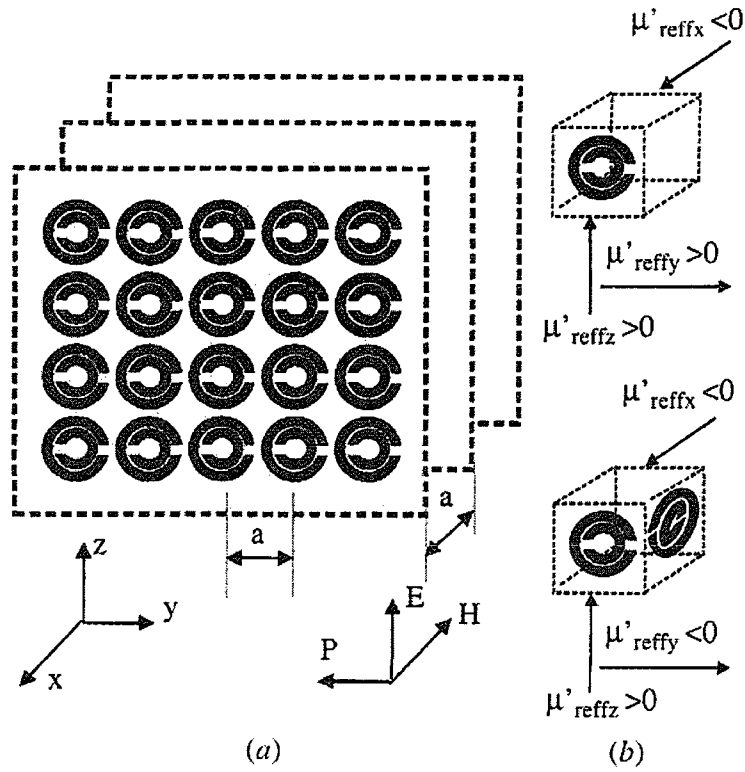


Figure 2.6 – MNG Metamaterial [24]; (a) SRRs array. (b) Unit cell (1D and 2D cases).

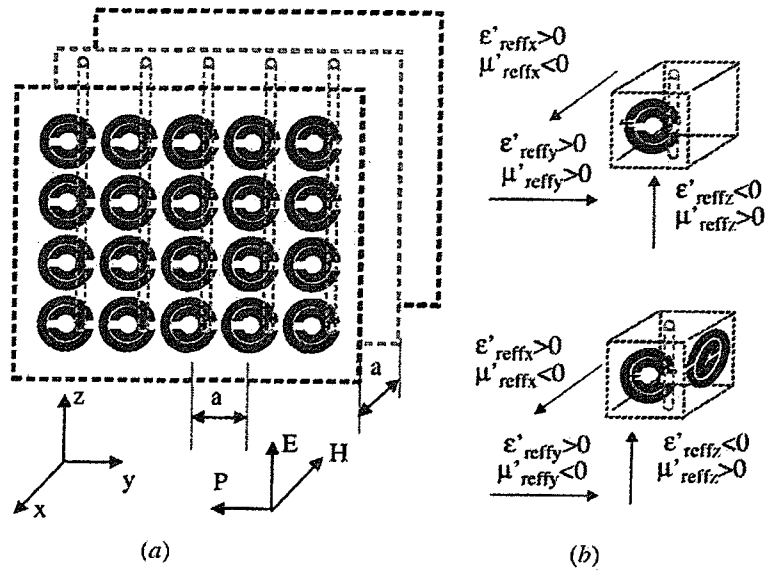


Figure 2.7 – DNG Metamaterial [24]; (a) Wires & SRRs. (b) Unit cell (1D & 2D cases).

2.2.4.1.3 DNG Metamaterial

The double-negative (DNG) metamaterial can be made from combination of the thin-wire-based ENG structure and the SRR-based MNG structure (Figure 2.7). It is assumed that the new composite material exhibited a macroscopic permittivity equal to that of the thin-wire-based ENG medium and a macroscopic permeability equal to the permeability of the SRR-based MNG medium. This is a simplified model which neglects any interactions between the wires and the SRRs [24].

The DNG metamaterial is also named the left-handed metamaterial (LHM), backward-wave (BW) media, and media with negative refractive index.

2.2.4.2 Negative Refractive Index

The main reason researchers have investigated metamaterials is the possibility to create a structure with a negative refractive index, since this property is not found in any naturally occurring material. Almost all materials encountered in optics, such as glass or water, have positive values for both permittivity ϵ and permeability μ . However, many metals (such as silver and gold) have negative ϵ at visible wavelengths. Materials having negative ϵ or μ (but not both) are opaque to electromagnetic radiation.

For plane waves propagating in negative refractive index metamaterials, the electric field, magnetic field, and poynting vector (or group velocity) follow a left-hand rule, thus giving rise to the name left-handed (meta) materials. It should be noted that the terms left-handed and right-handed can also arise in the study of chiral media (Section 2.2.5), but their use in that context is unrelated to this effect. Some researchers consider the qualifier left-handed for achiral materials as particularly infelicitous.

An example for negative index (or DNG or LHM) is flat lens focusing with left-handed metamaterial (LHM). A negative index of refraction should cause electromagnetic radiation to refract or bend at a negative angle when entering an LHM, as shown in the Figure 2.8 on the left. The Figure 2.8 on the right shows that this property could be used to bring radiation to a focus with a flat LHM lens. The advantage of a flat lens in comparison to a conventional curved lens is that the focal length could be varied simply by adjusting the distance between the lens and the electromagnetic wave source. In this in-house work, researchers at the national aeronautics and space administration (NASA) Glenn research center [78] developed a computational model for LHMs with the three-dimensional electromagnetic commercial code microwave studio, constructed an LHM flat lens, and used it to experimentally demonstrate the reversed refraction and flat lens focusing of microwave radiation.

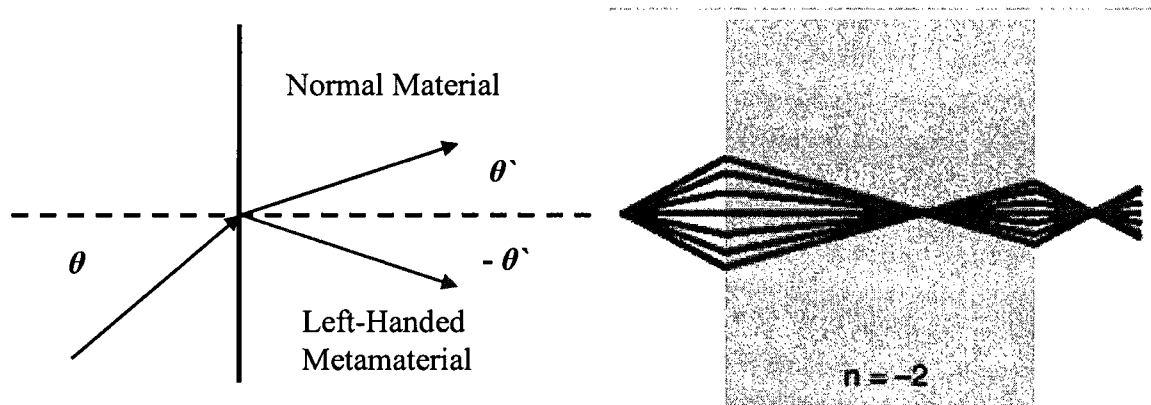


Figure 2.8 – Left: Refraction of an incident electromagnetic wave from free space by a conventional material and LHM. Right [78]: Electromagnetic radiation is focused by a flat slab of LHM with index $n = -2$.

The LHM flat lens configuration is a periodic array of metallic rings and wires based on work by researchers at the University of California at San Diego ([46] and [47]). A photograph of the constructed flat lens array of LHM cells is shown on the Figure 2.9. For microwave radiation at wavelengths about 10 times a cell length, this configuration provides negative effective values of electric permittivity and magnetic permeability, resulting in a negative value for the index of refraction. Preliminary testing has demonstrated a reversed refraction effect with focusing of the microwave radiation. Finite element models are being developed and an optics ray tracing code is being used to create new lens designs.

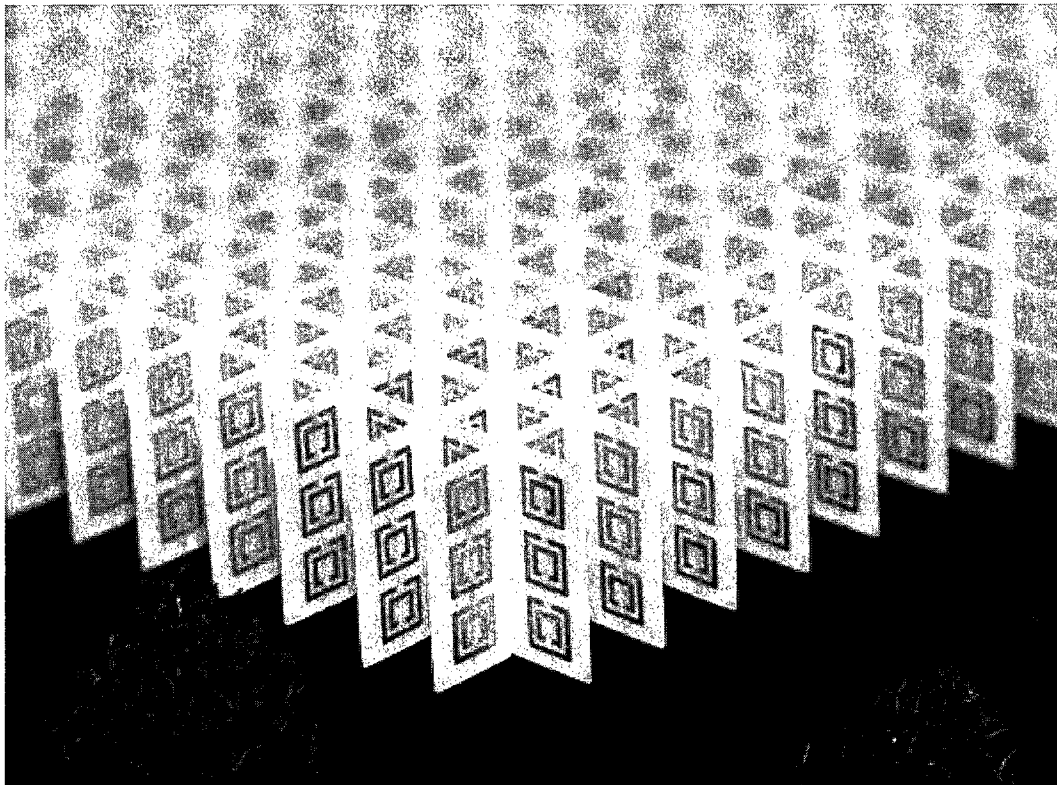


Figure 2.9 – LHM flat lens consisting of an array of 3 by 20 by 20 unit cells, with unit cell size of 5 mm. This geometry shows reversed refraction and left-handed focusing properties at microwave frequencies between 10 and 11 GHz [78].

2.2.5 Chiral Media

The term “chiral” is a Greek’s word and means “hand”. The following are some concept definitions of chiral media;

- Material with either a left or right handed helical arrangement,
- Having different left-handed and right-handed forms, not mirror symmetric,
- An object whose mirror image is not the same as itself,
- Any molecule that is not superimposable on its mirror image.

Molecules can be chiral if they contain one or more chiral centers. For the purposes of introductory organic chemistry, a chiral center can be defined as a hybridized carbon that is bonded to four different groups. On the other hand chiral molecule has a carbon atom with four different groups attached.

A chiral molecule is not superimposable with its mirror image. Like left and right hands (that have a thumb, fingers in the same order, but are mirror images and not the same), chiral molecules have the same things attached in the same order, but are mirror images and not the same (Figure 2.10). The best definition for a chiral molecule maybe is one that, “The necessary and sufficient condition for a chiral molecule is one, that is not superimposable on its mirror image” [79]. For example, you cannot place your right hand on your left and have all hand parts in the same place. They are related to each other as mirror images in three-dimensional space, and as such they can not be superimposed on top of each other.

Chiral media can also be defined from the macroscopic point of view. An object that is not chiral is said to be achiral (or non-chiral). Thus all objects are either chiral or achiral. The double helix is a chiral object [80] (Figure 2.11).

The term “chirality” is also Greek’s word and refers to the property of “handedness”. Chirality is an important chemical concept. For example the active ingredients in caraway seeds and spearmint demonstrate the concept. Though they have identical molecular structures, the two substances taste differently because they are opposite in chirality [81].

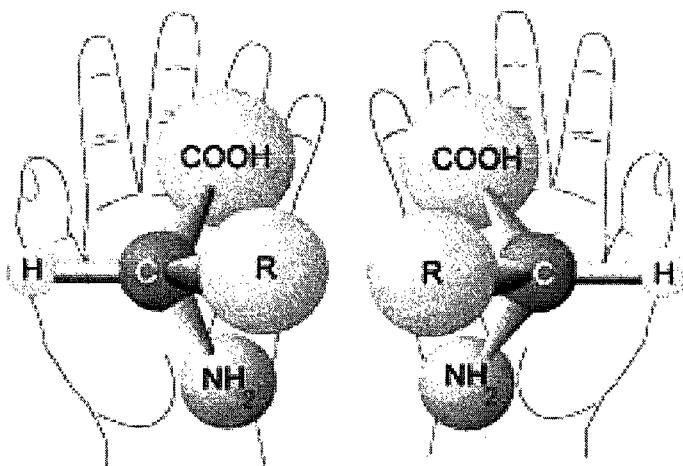


Figure 2.10 – Hands and chiral molecules [79].

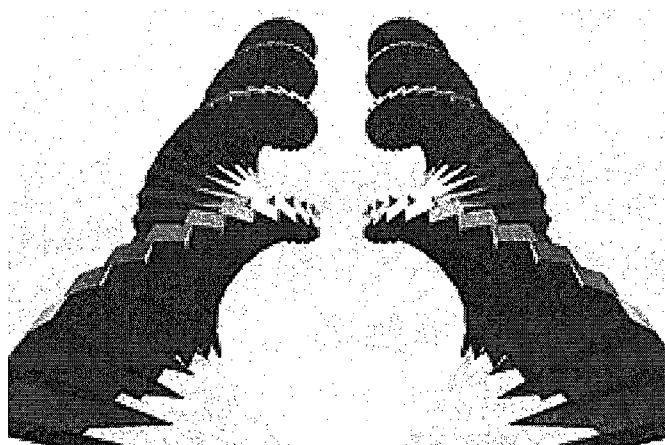


Figure 2.11 – Double helix is a chiral object [80].

Many biological and natural molecules are chiral, such as amino acids, carbohydrates, nucleic acids, sugars, proteins, hormones, glycine, tertiary amine, tartaric acid, snub polyhedron, DNA, and RNA. Some man made chiral objects are irregular tetrahedron, stringed instruments, double helix and hand gloves.

2.2.5.1 Electromagnetic Behaviours of Chiral Media

Chiral materials have been known and studied since 1813, when Biot first explained observations of color changes for white linearly polarized light transmitted through quartz [82]. He has shown that each frequency of linearly polarized light rotated by a different amount during transmission through a chiral medium. This phenomenon became known as optical rotation or alternatively as optical activity. The sodium light is usually used for the determination of optical activity. The rotation is different, may be zero, and may even reverse in direction compared with the rotation given with sodium light. In 1895, Cotton has shown that chiral media can transform a linearly polarized wave into an elliptically polarized wave [82].

Chiral media is a reciprocal medium characterized by different phase velocities for right and left circularly polarized waves. These are the same properties as an isotropic optically active media, therefore the same constitutive relationships are used. Chiral media responds with both electric and magnetic polarization to either electric or magnetic excitation. Chiral objects can generate both co- and cross-polarized fields simultaneously which is an advantage for some applications. In a lossless chiral medium, any linearly polarized wave undergoes a rotation of its polarization as it propagates. For a chiral cylinder, the chirality results in a coupling between the TM_z and TE_z scattering waves.

Therefore, the solution of the problem involving chiral medium is more complicated compared to achiral medium.

An isotropic chiral medium is a macroscopically continuous medium composed of equivalent chiral objects that are uniformly distributed and randomly oriented. The theory of electromagnetic wave propagation in isotropic chiral media differs from the more common aspects of isotropic achiral media. From the technical point of view, an isotropic achiral media is characterized by two parameters, in counterpoint to chiral medium characterized by three parameters, two common parameters (the electric permittivity and the magnetic permeability), and the new extra parameter chirality admittance which is responsible for optical activity. Also the electromagnetic chirality is known as optical activity in the optical regime.

2.2.5.2 Artificial Chiral Media

All objects in the nature are either chiral or achiral. Thus, there are natural chiral materials. However it seems, still there are some obstacles to use directly the natural chiral materials for real applications. Use of artificial materials by embedding pieces of inclusions in some host media (as discussed in Section 2.2.1) is interesting way that researchers are interested to do that. Helix is a one of the appropriate chiral object for fabrication of artificial chiral material.

The first attempt to explore the concept of artificial materials appears when in 1898 Bose made the first microwave experiment on twisted structures-geometries that were essentially artificial chiral elements [25]. In 1914, Lindman worked on artificial chiral media by embedding many randomly oriented small wire helices in a host medium

[26]. In 1956 Winkler [83], 1957 Tinoco and Freeman [84], and 1960 Tinoco and Woody [85], have done some experiments on microwave micropagation through dispersions of copper helices.

Also extensive investigations are reported about natural and artificial chiral material in the last twenty years with different subjects. In some theoretical and experimental investigations [86]-[117], thin wires in the form of helices or other chiral shapes are used as the composite inclusions embedded in the host materials to demonstrate the artificial chiral structures. As an example Busse and his group [99] have experimentally studied waveguide characterization of chiral material. Figure 2.12 shows their fabricated artificial chiral media using helices and foam. Furthermore, some other investigations [118]-[136] about chiral media are reported without demonstrating the artificial chiral structures. The subjects which are related to our work include; waveguiding, radiation, scattering, and coating.

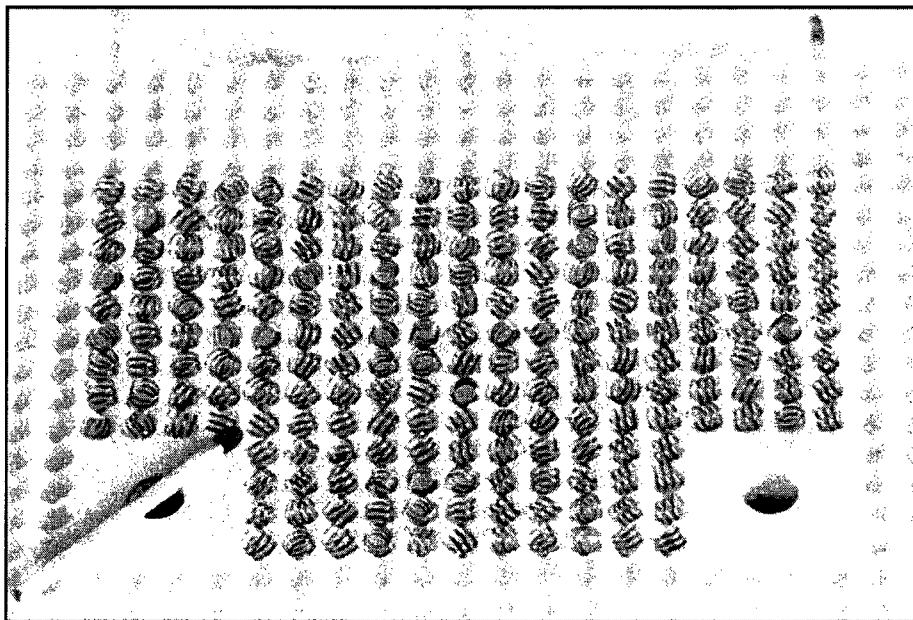


Figure 2.12 – Artificial chiral media (waveguide) using helices and foam [99].

Therefore, using the randomly oriented small wire helices in a host media is a good technique to fabricate artificial chiral media. The host media can be chosen so that they are soft and flexible to change the shape, and can easily be used for any electromagnetic devices.

2.2.6 Soft and Flexible Host Media

Most of the applications (or devices) which are made by artificial materials (i.e., metamaterial or chiral media) have rectangular shapes. The host media which were used for these purposes were hard and non flexible. Thus, it seems this technique can not be appropriate and applicable for a complicated shapes same as elliptic cylinder. As the new idea a soft and flexible host media, i.e., soft plastic can be used for these purposes.

According to this idea, artificial materials are not directly made for a special device. Instead, they are produced in general form by embedding a three-dimensional array of objects in a soft host media. The objects can have different size, shapes, and orientation for different kinds of materials. For example small (left- and right-hand) helices can be used to producing chiral media. Also, artificial materials can have different cell sizes for various ranges of frequencies. Of course, it is not possible to produce such kind of materials in a simple laboratory. They must be produced industrially with advanced technology. Then, these materials can be cut in many shapes and used for different devices.

3. Formulations for Elliptic Slot Antenna Coated by Nonconfocal Materials

The electromagnetic wave interaction with elliptic cylinder is typically expressed in terms of the elliptic cylindrical coordinate system eigenfunctions. In this chapter, we start with the elliptic cylindrical coordinate system, and then develop and express the solution in terms of eigenfunction expansions and other associate quantities of interest.

3.1 Elliptic Cylindrical Coordinate System

Consider an elliptic cylinder as shown in Figure 3.1 with its cross section in the (x, y) plane [137]. The semi-focal length f is given by $f^2 = a^2 - b^2$ where a is the semi-major axis and b is the semi-minor axis of the ellipse. The elliptic cylindrical coordinate system (ξ, η, z) is defined according to the transformation $x + j y = f \cosh(\xi + j \eta)$. Equating the real and imaginary parts of each side [138], in Cartesian coordinate system (x, y, z) , we obtain

$$x = f \cosh \xi \cos \eta, \quad (3.1)$$

$$y = f \sinh \xi \sin \eta, \quad (3.2)$$

$$z = z, \quad (3.3)$$

where ξ is the radial coordinate, $0 \leq \xi \leq \infty$, and η is the angular coordinate, $0 \leq \eta \leq 2\pi$.

The surface $\xi = \xi_0$ reduces to the elliptic cylinder

$$\left(\frac{x}{f \cosh \xi_0} \right)^2 + \left(\frac{y}{f \sinh \xi_0} \right)^2 = \cos^2 \eta + \sin^2 \eta = 1, \quad (3.4)$$

with semi-major axis $a = f \cosh \xi_0$ and semi-minor axis $b = f \sinh \xi_0$. The surface $\eta = \eta_0$ reduces to the hyperbolic cylinder

$$\left(\frac{x}{f \cos \eta_0}\right)^2 - \left(\frac{y}{f \sin \eta_0}\right)^2 = \cosh^2 \xi - \sinh^2 \xi = 1, \quad (3.5)$$

which crosses the x-axis at $\pm f \cos \eta_0$ and has asymptotes $y = \pm x \tan \eta_0$.

The corresponding scale factors in the elliptic cylindrical coordinate system are

$$\begin{aligned} h_\xi &= f \sqrt{\sinh^2 \xi + \sin^2 \eta} = f \sqrt{\cosh^2 \xi - \cos^2 \eta} \\ &= f \sqrt{\frac{1}{2}(\cosh 2\xi - \cos 2\eta)}, \end{aligned} \quad (3.6)$$

$$h_\eta = h_\xi, \quad (3.7)$$

$$h_z = 1. \quad (3.8)$$

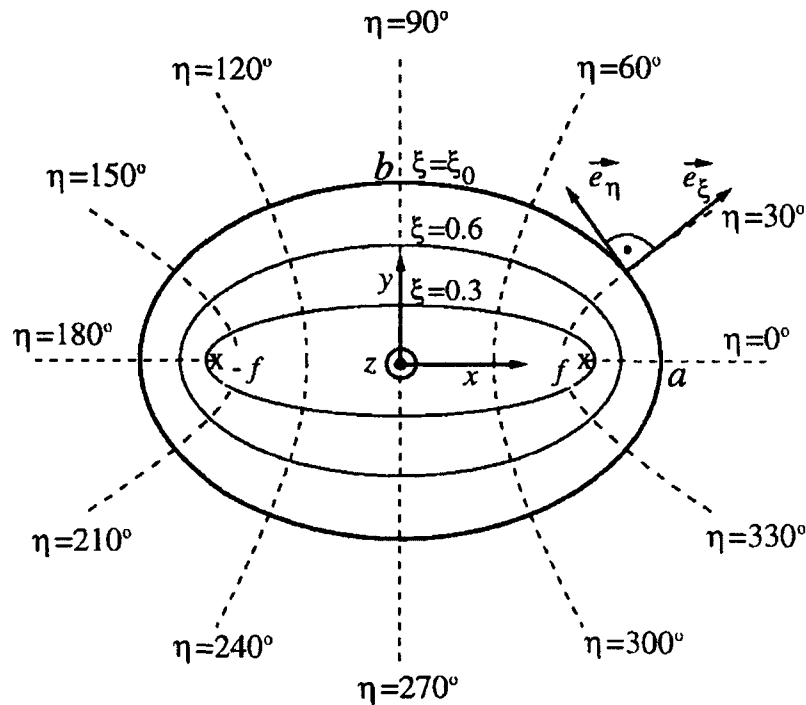


Figure 3.1 – Elliptic cylindrical coordinate system [137].

For a constant semi-focal length f and different values of ζ_0 (different surfaces), different elliptic cylinders can be obtained from Equation (3.4) which are confocal. Two elliptic cylinders are confocal if they have same focal points and no orientation with respect to each other, otherwise, they are nonconfocal. For examples two elliptic cylinders with different center points, and/or different focal length, and/or oriented axes with respect to each other, are nonconfocal cylinders.

The mathematical expressions for the problems with nonconfocal cylinders geometry may need one or more elliptic cylindrical coordinate systems. Each region of this geometry may use its own coordinate system to express the problem. However, for final solution some expressions must be transferred to other coordinate system. Therefore, solutions to the problems with nonconfocal cylinders geometries are more complicated compared to confocal ones.

The nonconfocal cylinders geometry offers more design options. Furthermore, there are some applications which have nonconfocal cylinders geometry. For example, an elliptic cylinder covered by a uniform sheet has a nonconfocal cylinders geometry.

3.2 Wave Equations

The two-dimensional Helmholtz wave equation, assuming no variation along z axis, in the elliptic cylindrical coordinate system is given by [138]

$$\left[\frac{\partial^2}{\partial \xi^2} + \frac{\partial^2}{\partial \eta^2} + 2q(\cosh 2\xi - \cos 2\eta) \right] \psi(\xi, \eta) = 0, \quad (3.9)$$

where

$$q = (k f)^2 / 4, \quad (3.10)$$

is a dimensionless parameter, and k is the propagation constant. Using the separation of variables technique, we assume a solution of the form

$$\psi(\xi, \eta) = R(\xi)S(\eta). \quad (3.11)$$

Substituting Equation (3.11) into (3.9) yields

$$\left[\frac{d^2}{d\eta^2} + (p - 2q \cos 2\eta) \right] S(\eta) = 0, \quad (3.12)$$

$$\left[\frac{d^2}{d\xi^2} - (p - 2q \cosh 2\xi) \right] R(\xi) = 0, \quad (3.13)$$

where p is the separation constant. Equations (3.12) and (3.13) are known as the angular Mathieu equation and radial (or modified) Mathieu equation, and their solutions are the angular Mathieu functions and radial (or modified) Mathieu functions, respectively.

3.2.1 Wave Equations in Chiral Media

Different kinds of materials can be used for coating the slotted cylinder. These materials are generally divided into chiral and achiral medium. The problem formulation for chiral medium is more complicated and more general compared to achiral medium. The expression of wave equations for chiral media can be used for achiral media, as well, by considering a zero chirality.

Therefore, this section presents the procedure for transforming the coupled wave equations for chiral media to a set of uncoupled wave equations so that classical eigenfunction techniques can be used [122]. The constitutive relationships for a chiral medium are

$$\vec{D} = \varepsilon_c \vec{E} - j\gamma\mu \vec{H}, \quad (3.14)$$

$$\vec{B} = \mu \vec{H} + j\gamma\mu \vec{E}, \quad (3.15)$$

where

$$\varepsilon_c = \varepsilon + \mu\gamma^2, \quad (3.16)$$

is the effective permittivity of the chiral medium, \vec{D} , \vec{B} , \vec{E} , and \vec{H} are the electric flux density, magnetic flux density, electric field, and magnetic field, respectively. Also ε is the permittivity, μ is the permeability, and γ is the chiral admittance of the medium. If μ , ε , or γ is complex the media is lossy. If $\gamma = 0$, then (3.14) and (3.15) reduce to the constitutive for an achiral medium.

In a chiral media with electric volume current density \vec{J} and electric charge density ρ , the matrix form of Maxwell's equations can be written [122] as

$$\nabla \times \begin{bmatrix} \vec{E} \\ \vec{H} \end{bmatrix} = [K] \begin{bmatrix} \vec{E} \\ \vec{H} \end{bmatrix} + \begin{bmatrix} \vec{0} \\ \vec{J} \end{bmatrix}, \quad (3.17)$$

$$\nabla \cdot \begin{bmatrix} \vec{E} \\ \vec{H} \end{bmatrix} = \frac{\rho}{\varepsilon} \begin{bmatrix} 1 \\ -j\gamma \end{bmatrix}, \quad (3.18)$$

where

$$[K] = \begin{bmatrix} \omega\mu\gamma & -j\omega\mu \\ j\omega\varepsilon_c & \omega\mu\gamma \end{bmatrix}, \quad (3.19)$$

$$\rho = \frac{j}{\omega} \nabla \cdot \vec{J}, \quad (3.20)$$

and ω is the angular velocity. Using (3.17) and (3.18), the source-free wave equation in chiral media is

$$\nabla^2 \begin{bmatrix} \vec{E} \\ \vec{H} \end{bmatrix} + [K]^2 \begin{bmatrix} \vec{E} \\ \vec{H} \end{bmatrix} = 0. \quad (3.21)$$

The coupling caused by $[K]$ in the wave equation can be removed by diagonalizing $[K]$ such that

$$[A]^{-1}[K][A] = \begin{bmatrix} k_R & 0 \\ 0 & -k_L \end{bmatrix}, \quad (3.22)$$

where

$$[A] = \begin{bmatrix} 1 & 1 \\ j\sqrt{\epsilon_c/\mu} & -j\sqrt{\epsilon_c/\mu} \end{bmatrix}, \quad (3.23)$$

and the chiral wave numbers are given by

$$k_R = \omega\sqrt{\mu\epsilon_c} + \omega\mu\gamma, \quad (3.24)$$

$$k_L = \omega\sqrt{\mu\epsilon_c} - \omega\mu\gamma. \quad (3.25)$$

We define

$$\begin{bmatrix} \vec{E} \\ \vec{H} \end{bmatrix} = [A] \begin{bmatrix} \vec{E}_R \\ \vec{E}_L \end{bmatrix}, \quad (3.26)$$

where \vec{E}_R and \vec{E}_L are the electric fields of right and left hand circularly polarized waves with propagation constants k_R and k_L , respectively. Substituting (3.26) into (3.17) and (3.18) results in a set of uncoupled equations for chiral media

$$\nabla \times \begin{bmatrix} \vec{E}_R \\ \vec{E}_L \end{bmatrix} = \begin{bmatrix} k_R \vec{E}_R \\ -k_L \vec{E}_L \end{bmatrix} + \vec{J} \frac{j}{2} \sqrt{\mu/\epsilon_c} \begin{bmatrix} -1 \\ 1 \end{bmatrix}, \quad (3.27)$$

$$\nabla \cdot \begin{bmatrix} \vec{E}_R \\ \vec{E}_L \end{bmatrix} = \frac{\rho}{2\varepsilon} \begin{bmatrix} 1 - \gamma\sqrt{\mu/\varepsilon_c} \\ 1 + \gamma\sqrt{\mu/\varepsilon_c} \end{bmatrix}. \quad (3.28)$$

Then the uncoupled source-free wave equation in chiral media is

$$\nabla^2 \begin{bmatrix} \vec{E}_R \\ \vec{E}_L \end{bmatrix} + \begin{bmatrix} k_R^2 \vec{E}_R \\ k_L^2 \vec{E}_L \end{bmatrix} = 0. \quad (3.29)$$

3.3 The Eigenfunction Expansions

As shown in Figure 3.2, consider the Cartesian coordinate system (x_c, y_c, z) or elliptic cylindrical coordinate system (ξ_c, η_c, z) as a local coordinate system and (x, y, z) or (ξ, η, z) as a global coordinate system. A perfectly conducting elliptic cylinder with semi-focal length f_c , semi-major axis a_c , and semi-minor axis b_c is centered at the origin of the local coordinate system. It has an axial slot along the z -axis with angular width $\eta_{c2} - \eta_{c1}$. This cylinder coated by a nonconfocal elliptic cylinder which is located at the origin of the global coordinate system with semi-focal length f , semi-major axis a , and semi-minor axis b . The major axis (x_c -axis) of the local coordinate system is oriented by an angle α with respect to the major axis (x -axis) of the global coordinate system, and its center is given by the polar coordinates (d, β) with respect to the center of the global coordinate system. The cross sections of this geometry in the x - y plane are shown in Figure 3.2 which include the three regions.

The inner region of the conducting cylinder (region 1), can be free space, dielectric, or metamaterial. The coated region (region 2), can be free space, dielectric, isorefractive, metamaterial, or chiral media. Region 3 is free space. In the following sections we consider an incident transverse magnetic (TM) polarized wave. The

eigenfunction expansions in regions 1 and 2 can be expressed in terms of the local coordinate system, while in region 3 they can be expressed in terms of the global coordinate system.

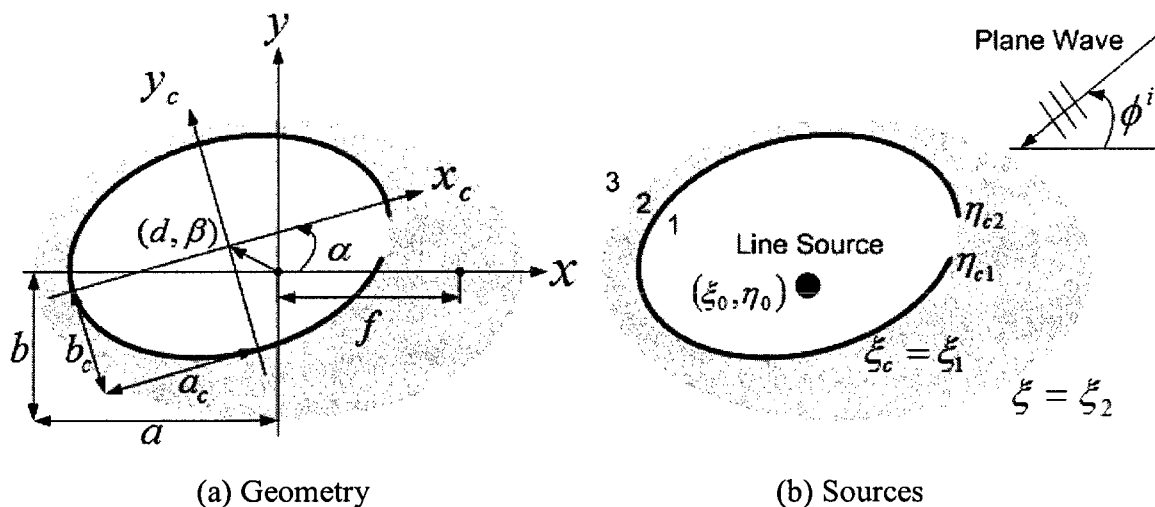


Figure 3.2 – Geometry of slotted elliptic cylinder coated by a nonconfocal material.

(a) Local and global coordinate systems. (b) Slot and its excitation sources.

3.3.1 Incident Wave

The source can be located in region 1 or region 3. Assume a line source for region 1, and a line source or plane wave for region 3. If the source is located in region 1, the slot acts as a transmitting antenna, and if the source is located in region 3, it acts as a receiving or coupling antenna.

In general, for an electric line source with unit amplitude, located at (ξ_0, η_0) , the incident electric fields are given by [9]

$$E_{z_c}^{li} = \sum_m A l_{\epsilon_m} R_{\epsilon_m}^{(4)}(c_1, \xi_c) S_{\epsilon_m}(c_1, \eta_c), \quad \xi_c \geq \xi_0 \quad (3.30)$$

$$E_z^{3i} = \sum_m A3_{\epsilon_m} R_{\epsilon_m}^{(1)}(c_3, \xi) S_{\epsilon_m}(c_3, \eta), \quad \xi \leq \xi_0 \quad (3.31)$$

where S is the angular Mathieu function, $R^{(l)}$ is the l^{th} kind of radial Mathieu function ($l = 1, \dots, 4$), $c_1 = k_1 f_c$, $c_3 = k_3 f$, k_l is wave number in region l , subscripts e and o denote even and odd types, respectively, and the summation (Σ) starts from 0 for even type and from 1 for odd type functions. Also

$$A1_{\epsilon_n} = 4R_{\epsilon_n}^{(1)}(c_1, \xi_0) S_{\epsilon_n}(c_1, \eta_0) / N_{\epsilon_n}(c_1), \quad (3.32)$$

$$A3_{\epsilon_n} = 4R_{\epsilon_n}^{(4)}(c_3, \xi_0) S_{\epsilon_n}(c_3, \eta_0) / N_{\epsilon_n}(c_3), \quad (3.33)$$

$$N_{\epsilon_n}(c_l) = \int_0^{2\pi} [S_{\epsilon_n}(c_l, \eta^+)]^2 d\eta^+, \quad (3.34)$$

$$\xi_0 = \cosh^{-1} \left\{ \left[\frac{1}{2} \left(\frac{\rho_0^2}{f_0^2} + 1 \right) + \sqrt{\frac{1}{4} \left(\frac{\rho_0^2}{f_0^2} + 1 \right)^2 - \frac{x_0^2}{f_0^2}} \right]^{1/2} \right\}, \quad (3.35)$$

$$\eta_0 = \cos^{-1} \left(\frac{x_0}{f_0 \cosh \xi_0} \right), \quad (3.36)$$

$$x_0 = \rho_0 \cos \phi^i, \quad (3.37)$$

$A1_{\epsilon_n}$ and $A3_{\epsilon_n}$ are expressed in local and global coordinate systems, respectively, $\eta^+ = \eta_c$ (or η) if $l = 1$ (or 3), $f_0 = f_c$ (or f) if source located in region 1 (or 3), ϕ^i is the incident angle with respect to the major axis of the corresponding (local or global) coordinate system, and ρ_0 is the radial distance from the origin to the source location. The origin is center of the local coordinate system if source located in region 1, and it is center of the global coordinate system if source located in region 3. For a plane wave, the incident electric field is given by (3.31) with

$$A3_{\epsilon_n} = j^n \sqrt{8\pi} E_0 S_{\epsilon_n}(c_3, \cos \phi^i) / N_{\epsilon_n}(c_3), \quad (3.38)$$

where E_0 is the amplitude of the incident field.

The corresponding magnetic fields for Equations (3.30) and (3.31) in the η_c and η directions, respectively, can be obtained by

$$\begin{aligned} H_{\eta_c}^{1i} &= \frac{-j}{\omega\mu_1 h_c} \frac{\partial E_{z_c}^{1i}}{\partial \xi_c} \\ &= \frac{-j}{\omega\mu_1 h_c} \sum_m A1_{\sigma_m} R_{\sigma_m}^{(4)'}(c_1, \xi_c) S_{\sigma_m}(c_1, \eta_c), \end{aligned} \quad (3.39)$$

$$\begin{aligned} H_{\eta}^{3i} &= \frac{-j}{\omega\mu_3 h} \frac{\partial E_z^{3i}}{\partial \xi} \\ &= \frac{-j}{\omega\mu_3 h} \sum_m A3_{\sigma_m} R_{\sigma_m}^{(1)'}(c_3, \xi) S_{\sigma_m}(c_3, \eta), \end{aligned} \quad (3.40)$$

where μ_1 and μ_3 are permeabilities of region 1 and region 3, respectively, h_c and h are scale factors and given by (3.6), and the prim indicates the derivative with respect to the corresponding argument.

3.3.2 Fields in Region 1 ($\xi_c < \xi_1$)

In the presence of a chiral media, the fields may be expanded as an infinite sum of vector wave functions, \vec{M}_m and \vec{N}_m [122], [139] which are related by

$$\nabla \times \vec{N}_m = k \vec{M}_m, \quad (3.41)$$

$$\nabla \times \vec{M}_m = k \vec{N}_m. \quad (3.42)$$

In elliptic cylindrical coordinate system (ξ, η, z) , \vec{M}_m and \vec{N}_m can be written as

$$\vec{N}_m^{(l)}(k) = \hat{u}_z R_{\sigma_m}^{(l)}(c, \xi) S_{\sigma_m}(c, \eta), \quad (3.43)$$

$$\begin{aligned}
\vec{M}_m^{(l)}(k) &= \frac{1}{k} \nabla \times \vec{N}_m^{(l)}(k) \\
&= \hat{u}_\xi M_\xi + \hat{u}_\eta M_\eta \\
&= \hat{u}_\xi \frac{1}{kh} R_{\sigma_m}^{(l)}(c, \xi) S'_{\sigma_m}(c, \eta) \\
&\quad - \hat{u}_\eta \frac{1}{kh} R_{\sigma_m}^{(l)'}(c, \xi) S_{\sigma_m}(c, \eta). \tag{3.44}
\end{aligned}$$

Therefore, the fields in region 1 will have TM_Z and TE_Z components, and the electric field is expanded as

$$\begin{aligned}
\vec{E}^1 &= \sum_m \left[B1_{\sigma_m} \vec{M}_m^{(1)}(k_1) + B2_{\sigma_m} \vec{N}_m^{(1)}(k_1) \right] \\
&= \hat{u}_{\xi_c} \frac{1}{k_1 h_c} \sum_m B1_{\sigma_m} R_{\sigma_m}^{(1)}(c_1, \xi_c) S'_{\sigma_m}(c_1, \eta_c) \\
&\quad - \hat{u}_{\eta_c} \frac{1}{k_1 h_c} \sum_m B1_{\sigma_m} R_{\sigma_m}^{(1)'}(c_1, \xi_c) S_{\sigma_m}(c_1, \eta_c) \\
&\quad + \hat{u}_{z_c} \sum_m B2_{\sigma_m} R_{\sigma_m}^{(1)}(c_1, \xi_c) S_{\sigma_m}(c_1, \eta_c), \tag{3.45}
\end{aligned}$$

where $B1_{\sigma_m}$ and $B2_{\sigma_m}$ are unknown expansion coefficients. The corresponding magnetic field can be written as

$$\begin{aligned}
\vec{H}^1 &= \frac{j}{\sqrt{\mu_1 / \epsilon_1}} \sum_m \left[B1_{\sigma_m} \vec{N}_m^{(1)}(k_1) + B2_{\sigma_m} \vec{M}_m^{(1)}(k_1) \right] \\
&= \hat{u}_{\xi_c} \frac{j}{\omega \mu_1 h_c} \sum_m B2_{\sigma_m} R_{\sigma_m}^{(1)}(c_1, \xi_c) S'_{\sigma_m}(c_1, \eta_c) \\
&\quad - \hat{u}_{\eta_c} \frac{j}{\omega \mu_1 h_c} \sum_m B2_{\sigma_m} R_{\sigma_m}^{(1)'}(c_1, \xi_c) S_{\sigma_m}(c_1, \eta_c)
\end{aligned}$$

$$+\hat{u}_{z_c} \frac{j}{\sqrt{\mu_1 / \varepsilon_1}} \sum_m B1_{\varepsilon_m} R_{\varepsilon_m}^{(1)}(c_1, \xi_c) S_{\varepsilon_m}(c_1, \eta_c). \quad (3.46)$$

3.3.3 Aperture Fields ($\xi_c = \xi_1$)

The unknown aperture fields on the slot are expressed in terms of sinusoidal Fourier representation of even and odd parts, i.e.,

$$E_{\eta_c}^a(\eta_c) = \frac{-1}{k_1 h_c} \sum_m b1_{\varepsilon_m} CS_{\varepsilon_m}(\eta_c), \quad (3.47)$$

$$E_{z_c}^a(\eta_c) = \sum_m b2_{\varepsilon_m} CS_{\varepsilon_m}(\eta_c), \quad (3.48)$$

where

$$CS_{\varepsilon_m}(\eta_c) = \begin{cases} \cos \frac{2m\pi}{\eta_{c2} - \eta_{c1}} \eta_c, \\ \sin \frac{2m\pi}{\eta_{c2} - \eta_{c1}} \eta_c, \end{cases} \quad (3.49)$$

and $b1_{\varepsilon_m}$ and $b2_{\varepsilon_m}$ are unknown expansion coefficients to be determined.

3.3.4 Fields in Region 2 ($\xi_c > \xi_1$ and $\xi \leq \xi_2$)

In region 2, the eigenfunction expansion must account for the polarization rotation inherent to chiral media. In a z -independent problem, these result in a coupling between the TM_Z and TE_Z fields, which prevents the eigenfunction expansion from being written as a simple superposition of TM_Z and TE_Z fields. However, the eigenfunction expansion can be written as a superposition of right and left hand circularly polarized fields. This is done by combining the vector wave functions \vec{M}_m and \vec{N}_m , to form right and left hand circularly polarized vector wave functions

$$\vec{E}_{Rm}^{(l)} = \vec{M}_m^{(l)}(k_R) + \vec{N}_m^{(l)}(k_R), \quad (3.50)$$

$$\vec{E}_{Lm}^{(l)} = -\vec{M}_m^{(l)}(k_L) + \vec{N}_m^{(l)}(k_L). \quad (3.51)$$

The electric field in the chiral medium (region 2) may be then represented as

$$\begin{aligned} \vec{E}^2 &= \vec{E}_R^2 + \vec{E}_L^2 \\ &= \sum_m C1_{\epsilon_m} \left[\vec{M}_m^{(1)}(k_R) + \vec{N}_m^{(1)}(k_R) \right] + \sum_m C2_{\epsilon_m} \left[-\vec{M}_m^{(1)}(k_L) + \vec{N}_m^{(1)}(k_L) \right] \\ &\quad + \sum_m D1_{\epsilon_m} \left[\vec{M}_m^{(2)}(k_R) + \vec{N}_m^{(2)}(k_R) \right] + \sum_m D2_{\epsilon_m} \left[-\vec{M}_m^{(2)}(k_L) + \vec{N}_m^{(2)}(k_L) \right] \\ &= \hat{u}_{\xi_c} \frac{1}{h_c} \left\{ \frac{1}{k_R} \sum_m C1_{\epsilon_m} R_{\epsilon_m}^{(1)}(c_R, \xi_c) S'_{\epsilon_m}(c_R, \eta_c) - \frac{1}{k_L} \sum_m C2_{\epsilon_m} R_{\epsilon_m}^{(1)}(c_L, \xi_c) S'_{\epsilon_m}(c_L, \eta_c) \right. \\ &\quad \left. + \frac{1}{k_R} \sum_m D1_{\epsilon_m} R_{\epsilon_m}^{(2)}(c_R, \xi_c) S'_{\epsilon_m}(c_R, \eta_c) - \frac{1}{k_L} \sum_m D2_{\epsilon_m} R_{\epsilon_m}^{(2)}(c_L, \xi_c) S'_{\epsilon_m}(c_L, \eta_c) \right\} \\ &\quad - \hat{u}_{\eta_c} \frac{1}{h_c} \left\{ \frac{1}{k_R} \sum_m C1_{\epsilon_m} R_{\epsilon_m}^{(1)'}(c_R, \xi_c) S_{\epsilon_m}(c_R, \eta_c) - \frac{1}{k_L} \sum_m C2_{\epsilon_m} R_{\epsilon_m}^{(1)'}(c_L, \xi_c) S_{\epsilon_m}(c_L, \eta_c) \right. \\ &\quad \left. + \frac{1}{k_R} \sum_m D1_{\epsilon_m} R_{\epsilon_m}^{(2)'}(c_R, \xi_c) S_{\epsilon_m}(c_R, \eta_c) - \frac{1}{k_L} \sum_m D2_{\epsilon_m} R_{\epsilon_m}^{(2)'}(c_L, \xi_c) S_{\epsilon_m}(c_L, \eta_c) \right\} \\ &\quad + \hat{u}_{z_c} \left\{ \sum_m C1_{\epsilon_m} R_{\epsilon_m}^{(1)}(c_R, \xi_c) S_{\epsilon_m}(c_R, \eta_c) + \sum_m C2_{\epsilon_m} R_{\epsilon_m}^{(1)}(c_L, \xi_c) S_{\epsilon_m}(c_L, \eta_c) \right. \\ &\quad \left. + \sum_m D1_{\epsilon_m} R_{\epsilon_m}^{(2)}(c_R, \xi_c) S_{\epsilon_m}(c_R, \eta_c) + \sum_m D2_{\epsilon_m} R_{\epsilon_m}^{(2)}(c_L, \xi_c) S_{\epsilon_m}(c_L, \eta_c) \right\}, \quad (3.52) \end{aligned}$$

where $c_R = k_R f_c$, $c_L = k_L f_c$, $C1_{\epsilon_m}$, $C2_{\epsilon_m}$, $D1_{\epsilon_m}$, and $D2_{\epsilon_m}$ are unknown expansion coefficients. The corresponding magnetic field can be written as

$$\begin{aligned}
\vec{H}^2 &= \frac{j}{\sqrt{\mu_2/\epsilon_2}} \left\{ \vec{E}_R^2 - \vec{E}_L^2 \right\} \\
&= \frac{j}{\sqrt{\mu_2/\epsilon_2}} \left\{ \sum_m C1_{\epsilon_m} \left[\vec{M}_m^{(1)}(k_R) + \vec{N}_m^{(1)}(k_R) \right] + \sum_m C2_{\epsilon_m} \left[\vec{M}_m^{(1)}(k_L) - \vec{N}_m^{(1)}(k_L) \right] \right. \\
&\quad \left. + \sum_m D1_{\epsilon_m} \left[\vec{M}_m^{(2)}(k_R) + \vec{N}_m^{(2)}(k_R) \right] + \sum_m D2_{\epsilon_m} \left[\vec{M}_m^{(2)}(k_L) - \vec{N}_m^{(2)}(k_L) \right] \right\} \\
&= \hat{u}_{\xi_c} \frac{j}{h_c \sqrt{\mu_2/\epsilon_2}} \left\{ \frac{1}{k_R} \sum_m C1_{\epsilon_m} R_{\epsilon_m}^{(1)}(c_R, \xi_c) S'_{\epsilon_m}(c_R, \eta_c) + \frac{1}{k_L} \sum_m C2_{\epsilon_m} R_{\epsilon_m}^{(1)}(c_L, \xi_c) S'_{\epsilon_m}(c_L, \eta_c) \right. \\
&\quad \left. + \frac{1}{k_R} \sum_m D1_{\epsilon_m} R_{\epsilon_m}^{(2)}(c_R, \xi_c) S'_{\epsilon_m}(c_R, \eta_c) + \frac{1}{k_L} \sum_m D2_{\epsilon_m} R_{\epsilon_m}^{(2)}(c_L, \xi_c) S'_{\epsilon_m}(c_L, \eta_c) \right\} \\
&\quad - \hat{u}_{\eta_c} \frac{j}{h_c \sqrt{\mu_2/\epsilon_2}} \left\{ \frac{1}{k_R} \sum_m C1_{\epsilon_m} R_{\epsilon_m}^{(1)'}(c_R, \xi_c) S_{\epsilon_m}(c_R, \eta_c) + \frac{1}{k_L} \sum_m C2_{\epsilon_m} R_{\epsilon_m}^{(1)'}(c_L, \xi_c) S_{\epsilon_m}(c_L, \eta_c) \right. \\
&\quad \left. + \frac{1}{k_R} \sum_m D1_{\epsilon_m} R_{\epsilon_m}^{(2)'}(c_R, \xi_c) S_{\epsilon_m}(c_R, \eta_c) + \frac{1}{k_L} \sum_m D2_{\epsilon_m} R_{\epsilon_m}^{(2)'}(c_L, \xi_c) S_{\epsilon_m}(c_L, \eta_c) \right\} \\
&\quad + \hat{u}_{z_c} \frac{j}{\sqrt{\mu_2/\epsilon_2}} \left\{ \sum_m C1_{\epsilon_m} R_{\epsilon_m}^{(1)}(c_R, \xi_c) S_{\epsilon_m}(c_R, \eta_c) - \sum_m C2_{\epsilon_m} R_{\epsilon_m}^{(1)}(c_L, \xi_c) S_{\epsilon_m}(c_L, \eta_c) \right. \\
&\quad \left. + \sum_m D1_{\epsilon_m} R_{\epsilon_m}^{(2)}(c_R, \xi_c) S_{\epsilon_m}(c_R, \eta_c) - \sum_m D2_{\epsilon_m} R_{\epsilon_m}^{(2)}(c_L, \xi_c) S_{\epsilon_m}(c_L, \eta_c) \right\}. \quad (3.53)
\end{aligned}$$

3.3.5 Fields in Region 3 ($\xi > \xi_2$)

The fields in region 3 will have TM_Z and TE_Z components. Therefore, the electric field is expanded as

$$\begin{aligned}
\vec{E}^3 &= \sum_m \left[F1_{\epsilon_m} \vec{M}_m^{(4)}(k_3) + F2_{\epsilon_m} \vec{N}_m^{(4)}(k_3) \right] \\
&= \hat{u}_{\xi} \frac{1}{k_3 h} \sum_m F1_{\epsilon_m} R_{\epsilon_m}^{(4)}(c_3, \xi) S'_{\epsilon_m}(c_3, \eta)
\end{aligned}$$

$$\begin{aligned}
& -\hat{u}_\eta \frac{1}{k_3 h} \sum_m F1_{\epsilon_m} R_{\epsilon_m}^{(4)'}(c_3, \xi) S_{\epsilon_m}(c_3, \eta) \\
& + \hat{u}_z \sum_m F2_{\epsilon_m} R_{\epsilon_m}^{(4)}(c_3, \xi) S_{\epsilon_m}(c_3, \eta),
\end{aligned} \tag{3.54}$$

where $F1_{\epsilon_m}$ and $F2_{\epsilon_m}$ are unknown expansion coefficients. The corresponding magnetic field can be written as

$$\begin{aligned}
\vec{H}^3 &= \frac{j}{\sqrt{\mu_3 / \epsilon_3}} \sum_m \left[F1_{\epsilon_m} \vec{N}_m^{(4)}(k_3) + F2_{\epsilon_m} \vec{M}_m^{(4)}(k_3) \right] \\
&= \hat{u}_\xi \frac{j}{\omega \mu_3 h} \sum_m F2_{\epsilon_m} R_{\epsilon_m}^{(4)}(c_3, \xi) S_{\epsilon_m}'(c_3, \eta) \\
&\quad - \hat{u}_\eta \frac{j}{\omega \mu_3 h} \sum_m F2_{\epsilon_m} R_{\epsilon_m}^{(4)'}(c_3, \xi) S_{\epsilon_m}(c_3, \eta) \\
&\quad + \hat{u}_z \frac{j}{\sqrt{\mu_3 / \epsilon_3}} \sum_m F1_{\epsilon_m} R_{\epsilon_m}^{(4)}(c_3, \xi) S_{\epsilon_m}(c_3, \eta).
\end{aligned} \tag{3.55}$$

3.4 Boundary Conditions

The unknown expansion coefficients, $B1_{\epsilon_m}$, $B2_{\epsilon_m}$, $C1_{\epsilon_m}$, $C2_{\epsilon_m}$, $D1_{\epsilon_m}$, $D2_{\epsilon_m}$, $F1_{\epsilon_m}$, and $F2_{\epsilon_m}$ together with $b1_{\epsilon_m}$ and $b2_{\epsilon_m}$ may be determined by imposing the boundary conditions on the surfaces of slotted and coated cylinders defined by $\xi_c = \xi_1$ and $\xi = \xi_2$. It is known that the tangential components of the electric field across an interface between two media with no impressed magnetic current densities along the boundary of the interface are continuous and they vanish on the perfect conducting surfaces. Also, the tangential components of the magnetic field across an interface between two media, neither of which is a perfect conductor, are continuous [140].

The boundary conditions at $\xi = \xi_2$ can be applied after the transformation of the field components inside the coating (region 2) in terms of the global coordinate system. This can be done using the addition theorem for Mathieu functions [141]-[144], so that components $E_{\eta_c}^2$, $E_{z_c}^2$, $H_{\eta_c}^2$, and $H_{z_c}^2$ in the local coordinate system change to similar components (E_η^2 , E_z^2 , H_η^2 , and H_z^2 , respectively) in the global coordinate system, as

$$E_\eta^2 = \frac{-1}{h} \left\{ \frac{1}{k_R} \sum_m C1_{\epsilon_m} \sum_l \left[WE_{\epsilon_l m} R_{el}^{(1)'}(c_{R2}, \xi) S_{el}(c_{R2}, \eta) + WO_{\epsilon_l m} R_{ol}^{(1)'}(c_{R2}, \xi) S_{ol}(c_{R2}, \eta) \right] \right. \\ \left. - \frac{1}{k_L} \sum_m C2_{\epsilon_m} \sum_l \left[WE_{\epsilon_l m} R_{el}^{(1)'}(c_{L2}, \xi) S_{el}(c_{L2}, \eta) + WO_{\epsilon_l m} R_{ol}^{(1)'}(c_{L2}, \xi) S_{ol}(c_{L2}, \eta) \right] \right. \\ \left. + \frac{1}{k_R} \sum_m D1_{\epsilon_m} \sum_l \left[WE_{\epsilon_l m} R_{el}^{(2)'}(c_{R2}, \xi) S_{el}(c_{R2}, \eta) + WO_{\epsilon_l m} R_{ol}^{(2)'}(c_{R2}, \xi) S_{ol}(c_{R2}, \eta) \right] \right. \\ \left. - \frac{1}{k_L} \sum_m D2_{\epsilon_m} \sum_l \left[WE_{\epsilon_l m} R_{el}^{(2)'}(c_{L2}, \xi) S_{el}(c_{L2}, \eta) + WO_{\epsilon_l m} R_{ol}^{(2)'}(c_{L2}, \xi) S_{ol}(c_{L2}, \eta) \right] \right\}, \quad (3.56)$$

$$E_z^2 = \sum_m C1_{\epsilon_m} \sum_l \left[WE_{\epsilon_l m} R_{el}^{(1)}(c_{R2}, \xi) S_{el}(c_{R2}, \eta) + WO_{\epsilon_l m} R_{ol}^{(1)}(c_{R2}, \xi) S_{ol}(c_{R2}, \eta) \right] \\ + \sum_m C2_{\epsilon_m} \sum_l \left[WE_{\epsilon_l m} R_{el}^{(1)}(c_{L2}, \xi) S_{el}(c_{L2}, \eta) + WO_{\epsilon_l m} R_{ol}^{(1)}(c_{L2}, \xi) S_{ol}(c_{L2}, \eta) \right] \\ + \sum_m D1_{\epsilon_m} \sum_l \left[WE_{\epsilon_l m} R_{el}^{(2)}(c_{R2}, \xi) S_{el}(c_{R2}, \eta) + WO_{\epsilon_l m} R_{ol}^{(2)}(c_{R2}, \xi) S_{ol}(c_{R2}, \eta) \right] \\ + \sum_m D2_{\epsilon_m} \sum_l \left[WE_{\epsilon_l m} R_{el}^{(2)}(c_{L2}, \xi) S_{el}(c_{L2}, \eta) + WO_{\epsilon_l m} R_{ol}^{(2)}(c_{L2}, \xi) S_{ol}(c_{L2}, \eta) \right], \quad (3.57)$$

$$H_\eta^2 = \frac{-j}{h\sqrt{\mu_2/\epsilon_2}} \left\{ \frac{1}{k_R} \sum_m C1_{\epsilon_m} \sum_l \left[WE_{\epsilon_l m} R_{el}^{(1)'}(c_{R2}, \xi) S_{el}(c_{R2}, \eta) \right. \right. \\ \left. \left. + WO_{\epsilon_l m} R_{ol}^{(1)'}(c_{R2}, \xi) S_{ol}(c_{R2}, \eta) \right] \right. \\ \left. + \frac{1}{k_L} \sum_m C2_{\epsilon_m} \sum_l \left[WE_{\epsilon_l m} R_{el}^{(1)'}(c_{L2}, \xi) S_{el}(c_{L2}, \eta) + WO_{\epsilon_l m} R_{ol}^{(1)'}(c_{L2}, \xi) S_{ol}(c_{L2}, \eta) \right] \right\}$$

$$\begin{aligned}
& + \frac{1}{k_R} \sum_m D1_{\epsilon_m} \sum_l \left[WE_{\epsilon_{lm}} R_{el}^{(2)'}(c_{R2}, \xi) S_{el}(c_{R2}, \eta) + WO_{\epsilon_{lm}} R_{ol}^{(2)'}(c_{R2}, \xi) S_{ol}(c_{R2}, \eta) \right] \\
& + \frac{1}{k_L} \sum_m D2_{\epsilon_m} \sum_l \left[WE_{\epsilon_{lm}} R_{el}^{(2)'}(c_{L2}, \xi) S_{el}(c_{L2}, \eta) + WO_{\epsilon_{lm}} R_{ol}^{(2)'}(c_{L2}, \xi) S_{ol}(c_{L2}, \eta) \right] \Bigg\}, \quad (3.58)
\end{aligned}$$

$$\begin{aligned}
H_z^2 = \frac{j}{\sqrt{\mu_2 / \epsilon_2}} & \left\{ \sum_m C1_{\epsilon_m} \sum_l \left[WE_{\epsilon_{lm}} R_{el}^{(1)}(c_{R2}, \xi) S_{el}(c_{R2}, \eta) + WO_{\epsilon_{lm}} R_{ol}^{(1)}(c_{R2}, \xi) S_{ol}(c_{R2}, \eta) \right] \right. \\
& - \sum_m C2_{\epsilon_m} \sum_l \left[WE_{\epsilon_{lm}} R_{el}^{(1)}(c_{L2}, \xi) S_{el}(c_{L2}, \eta) + WO_{\epsilon_{lm}} R_{ol}^{(1)}(c_{L2}, \xi) S_{ol}(c_{L2}, \eta) \right] \\
& + \sum_m D1_{\epsilon_m} \sum_l \left[WE_{\epsilon_{lm}} R_{el}^{(2)}(c_{R2}, \xi) S_{el}(c_{R2}, \eta) + WO_{\epsilon_{lm}} R_{ol}^{(2)}(c_{R2}, \xi) S_{ol}(c_{R2}, \eta) \right] \\
& \left. - \sum_m D2_{\epsilon_m} \sum_l \left[WE_{\epsilon_{lm}} R_{el}^{(2)}(c_{L2}, \xi) S_{el}(c_{L2}, \eta) + WO_{\epsilon_{lm}} R_{ol}^{(2)}(c_{L2}, \xi) S_{ol}(c_{L2}, \eta) \right] \right\}, \quad (3.59)
\end{aligned}$$

where $c_{R2} = k_R f$, $c_{L2} = k_L f$, and the l -summation (Σ) starts from 0 for even type (WE) and from 1 for odd type (WO). Details of WE and WO are given in Appendix A.

Therefore, the boundary conditions at $\xi_c = \xi_1$ are

$$E_{\eta_c}^1 = \begin{cases} E_{\eta_c}^a, & \eta_{c1} < \eta_c < \eta_{c2} \\ 0, & \text{else} \end{cases} \quad (3.60)$$

$$E_{z_c}^{li} + E_{z_c}^1 = \begin{cases} E_{z_c}^a, & \eta_{c1} < \eta_c < \eta_{c2} \\ 0, & \text{else} \end{cases} \quad (3.61)$$

$$E_{\eta_c}^2 = \begin{cases} E_{\eta_c}^a, & \eta_{c1} < \eta_c < \eta_{c2} \\ 0, & \text{else} \end{cases} \quad (3.62)$$

$$E_{z_c}^2 = \begin{cases} E_{z_c}^a, & \eta_{c1} < \eta_c < \eta_{c2} \\ 0, & \text{else} \end{cases} \quad (3.63)$$

$$H_{\eta_c}^{li} + H_{\eta_c}^1 = H_{\eta_c}^2, \quad \eta_{c1} < \eta_c < \eta_{c2} \quad (3.64)$$

$$H_{z_c}^1 = H_{z_c}^2, \quad \eta_{c1} < \eta_c < \eta_{c2} \quad (3.65)$$

and the boundary conditions at $\zeta = \zeta_2$ are

$$E_\eta^2 = E_\eta^3, \quad (3.66)$$

$$E_z^2 = E_z^{3i} + E_z^3, \quad (3.67)$$

$$H_\eta^2 = H_\eta^{3i} + H_\eta^3, \quad (3.68)$$

$$H_z^2 = H_z^3. \quad (3.69)$$

Equations (3.60) – (3.69) are the boundaries conditions in the general case. Depending on the source locating (inside or outside the cylinder), E_z^{3i} (and H_η^{3i}), or E_z^{1i} (and H_η^{1i}), become zero, respectively.

3.5 Finding the Coefficients

To find the unknown expansion coefficients, we substitute the corresponding expressions into (3.60) – (3.69). After substituting, multiply both sides of Equations (3.60) and (3.61) by $S_{\epsilon_n}(c_1, \eta_c)$, multiply both sides of Equations (3.62) and (3.63) by $S_{\epsilon_n}(c_R, \eta_c)$, multiply both sides of Equations (3.64) and (3.65) by $CS_{\epsilon_n}(\eta_c)$, and multiply both sides of Equations (3.66) – (3.69) by $S_{\epsilon_n}(c_{L2}, \eta)$. Then, integrating over the counters and using the orthogonality properties of Mathieu functions, the terms involving even functions decouple completely from those of odd functions, and vice versa. Finally we have

$$B1_{\epsilon_n} = \frac{1}{N_{\epsilon_n}(c_1)J'_{\epsilon_n}(c_1)} \sum_m Q_{\epsilon_{nm}}(c_1) b1_{\epsilon_m}, \quad (3.70)$$

$$\frac{H_{\epsilon_n}(c_1)}{J_{\epsilon_n}(c_1)} A1_{\epsilon_n} + B2_{\epsilon_n} = \frac{1}{N_{\epsilon_n}(c_1)J_{\epsilon_n}(c_1)} \sum_m Q_{\epsilon_{nm}}(c_1) b2_{\epsilon_m}, \quad (3.71)$$

$$\begin{aligned}
& C1_{\epsilon_n} + \frac{K'_{\epsilon_n}(c_R)}{J'_{\epsilon_n}(c_R)} D1_{\epsilon_n} \\
& - \frac{k_R}{k_L} \frac{1}{N_{\epsilon_n}(c_R) J'_{\epsilon_n}(c_R)} \sum_m M_{\epsilon_{nm}}(c_R, c_L) \left\{ J'_{\epsilon_m}(c_L) C2_{\epsilon_m} + K'_{\epsilon_m}(c_L) D2_{\epsilon_m} \right\} \\
& = \frac{k_R}{k_L} \frac{1}{N_{\epsilon_n}(c_R) J'_{\epsilon_n}(c_R)} \sum_m Q_{\epsilon_{nm}}(c_R) b1_{\epsilon_m}, \quad (3.72)
\end{aligned}$$

$$\begin{aligned}
& C1_{\epsilon_n} + \frac{K'_{\epsilon_n}(c_R)}{J'_{\epsilon_n}(c_R)} D1_{\epsilon_n} + \frac{1}{N_{\epsilon_n}(c_R) J'_{\epsilon_n}(c_R)} \sum_m M_{\epsilon_{nm}}(c_R, c_L) \left\{ J'_{\epsilon_m}(c_L) C2_{\epsilon_m} + K'_{\epsilon_m}(c_L) D2_{\epsilon_m} \right\} \\
& = \frac{1}{N_{\epsilon_n}(c_R) J'_{\epsilon_n}(c_R)} \sum_m Q_{\epsilon_{nm}}(c_R) b2_{\epsilon_m}, \quad (3.73)
\end{aligned}$$

$$\begin{aligned}
& \sum_m Q_{\epsilon_{mn}}(c_1) \left\{ H'_{\epsilon_m}(c_1) A1_{\epsilon_m} + J'_{\epsilon_m}(c_1) B2_{\epsilon_m} \right\} \\
& = \frac{\omega\mu_1}{k_R \sqrt{\mu_2 / \epsilon_2}} \sum_m Q_{\epsilon_{mn}}(c_R) \left\{ J'_{\epsilon_m}(c_R) C1_{\epsilon_m} + K'_{\epsilon_m}(c_R) D1_{\epsilon_m} \right\} \\
& + \frac{\omega\mu_1}{k_L \sqrt{\mu_2 / \epsilon_2}} \sum_m Q_{\epsilon_{mn}}(c_L) \left\{ J'_{\epsilon_m}(c_L) C2_{\epsilon_m} + K'_{\epsilon_m}(c_L) D2_{\epsilon_m} \right\}, \quad (3.74)
\end{aligned}$$

$$\begin{aligned}
& \frac{\sqrt{\mu_2 / \epsilon_2}}{\sqrt{\mu_1 / \epsilon_1}} \sum_m Q_{\epsilon_{mn}}(c_1) J'_{\epsilon_m}(c_1) B1_{\epsilon_m} = \sum_m Q_{\epsilon_{mn}}(c_R) \left\{ J'_{\epsilon_m}(c_R) C1_{\epsilon_m} + K'_{\epsilon_m}(c_R) D1_{\epsilon_m} \right\} \\
& - \sum_m Q_{\epsilon_{mn}}(c_L) \left\{ J'_{\epsilon_m}(c_L) C2_{\epsilon_m} + K'_{\epsilon_m}(c_L) D2_{\epsilon_m} \right\}, \quad (3.75)
\end{aligned}$$

$$\begin{aligned}
& \frac{k_L}{k_R} \sum_l M_{\epsilon_{nl}}(c_{L2}, c_{R2}) J'_{\epsilon_l}(c_{R2}) \sum_m \left\{ \begin{bmatrix} WE_{\epsilon_{lm}} \\ WO_{\epsilon_{lm}} \end{bmatrix} C1_{em} + \begin{bmatrix} WE_{\circ_{lm}} \\ WO_{\circ_{lm}} \end{bmatrix} C1_{om} \right\} \\
& - N_{\epsilon_n}(c_{L2}) J'_{\epsilon_n}(c_{L2}) \sum_m \left\{ \begin{bmatrix} WE_{\epsilon_{nm}} \\ WO_{\epsilon_{nm}} \end{bmatrix} C2_{em} + \begin{bmatrix} WE_{\circ_{nm}} \\ WO_{\circ_{nm}} \end{bmatrix} C2_{om} \right\}
\end{aligned}$$

$$\begin{aligned}
& + \frac{k_L}{k_R} \sum_l M_{\epsilon_{nl}}(c_{L2}, c_{R2}) K'_{\epsilon_l}(c_{R2}) \sum_m \left\{ \begin{bmatrix} WE_{\epsilon_{lm}} \\ WO_{\epsilon_{lm}} \end{bmatrix} D1_{em} + \begin{bmatrix} WE_{\circ_{lm}} \\ WO_{\circ_{lm}} \end{bmatrix} D1_{om} \right\} \\
& - N_{\epsilon_n}(c_{L2}) K'_{\epsilon_n}(c_{L2}) \sum_m \left\{ \begin{bmatrix} WE_{\epsilon_{nm}} \\ WO_{\epsilon_{nm}} \end{bmatrix} D2_{em} + \begin{bmatrix} WE_{\circ_{nm}} \\ WO_{\circ_{nm}} \end{bmatrix} D2_{om} \right\} \\
& = \frac{k_L}{k_3} \sum_m M_{\epsilon_{nm}}(c_{L2}, c_3) H'_{\epsilon_m}(c_3) F1_{\epsilon_m}, \tag{3.76}
\end{aligned}$$

$$\begin{aligned}
& \sum_l M_{\epsilon_{nl}}(c_{L2}, c_{R2}) J'_{\epsilon_l}(c_{R2}) \sum_m \left\{ \begin{bmatrix} WE_{\epsilon_{lm}} \\ WO_{\epsilon_{lm}} \end{bmatrix} C1_{em} + \begin{bmatrix} WE_{\circ_{lm}} \\ WO_{\circ_{lm}} \end{bmatrix} C1_{om} \right\} \\
& + N_{\epsilon_n}(c_{L2}) J'_{\epsilon_n}(c_{L2}) \sum_m \left\{ \begin{bmatrix} WE_{\epsilon_{nm}} \\ WO_{\epsilon_{nm}} \end{bmatrix} C2_{em} + \begin{bmatrix} WE_{\circ_{nm}} \\ WO_{\circ_{nm}} \end{bmatrix} C2_{om} \right\} \\
& + \sum_l M_{\epsilon_{nl}}(c_{L2}, c_{R2}) K'_{\epsilon_l}(c_{R2}) \sum_m \left\{ \begin{bmatrix} WE_{\epsilon_{lm}} \\ WO_{\epsilon_{lm}} \end{bmatrix} D1_{em} + \begin{bmatrix} WE_{\circ_{lm}} \\ WO_{\circ_{lm}} \end{bmatrix} D1_{om} \right\} \\
& + N_{\epsilon_n}(c_{L2}) K'_{\epsilon_n}(c_{L2}) \sum_m \left\{ \begin{bmatrix} WE_{\epsilon_{nm}} \\ WO_{\epsilon_{nm}} \end{bmatrix} D2_{em} + \begin{bmatrix} WE_{\circ_{nm}} \\ WO_{\circ_{nm}} \end{bmatrix} D2_{om} \right\} \\
& = \sum_m M_{\epsilon_{nm}}(c_{L2}, c_3) \left\{ J'_{\epsilon_m}(c_3) A3_{\epsilon_m} + H'_{\epsilon_m}(c_3) F2_{\epsilon_m} \right\}, \tag{3.77}
\end{aligned}$$

$$\begin{aligned}
& \frac{k_L}{k_R} \sum_l M_{\epsilon_{nl}}(c_{L2}, c_{R2}) J'_{\epsilon_l}(c_{R2}) \sum_m \left\{ \begin{bmatrix} WE_{\epsilon_{lm}} \\ WO_{\epsilon_{lm}} \end{bmatrix} C1_{em} + \begin{bmatrix} WE_{\circ_{lm}} \\ WO_{\circ_{lm}} \end{bmatrix} C1_{om} \right\} \\
& + N_{\epsilon_n}(c_{L2}) J'_{\epsilon_n}(c_{L2}) \sum_m \left\{ \begin{bmatrix} WE_{\epsilon_{nm}} \\ WO_{\epsilon_{nm}} \end{bmatrix} C2_{em} + \begin{bmatrix} WE_{\circ_{nm}} \\ WO_{\circ_{nm}} \end{bmatrix} C2_{om} \right\} \\
& + \frac{k_L}{k_R} \sum_l M_{\epsilon_{nl}}(c_{L2}, c_{R2}) K'_{\epsilon_l}(c_{R2}) \sum_m \left\{ \begin{bmatrix} WE_{\epsilon_{lm}} \\ WO_{\epsilon_{lm}} \end{bmatrix} D1_{em} + \begin{bmatrix} WE_{\circ_{lm}} \\ WO_{\circ_{lm}} \end{bmatrix} D1_{om} \right\}
\end{aligned}$$

$$\begin{aligned}
& + N_{\epsilon_n}(c_{L2})K'_{\epsilon_n}(c_{L2})\sum_m \left\{ \begin{bmatrix} WE_{\epsilon_{nm}} \\ WO_{\epsilon_{nm}} \end{bmatrix} D2_{em} + \begin{bmatrix} WE_{\circ_{nm}} \\ WO_{\circ_{nm}} \end{bmatrix} D2_{om} \right\} \\
& = \frac{k_L \sqrt{\mu_2 / \epsilon_2}}{\omega \mu_3} \sum_m M_{\epsilon_{nm}}(c_{L2}, c_3) \left\{ J'_{\epsilon_m}(c_3) A3_{\epsilon_m} + H'_{\epsilon_m}(c_3) F2_{\epsilon_m} \right\}, \quad (3.78)
\end{aligned}$$

$$\begin{aligned}
& \sum_l M_{\epsilon_{nl}}(c_{L2}, c_{R2}) J_{\epsilon_l}(c_{R2}) \sum_m \left\{ \begin{bmatrix} WE_{\epsilon_{lm}} \\ WO_{\epsilon_{lm}} \end{bmatrix} C1_{em} + \begin{bmatrix} WE_{\circ_{lm}} \\ WO_{\circ_{lm}} \end{bmatrix} C1_{om} \right\} \\
& - N_{\epsilon_n}(c_{L2}) J_{\epsilon_n}(c_{L2}) \sum_m \left\{ \begin{bmatrix} WE_{\epsilon_{nm}} \\ WO_{\epsilon_{nm}} \end{bmatrix} C2_{em} + \begin{bmatrix} WE_{\circ_{nm}} \\ WO_{\circ_{nm}} \end{bmatrix} C2_{om} \right\} \\
& + \sum_l M_{\epsilon_{nl}}(c_{L2}, c_{R2}) K_{\epsilon_l}(c_{R2}) \sum_m \left\{ \begin{bmatrix} WE_{\epsilon_{lm}} \\ WO_{\epsilon_{lm}} \end{bmatrix} D1_{em} + \begin{bmatrix} WE_{\circ_{lm}} \\ WO_{\circ_{lm}} \end{bmatrix} D1_{om} \right\} \\
& - N_{\epsilon_n}(c_{L2}) K_{\epsilon_n}(c_{L2}) \sum_m \left\{ \begin{bmatrix} WE_{\epsilon_{nm}} \\ WO_{\epsilon_{nm}} \end{bmatrix} D2_{em} + \begin{bmatrix} WE_{\circ_{nm}} \\ WO_{\circ_{nm}} \end{bmatrix} D2_{om} \right\} \\
& = \frac{\sqrt{\mu_2 / \epsilon_2}}{\sqrt{\mu_3 / \epsilon_3}} \sum_m M_{\epsilon_{nm}}(c_{L2}, c_3) H_{\epsilon_m}(c_3) F1_{\epsilon_m}, \quad (3.79)
\end{aligned}$$

where

$$J_{\epsilon_n}(c_i) = R_{\epsilon_n}^{(1)}(c_i, \xi_j), \quad (3.80)$$

$$K_{\epsilon_n}(c_i) = R_{\epsilon_n}^{(2)}(c_i, \xi_j), \quad (3.81)$$

$$H_{\epsilon_n}(c_i) = R_{\epsilon_n}^{(4)}(c_i, \xi_j), \quad (3.82)$$

$$Q_{\epsilon_{nm}}(c_l) = \int_{\eta_{c1}}^{\eta_{c2}} S_{\epsilon_n}(c_l, \eta_c) C S_{\epsilon_m}(\eta_c) d\eta_c, \quad (3.83)$$

$$M_{\epsilon_{nm}}(c_i, c_j) = \int_0^{2\pi} S_{\epsilon_n}(c_i, \eta^+) S_{\epsilon_m}(c_j, \eta^+) d\eta^+. \quad (3.84)$$

In Equations (3.80) – (3.82), $j = 1$ if $i = 1, R, L$, and $j = 2$ if $i = R2, L2, 3$. In Equation (3.84), $\eta^+ = \eta_c$ if $\xi_c = \xi_1$, and $\eta^+ = \eta$ if $\xi = \xi_2$.

The unknown expansion coefficients can be found by solving the system of linear equations (3.70) – (3.79). After solving the matrix forms, the expansion coefficients are given as follows,

$$B1_e = G2_e b1_e, \quad (3.85)$$

$$B2_e = -G3_e A1_e + G5_e b2_e, \quad (3.86)$$

$$b1_e = T130 A1_e + T131 A1_o + T132 A3_e + T133 A3_o + T134 b1_o, \quad (3.87)$$

$$b1_o = T143 A1_e + T144 A1_o + T145 A3_e + T146 A3_o, \quad (3.88)$$

$$b2_e = T104 A1_e + T105 A3_e + T106 A3_o + T107 b1_e + T108 b1_o + T109 b2_o, \quad (3.89)$$

$$b2_o = T116 A1_e + T117 A1_o + T118 A3_e + T119 A3_o + T120 b1_e + T121 b1_o, \quad (3.90)$$

$$C1_e = G10_e b1_e + G8_e C2_e - G7_e D1_e + G9_e D2_e, \quad (3.91)$$

$$C2_e = -T12 b1_e - T13 b1_o + T14 C2_o + T15 D1_e + T16 D1_o + T17 D2_e + T18 D2_o, \quad (3.92)$$

$$C2_o = T31 b1_e + T32 b1_o + T33 D1_e + T34 D1_o + T35 D2_e + T36 D2_o, \quad (3.93)$$

$$D1_e = T82 A3_e - T83 A3_o + T84 b1_e + T85 b1_o + T86 b2_e - T87 D1_o, \quad (3.94)$$

$$D1_o = T92 A3_e + T93 A3_o - T94 b1_e - T95 b1_o - T96 b2_e + T97 b2_o, \quad (3.95)$$

$$D2_e = T51 A3_e + T52 b1_e + T53 b1_o + T54 D1_e + T55 D1_o + T56 D2_o, \quad (3.96)$$

$$D2_o = -T72 A3_e + T73 A3_o + T74 b1_e + T75 b1_o + T76 D1_e + T77 D1_o, \quad (3.97)$$

$$F1_e = T1 C1_e + T2 C1_o - T3 C2_e - T4 C2_o + T5 D1_e + T6 D1_o - T7 D2_e - T8 D2_o, \quad (3.98)$$

$$F1_o = T19 C1_e + T20 C1_o - T21 C2_e - T22 C2_o \\ + T23 D1_e + T24 D1_o - T25 D2_e - T26 D2_o, \quad (3.99)$$

$$\begin{aligned}
F2_e = & -T37 A3_e + T38 C1_e + T39 C1_o + T40 C2_e + T41 C2_o \\
& + T42 D1_e + T43 D1_o + T44 D2_e + T45 D2_o, \quad (3.100)
\end{aligned}$$

$$\begin{aligned}
F2_o = & -T57 A3_o + T58 C1_e + T59 C1_o + T60 C2_e + T61 C2_o \\
& + T62 D1_e + T63 D1_o + T64 D2_e + T65 D2_o, \quad (3.101)
\end{aligned}$$

where matrices $T1$ through $T146$ are combinations of the matrices $G1$ through $G48$. The matrices $G1$ through $G48$ are given in Appendix *B*, and matrices $T1$ through $T146$ are given in Appendix *C*.

3.6 Far Zone Fields

After finding the unknown expansion coefficients, the different antenna parameters such as the antenna gain, aperture conductance, and the aperture voltage can be calculated. Due to chiral media, there are two (co- and cross-) polarized waves everywhere.

The asymptotic form for the forth kind of the radial Mathieu function is given by [145]

$$\begin{aligned}
R_{\circ m}^{(4)}(c, \cosh \xi) &= R_{\circ m}^{(1)}(c, \cosh \xi) - jR_{\circ m}^{(2)}(c, \cosh \xi) \\
&\stackrel{\xi \rightarrow \infty}{\cong} \frac{1}{\sqrt{c \cosh \xi}} \left\{ \cos \left[c \cosh \xi - \frac{\pi}{2}(M + 1/2) \right] \right. \\
&\quad \left. - j \sin \left[c \cosh \xi - \frac{\pi}{2}(M + 1/2) \right] \right\} \\
&= \frac{1}{\sqrt{k\rho}} e^{-jk\rho} e^{j\frac{\pi}{2}(M+1/2)}
\end{aligned}$$

$$= \sqrt{\frac{j}{k\rho}} j^m e^{-jk\rho}, \quad (3.102)$$

where $M = 2m$ for even orders, $M = 2m + 1$ for odd orders, $\rho \underset{\xi \rightarrow \infty}{\cong} f \cosh \xi$, and

$$k\rho \underset{\xi \rightarrow \infty}{\cong} kf \cosh \xi = c \cosh \xi. \quad (3.103)$$

From (3.54) and (3.102), the far zone co-polarized electric field is

$$E_z^3(\rho, \phi) = \sqrt{\frac{j}{k_3\rho}} e^{-jk_3\rho} \sum_m j^m F2_{\epsilon_m} S_{\epsilon_m}(c_3, \cos \phi), \quad (3.104)$$

where ρ and ϕ denote the polar coordinates in the circular cylindrical coordinate system.

For the far zone cross-polarized electric field, the asymptotic expansion of derivative of modified Mathieu function is needed. Using the asymptotic expansion of the fourth kind of the radial Mathieu function (Equation (3.102)), we have

$$\begin{aligned} R_{\epsilon_m}^{(4)'}(c, \cosh \xi) &= \frac{dR_{\epsilon_m}^{(4)}(c, \cosh \xi)}{d\rho} \cdot \frac{d\rho}{d\xi} \\ &\underset{\xi \rightarrow \infty}{\cong} -\sqrt{\frac{j}{k}} \frac{j^m e^{-jk\rho}}{\rho} \left(jk\sqrt{\rho} + \frac{1}{2\sqrt{\rho}} \right) \cdot f \sinh \xi \\ &\underset{\xi \rightarrow \infty}{\cong} -\sqrt{\frac{jk}{\rho}} j^{m+1} e^{-jk\rho} \cdot f \sinh \xi. \end{aligned} \quad (3.105)$$

From (3.54) and (3.105) we have

$$E_\eta^3(\rho, \phi) = -\sqrt{\frac{jk_3}{\rho}} \frac{f \sinh \xi}{k_3 h} e^{-jk_3\rho} \sum_m j^{m+1} F1_{\epsilon_m} S_{\epsilon_m}(c_3, \cos \phi), \quad (3.106)$$

where the scale factor h is given in Equation (3.6) as

$$\begin{aligned} h &= f \sqrt{\cosh^2 \xi - \cos^2 \eta} \\ &\underset{\xi \rightarrow \infty}{\cong} f \cosh \xi \end{aligned}$$

$$\underset{\xi \rightarrow \infty}{\cong} f \sinh \xi. \quad (3.107)$$

Substituting Equation (3.107) into (3.106), the far zone cross-polarized electric field can be written as

$$E_{\eta}^3(\rho, \phi) = -\sqrt{\frac{j}{k_3 \rho}} e^{-jk_3 \rho} \sum_m j^{m+1} F1_{\epsilon_m} S_{\epsilon_m}(c_3, \cos \phi). \quad (3.108)$$

The time-average power density in the far zone co-polarized field is

$$S(\rho, \phi) = \frac{1}{\sqrt{\mu_3 / \epsilon_3} k_3 \rho} \left| \sum_m j^m F2_{\epsilon_m} S_{\epsilon_m}(c_3, \cos \phi) \right|^2. \quad (3.109)$$

The average power density of $S(\rho, \phi)$ over an imaginary cylindrical surface with radius ρ can be written

$$\begin{aligned} S_{av}(\rho) &= \frac{1}{2\pi} \int_0^{2\pi} S(\rho, \phi) d\phi \\ &= \frac{1}{2\pi \sqrt{\mu_3 / \epsilon_3} k_3 \rho} \sum_m \left| F2_{\epsilon_m} \right|^2 N_{\epsilon_m}(c_3). \end{aligned} \quad (3.110)$$

Using Equation (3.108), the corresponding power equations for cross-polarized field, similar to (3.109) and (3.110) can be found. The antenna gain is given by

$$G(\phi) = S(\rho, \phi) / S_{av}(\rho). \quad (3.111)$$

The radiated time-average power through an imaginary cylindrical surface with length L and radius ρ is given by [11]

$$\begin{aligned} W &= 2\pi\rho LS_{av}(\rho) \\ &= |V|^2 G_a L, \end{aligned} \quad (3.112)$$

where V denotes the aperture voltage,

$$V = \int \vec{E} \cdot \vec{dl}, \quad (3.113)$$

and G_a denotes the aperture conductance per unit length,

$$G_a = 2\pi\rho S_{av}(\rho)/|V|^2. \quad (3.114)$$

Equations (3.112) – (3.114) are given in general forms. However, using Equations (3.48) and (3.113), the aperture voltage due to co-polarized aperture field can be calculated by

$$V|_{co} = \int \int_{\eta_{c1}}^{\eta_{c2}} E_{z_c}^a(\eta_c) d\eta_c dl. \quad (3.115)$$

Considering the aperture voltage per unit length, Equation (3.115) reduces to

$$V|_{co} = \int_{\eta_{c1}}^{\eta_{c2}} E_{z_c}^a(\eta_c) d\eta_c. \quad (3.116)$$

Similarly, using Equation (3.47) and (3.113), the aperture voltage due to cross-polarized aperture field can be calculated by

$$\begin{aligned} V|_{cross} &= \int \int_{\eta_{c1}}^{\eta_{c2}} E_{\eta_c}^a(\eta_c) d\eta_c dl \\ &= r(\eta_{c2} - \eta_{c1}) \int_{\eta_{c1}}^{\eta_{c2}} E_{\eta_c}^a(\eta_c) d\eta_c, \end{aligned} \quad (3.117)$$

where r is the average radius of the arc which is made by aperture on conducting cylinder surface, and $(\eta_{c2} - \eta_{c1})$ is aperture width (in radian). Substituting Equations (3.116) and (3.117) into (3.114), the aperture conductance due to co- and cross-polarized aperture fields can be obtained, respectively.

3.7 Formulation for the TE Case

The same procedure of Section 3.3 can be used to express eigenfunction expansions for the TE case. However, the boundary conditions at $\zeta_c = \zeta_1$ for TE case will change as follows,

$$H_{\eta_c}^1 = H_{\eta_c}^a, \quad \eta_{c1} < \eta_c < \eta_{c2} \quad (3.118)$$

$$H_{z_c}^{1i} + H_{z_c}^1 = H_{z_c}^a, \quad \eta_{c1} < \eta_c < \eta_{c2}, \quad (3.119)$$

$$H_{\eta_c}^2 = H_{\eta_c}^a, \quad \eta_{c1} < \eta_c < \eta_{c2} \quad (3.120)$$

$$H_{z_c}^2 = H_{z_c}^a, \quad \eta_{c1} < \eta_c < \eta_{c2} \quad (3.121)$$

$$E_{\eta_c}^{1i} + E_{\eta_c}^1 = E_{\eta_c}^2, \quad (3.122)$$

$$E_{z_c}^1 = E_{z_c}^2. \quad (3.123)$$

The boundary conditions at $\zeta = \zeta_2$ for TE case are similar to the boundary conditions for TM case which are given in Equations (3.65) – (3.68), except E (electric field) should be changed to H (magnetic field), and vice versa.

To find the unknown expansion coefficients for the TE case we have to substitute the corresponding expressions into (3.118) – (3.123) and into the equations which are similar to (3.66) – (3.69), and use the same method of Section 3.5. Therefore, for (3.118) – (3.123), after substituting the corresponding expressions, we multiply both sides of (3.118) – (3.121) by $CS_{\epsilon_n}(\eta_c)$, and multiply both sides of (3.122) and (3.123) by $S_{\epsilon_n}(c_1, \eta_c)$. Then, integrating over the counters and using the orthogonality properties of Mathieu functions, the terms involving even functions decouple completely from those of odd functions, and vice versa. Finally we have

$$\sum_m Q_{\epsilon_{mn}}(c_1) J'_{\epsilon_m}(c_1) B1_{\epsilon_m} = \sum_n Q1_{\epsilon_{mn}} b1_{\epsilon_n}, \quad (3.124)$$

$$\sum_m Q_{\epsilon_{mn}}(c_1) \{ H_{\epsilon_m}(c_1) A1_{\epsilon_m} + J_{\epsilon_m}(c_1) B2_{\epsilon_m} \} = \sum_n Q1_{\epsilon_{mn}} b2_{\epsilon_n}, \quad (3.125)$$

$$\frac{k_1}{k_R} \sum_m Q_{\epsilon_{mn}}(c_R) \{ J'_{\epsilon_m}(c_R) C1_{\epsilon_m} + K'_{\epsilon_m}(c_R) D1_{\epsilon_m} \}$$

$$-\frac{k_1}{k_L} \sum_m Q_{\epsilon_m n}^{\epsilon_m} (c_L) \left\{ J_{\epsilon_m}^{\epsilon_m} (c_L) C 2_{\epsilon_m} + K_{\epsilon_m}^{\epsilon_m} (c_L) D 2_{\epsilon_m} \right\} = \sum_n Q 1_{\epsilon_m n}^{\epsilon_m} b 1_{\epsilon_n}, \quad (3.126)$$

$$\begin{aligned} & \sum_m Q_{\epsilon_m n}^{\epsilon_m} (c_R) \left\{ J_{\epsilon_m}^{\epsilon_m} (c_R) C 1_{\epsilon_m} + K_{\epsilon_m}^{\epsilon_m} (c_R) D 1_{\epsilon_m} \right\} \\ & + \sum_m Q_{\epsilon_m n}^{\epsilon_m} (c_L) \left\{ J_{\epsilon_m}^{\epsilon_m} (c_L) C 2_{\epsilon_m} + K_{\epsilon_m}^{\epsilon_m} (c_L) D 2_{\epsilon_m} \right\} = \sum_n Q 1_{\epsilon_m n}^{\epsilon_m} b 2_{\epsilon_n}, \end{aligned} \quad (3.127)$$

$$\begin{aligned} & \frac{H_{\epsilon_n}^{\epsilon_n} (c_1)}{J_{\epsilon_n}^{\epsilon_n} (c_1)} A 1_{\epsilon_n} + B 2_{\epsilon_n} \\ & = \frac{\omega \epsilon_1 \sqrt{\mu_2 / \epsilon_2}}{k_R N_{\epsilon_n}^{\epsilon_n} (c_1) J_{\epsilon_n}^{\epsilon_n} (c_1)} \sum_m M_{\epsilon_n m}^{\epsilon_n} (c_1, c_R) \left\{ J_{\epsilon_m}^{\epsilon_m} (c_R) C 1_{\epsilon_m} + K_{\epsilon_m}^{\epsilon_m} (c_R) D 1_{\epsilon_m} \right\} \\ & + \frac{\omega \epsilon_1 \sqrt{\mu_2 / \epsilon_2}}{k_L N_{\epsilon_n}^{\epsilon_n} (c_1) J_{\epsilon_n}^{\epsilon_n} (c_1)} \sum_m M_{\epsilon_n m}^{\epsilon_n} (c_1, c_L) \left\{ J_{\epsilon_m}^{\epsilon_m} (c_L) C 2_{\epsilon_m} + K_{\epsilon_m}^{\epsilon_m} (c_L) D 2_{\epsilon_m} \right\}, \end{aligned} \quad (3.128)$$

$$\begin{aligned} B 1_{\epsilon_n} & = \frac{\sqrt{\mu_2 / \epsilon_2}}{\sqrt{\mu_1 / \epsilon_1}} \frac{1}{N_{\epsilon_n}^{\epsilon_n} (c_1) J_{\epsilon_n}^{\epsilon_n} (c_1)} \sum_m M_{\epsilon_n m}^{\epsilon_n} (c_1, c_R) \left\{ J_{\epsilon_m}^{\epsilon_m} (c_R) C 1_{\epsilon_m} + K_{\epsilon_m}^{\epsilon_m} (c_R) D 1_{\epsilon_m} \right\} \\ & - \frac{\sqrt{\mu_2 / \epsilon_2}}{\sqrt{\mu_1 / \epsilon_1}} \frac{1}{N_{\epsilon_n}^{\epsilon_n} (c_1) J_{\epsilon_n}^{\epsilon_n} (c_1)} \sum_m M_{\epsilon_n m}^{\epsilon_n} (c_1, c_L) \left\{ J_{\epsilon_m}^{\epsilon_m} (c_L) C 2_{\epsilon_m} + K_{\epsilon_m}^{\epsilon_m} (c_L) D 2_{\epsilon_m} \right\}, \end{aligned} \quad (3.129)$$

where

$$Q 1_{\epsilon_m n}^{\epsilon_m} = \int_{\eta_{c1}}^{\eta_{c2}} C S_{\epsilon_m}^{\epsilon_m} (\eta_c) C S_{\epsilon_n}^{\epsilon_n} (\eta_c) d\eta_c. \quad (3.130)$$

The unknown expansion coefficients for the TE case can be found by solving the system of linear equations (3.124) – (3.129), and a system similar to (3.76) – (3.79). After solving the matrix forms, the expansion coefficients for the TE case are given as follows,

$$B 1_{\epsilon} = T 1_{\epsilon} b 1_{\epsilon}, \quad (3.131)$$

$$B 2_{\epsilon} = -T 2_{\epsilon} A 1_{\epsilon} + T 3_{\epsilon} b 2_{\epsilon}, \quad (3.132)$$

$$b 1_{\epsilon} = T 142 A 1_{\epsilon} + T 143 A 1_{\epsilon} + T 144 A 3_{\epsilon} + T 145 A 3_{\epsilon} + T 146 b 1_{\epsilon}, \quad (3.133)$$

$$b1_o = T155 A1_e + T156 A1_o + T157 A3_e + T158 A3_o, \quad (3.134)$$

$$b2_e = T115 A1_e + T116 A1_o + T117 A3_e + T118 A3_o \\ + T119 B1_e + T120 B1_o - T121 b2_o, \quad (3.135)$$

$$b2_o = T128 A1_e + T129 A1_o + T130 A3_e + T131 A3_o + T132 B1_e + T133 B1_o, \quad (3.136)$$

$$C1_e = T4_e B1_e + T5_e C2_e - T6_e D1_e + T7_e D2_e, \quad (3.137)$$

$$C2_e = -T19 B1_e - T20 B1_o + T21 C2_o \\ + T22 D1_e + T23 D1_o + T24 D2_e + T25 D2_o, \quad (3.138)$$

$$C2_o = T38 B1_e + T39 B1_o + T40 D1_e + T41 D1_o + T42 D2_e + T43 D2_o, \quad (3.139)$$

$$D1_e = -T89 A1_e + T90 A3_e + T91 A3_o + T92 B1_e + T93 B1_o - T94 B2_e + T95 D1_o, \quad (3.140)$$

$$D1_o = -T100 A1_e - T101 A1_o + T102 A3_e + T103 A3_o \\ + T104 B1_e + T105 B1_o - T106 B2_e - T107 B2_o, \quad (3.141)$$

$$D2_e = T58 A3_e + T59 B1_e + T60 B1_o + T61 D1_e + T62 D1_o + T63 D2_o, \quad (3.142)$$

$$D2_o = -T79 A3_e + T80 A3_o + T81 B1_e + T82 B1_o + T83 D1_e + T84 D1_o, \quad (3.143)$$

$$F1_e = T8 C1_e + T9 C1_o - T10 C2_e - T11 C2_o \\ + T12 D1_e + T13 D1_o - T14 D2_e - T15 D2_o, \quad (3.144)$$

$$F1_o = T26 C1_e + T27 C1_o - T28 C2_e - T29 C2_o \\ + T30 D1_e + T31 D1_o - T32 D2_e - T33 D2_o, \quad (3.145)$$

$$F2_e = -T44 A3_e + T45 C1_e + T46 C1_o + T47 C2_e + T48 C2_o \\ + T49 D1_e + T50 D1_o + T51 D2_e + T52 D2_o, \quad (3.146)$$

$$F2_o = -T64 A3_o + T65 C1_e + T66 C1_o + T67 C2_e + T68 C2_o$$

$$+T69D1_e + T70D1_o + T71D2_e + T72D2_o, \quad (3.147)$$

where matrices $T1$ through $T158$ are combinations of the matrices $G1$ through $G48$. The matrices $G1$ through $G48$ are given in Appendix D , and matrices $T1$ through $T158$ are given in Appendix E .

After finding the unknown expansion coefficients, the required quantities for the TE case can be calculated using similar method to that of Section 3.6.

4. Transmitting and Receiving Characteristics of Elliptic Slot Antennas

In this chapter selected numerical results are presented and discussed for a variety of geometrical and material parameters. The numerical results of the antenna gain, aperture conductance, and aperture voltage are generated for both TM and TE cases, and for co- and cross-polarized waves. In each case, the infinite series is terminated to include only N terms of both the even and odd functions, where N , in general, is a suitable truncation number proportional to the structure's electrical size and shape. The infinite series of aperture fields is terminated to include only M terms of both the even and odd functions, where M is a suitable truncation number proportional to the structure's electrical size and aperture width.

Accuracy of the characteristic values and convergence of the Fourier coefficients are very important for numerical values of the Mathieu functions. The designated software program for this purpose is able to control the accuracy of computations though several internal checks the computed functions.

Details of the geometrical and material parameters, as well as, a symbol which is showing the situation of nonconfocal cylinders are given on the some figures of this chapter. The geometrical parameters and cylinders situations are based on the geometry which is analyzed and discussed in Chapter 3. For convenience, the details of each example can be compared to the general geometry which is shown in Figure 4.1.

4.1 Validation

Although the designated software program is internally able to control the accuracy of computations, more validation of the theoretical formulations and accuracy of the software program, is investigated.

4.1.1 Validation: Analytical Closed Form Solutions

Use of the other available solutions is one of the ways for checking the overall accuracy of the formulated solution and its associated software. In this section, some numerical results in special cases are generated and compared to the results which are analytically generated by other researchers.

As the first example, consider an electrically very small core cylinder with full slot ($\eta_{c2} - \eta_{c1} = 360^\circ$) coated by a chiral media. The scattered field from this cylinder should be the same as the scattered field from a pure chiral cylinder. Figure 4.2 shows the co- and cross-polarized scattering echo widths for a very small core cylinder coated by a nonconfocal chiral media. Inside the slotted cylinder is a dielectric with the same permeability and permittivity of the coated chiral media. The source is a TM polarized plane wave with incident angle $\phi^i = 180^\circ$. Other parameters are given on the figure. These results are in excellent agreement with the results given in [120] and [128] for scattering echo widths due to a circular chiral cylinder.

Many other checks were also done by considering the fact that the scattered field from a conducting elliptic cylinder with very narrow slot ($\eta_{c2} - \eta_{c1} \approx 0^\circ$) should be the same as the scattered field from a conducting elliptic cylinder without slot. In all considered cases with different geometrical and material parameters for TM and TE

polarized waves, the calculated scattered fields from a narrow slotted cylinder coated by a confocal dielectric were completely agreement with the results given in [146] for the scattering echo widths due to a conducting elliptic cylinder coated by a confocal dielectric.

Furthermore, as a second verification example, Figure 4.3 shows the scattering echo widths from a narrow slotted elliptic cylinder coated by a nonconfocal dielectric. The source is a TM polarized plane wave with incident angles $\phi^i = 0^\circ$ and 90° . Other parameters are given on the figure. These results are very good agreement with the results given in [142] for scattering echo widths from a conducting elliptic cylinder coated by a nonconfocal dielectric.

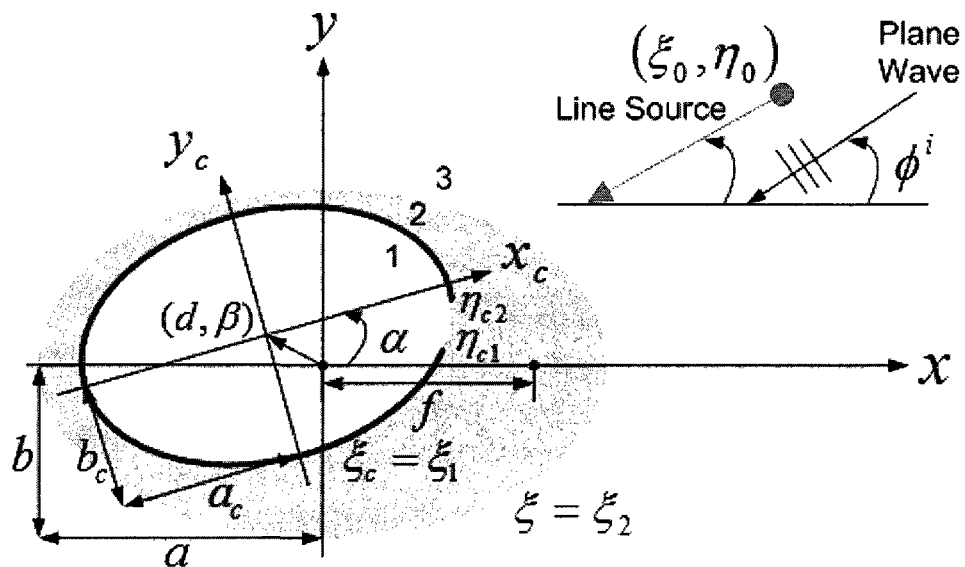


Figure 4.1 – General Geometry of slotted elliptic cylinder coated by a nonconfocal material.

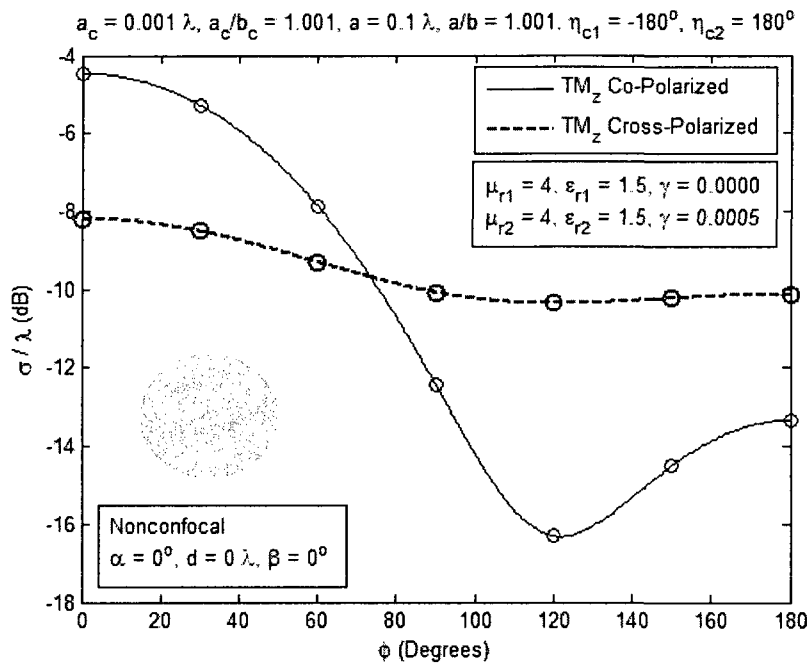


Figure 4.2 – Scattering by a chiral cylinder. The curves with ‘O O O’ are the results given in [120] and [128].

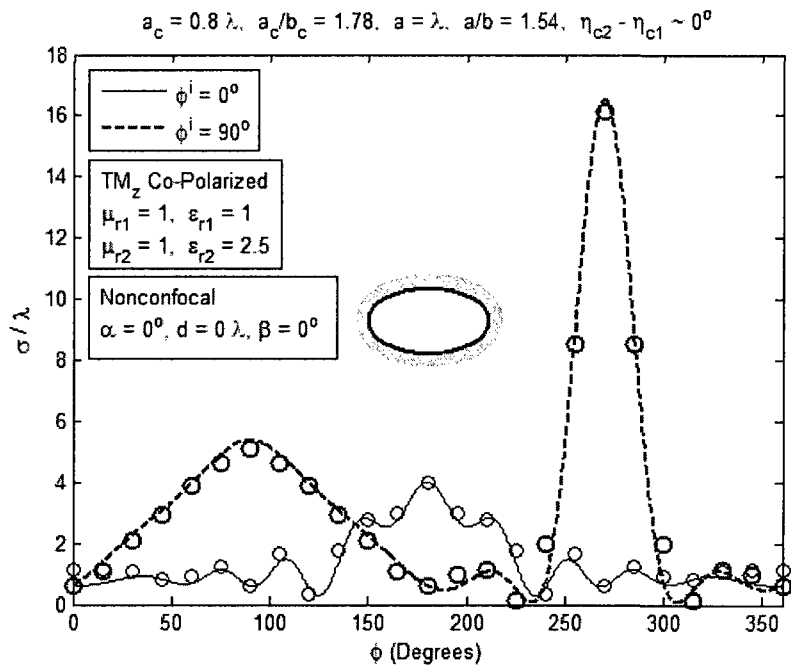


Figure 4.3 – Scattering by a very narrow slotted elliptic cylinder coated by a nonconfocal dielectric. The curves with ‘O O O’ are the results given in [142].

4.1.2 Validation: Simulation

Simulation is the other way that can be used for verification of the validation. In this section, we consider a slotted conducting elliptic cylinder with semi-major axis $a_c = \lambda/3$, axial ratio $a_c/b_c = 2$, and slot angle width 20° ($\eta_{c1} = -10^\circ$ and $\eta_{c2} = 10^\circ$). This cylinder coated by a nonconfocal material with semi-major axis $a = 1.4 a_c$ and axial ratio $a/b = 1.4$. The distance between the center of core cylinder (origin of the local coordinate system) and the center of coated cylinder (origin of the global coordinate system), $d = 0.13 \lambda$. An electric line source is located inside the core cylinder at $\rho = 0.13 \lambda$ and $\phi^i = 0^\circ$ (the center of coated cylinder). Figure 4.4 shows the simulated model of this geometry by HFSS (high frequency structure simulator) software.

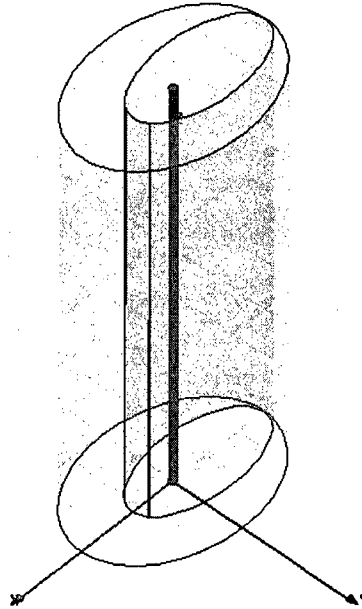


Figure 4.4 – The HFSS model of a slotted conducting elliptic cylinder coated by a nonconfocal material.

Figures 4.5 and 4.6 show the numerical results which are analytically generated and compared to the results which are simulated by HFSS. Inside the conducting cylinders are free space and other parameters are given on the figures. In analytical solution the length of cylinders and line source are assumed to be infinite long, while in HFSS they are limited (i.e., five times of λ). The normalized radiation patterns from the slotted conducting elliptic cylinders coated by nonconfocal dielectric and isorefractive materials are shown in Figures 4.5 and 4.6, respectively. In both figures the analytical generated results are very good agreement with the simulated results.

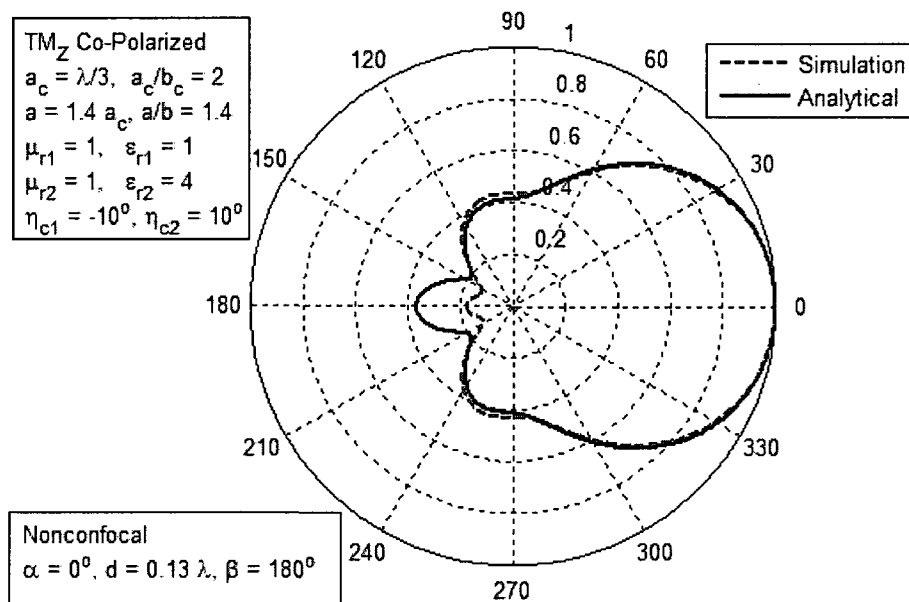


Figure 4.5 – Normalized radiation patterns from a slotted conducting elliptic cylinder coated by a dielectric.

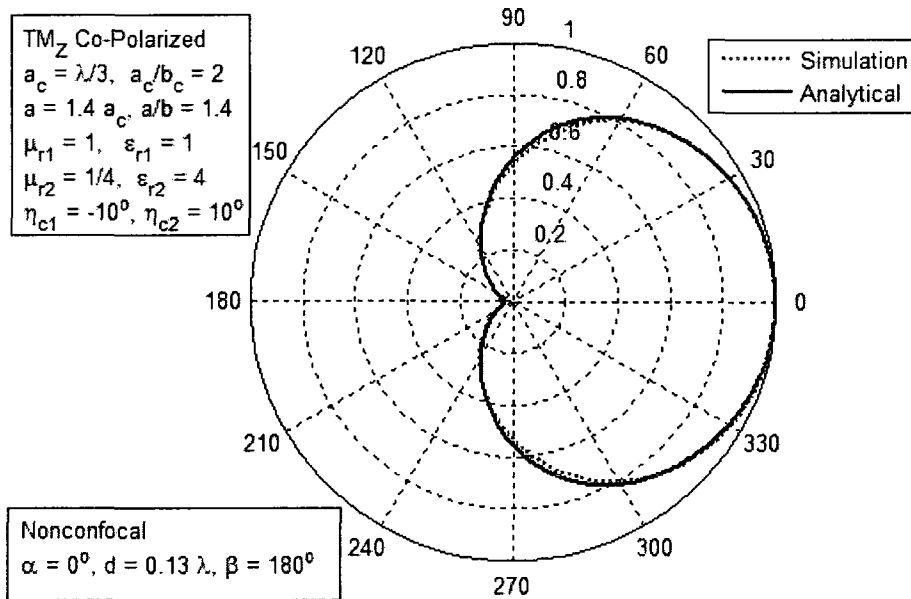


Figure 4.6 – Normalized radiation patterns from a slotted conducting elliptic cylinder coated by an isorefractive material.

4.2 Effect of Geometrical and Material Parameters

In this section, we consider the cases which are the main purpose of this thesis. The effects of geometrical and material parameters on antenna gain, aperture conductance, and aperture voltage are presented and discussed in the following numerical results. More details of geometrical and material parameters are given on the figures.

4.2.1 Antenna Gain

A useful quantity describing the performance of an antenna is the gain. Gain of an antenna is defined as the ratio of the radiation intensity in a given direction, to the intensity that would be produced by an ideal lossless antenna that radiates isotropically.

The effect of chirality on slot antenna gain is shown in Figures 4.7 and 4.8. For both geometries the nonconfocal coating cylinder is a chiral media with different chiralities. An electric line source is located at the center of each core cylinder and the excited wave is a TM polarized wave. Due to chiral media, there are two (co- and cross-) polarized waves everywhere which is an advantage for some applications. Figure 4.7 shows the co-polarized antenna gain from the slotted elliptic cylinder with semi-major axis $a_c = \lambda$, axial ratio $a_c/b_c = 2$, and slot angle width 10° ($\eta_{c1} = -5^\circ$ and $\eta_{c2} = 5^\circ$), coated by a cylinder with semi-major axis $a = 1.1 a_c$ and axial ratio $a/b = 2$. Figure 4.8 shows the cross-polarized antenna gain from the slotted elliptic cylinder with semi-major axis $a_c = \lambda/3$, axial ratio $a_c/b_c = 2$, and slot angle width 14° ($\eta_{c1} = -7^\circ$ and $\eta_{c2} = 7^\circ$), coated by a cylinder with semi-major axis $a = 1.2 a_c$ and axial ratio $a/b = 2$. As shown in these figures, the main and side lobes of the co-polarized antenna gains and the main lobes of the cross-polarized antenna gains increase by increasing the chirality. Also, the co-polarized antenna gains have small back lobes, while the cross-polarized gains have large back lobes.

In nonconfocal coating, more material can be placed in front of the slot which is an advantage. Figures 4.9, 4.10, and 4.11 show the results for the geometries in which the coating thicknesses in front of slots are more than the coating thicknesses of the other parts of conducting cylinders. The coated materials are chiral media with different chiralities. Figures 4.9 and 4.10 show the co- and cross-polarized antenna gains for TE case while Figure 4.11 shows the co-polarized antenna gain for TM case. The results of Figure 4.9 are due to a slotted elliptic cylinder with semi-major axis $a_c = \lambda/2$, axial ratio $a_c/b_c = 2$, and slot angle width 10° ($\eta_{c1} = 85^\circ$ and $\eta_{c2} = 95^\circ$) coated by a nonconfocal

cylinder with semi-major axis $a = 0.75 \lambda$ and axial ratio $a/b = 1.5$. The core cylinder is located at $d = \lambda/4$ and $\beta = 270^\circ$ with respect to the coating cylinder. A magnetic line source is located inside the core cylinder at $\rho_0 = \lambda/8$ and $\phi^i = \pi/2$. Figure 4.10 shows the results for a slotted elliptic cylinder with semi-major axis $a_c = \lambda/3$, axial ratio $a_c/b_c = 2$, and slot angle width 10° ($\eta_{c1} = 85^\circ$ and $\eta_{c2} = 95^\circ$) coated by a nonconfocal cylinder with semi-major axis $a = \lambda/2$ and axial ratio $a/b = 2$. The core cylinder is located at $d = \lambda/12$ and $\beta = 270^\circ$ with respect to the coating cylinder. A magnetic line source is located inside the core cylinder at $\rho_0 = \lambda/12$ and $\phi^i = \pi/2$. Figure 4.11 shows the results for a slotted elliptic cylinder with semi-major axis $a_c = \lambda/3$, axial ratio $a_c/b_c = 2$, and slot angle width 10° ($\eta_{c1} = -5^\circ$ and $\eta_{c2} = 5^\circ$) coated by a nonconfocal cylinder with semi-major axis $a = \lambda/2$, and axial ratio $a/b = 2$. The core cylinder is located at $d = \lambda/6$ and $\beta = 180^\circ$ with respect to the coating cylinder. An electric line source is located at the center of core cylinder. As shown in Figures 4.9, 4.10 and 4.11 the antenna gains at desired angles (90° , 90° and 0° , respectively) increase by increasing the chirality. Again, the side and back lobes of some results for cross-polarized antenna gains are large.

The effects of different kinds of nonconfocal coated materials on the co-polarized antenna gains for TM and TE cases are shown in Figures 4.12 and 4.13, respectively. In both geometries, the slotted conducting cylinder has semi-major axis $a_c = \lambda/3$, axial ratio $a_c/b_c = 2$, and slot angle width 10° coated by different kinds of materials with semi-major axis $a = \lambda/2$ and axial ratio $a/b = 2$. Figure 4.12 shows the results for slotted conducting cylinder which is located at $d = \lambda/12$ and $\beta = 180^\circ$ with respect to the coating cylinder. An electric line source is located at the center of core cylinder. As shown in Figure 4.12 the conducting cylinder with chiral media coating has the most gain and with metamaterial

coating has the lowest gain (around 0°) for this geometry. However, the back lobe of the antenna gain due to chiral media coating is larger than the other ones. Figure 4.13 shows the results for slotted conducting cylinder which is located at $d = \lambda/12$ and $\beta = 270^\circ$ with respect to the coating cylinder. A magnetic line source is located inside the core cylinder at $\rho_0 = \lambda/12$ and $\phi^i = \pi/2$. As shown in this figure the antenna gain due to chiral media coating is more than the antenna gains due to dielectric and isorefractive material coating (around 90°) for this geometry. Also, the back lobes of antenna gains due to these geometry and coating materials are large.

Figure 4.14 shows the effect of coating thickness on co-polarized antenna gains due to chiral media coating with different chiralities. In this geometry the slotted elliptic cylinder has semi-major axis $a_c = \lambda/3$, axial ratio $a_c/b_c = 3$, and slot angle width 10° ($\eta_{c1} = 85^\circ$ and $\eta_{c2} = 95^\circ$). A magnetic line source is located inside the core cylinder at $\rho_0 = \lambda/18$ and $\phi^i = \pi/2$, and the excited wave is a TE polarized wave. The coating axial ratio $a/b = 3$ and coating thicknesses are calculated from the semi-minor axis b_c . As shown in this figure, the antenna gain increases by increasing the chirality. Also, it increases by increasing the coating thickness for chiral admittances $\gamma = 0.0010$ and $\gamma = 0.0020$.

The effects of coating thicknesses on antenna gain due to coating materials dielectric, isorefractive, and chiral media are shown in Figures 4.15. In this geometry the slotted elliptic cylinder has semi-major axis $a_c = \lambda/3$, axial ratio $a_c/b_c = 3$, and slot angle width 20° ($\eta_{c1} = -10^\circ$ and $\eta_{c2} = 10^\circ$). An electric line source is located at the center of core cylinder, and the excited wave is a TM polarized wave. The coating axial ratio $a/b = 3$ and coating thicknesses are calculated from the semi-major axis a_c . As shown in this figure, by increasing the coating thickness, the gain due to isorefractive coating decreases

while the gains due to dielectric and chiral media coating increase for coating thickness more than 0.1λ .

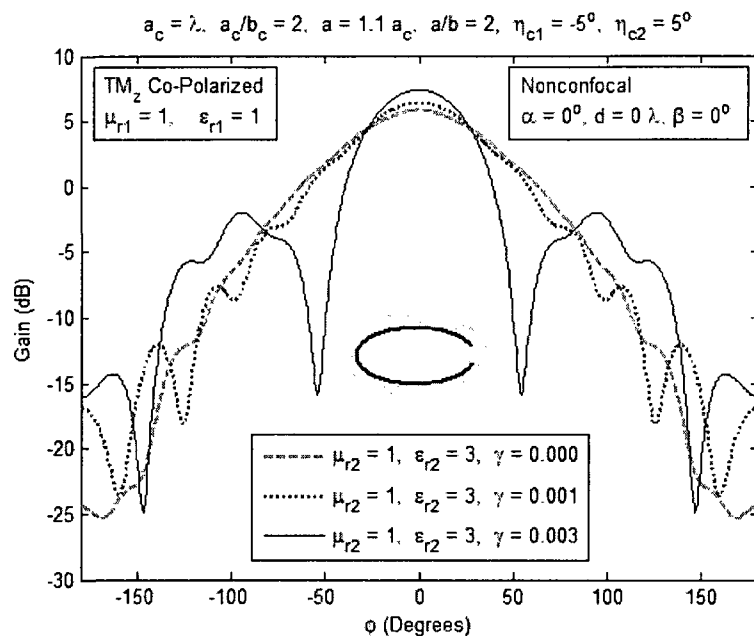


Figure 4.7 – Effect of chirality on antenna gain in TM_z co-polarized.

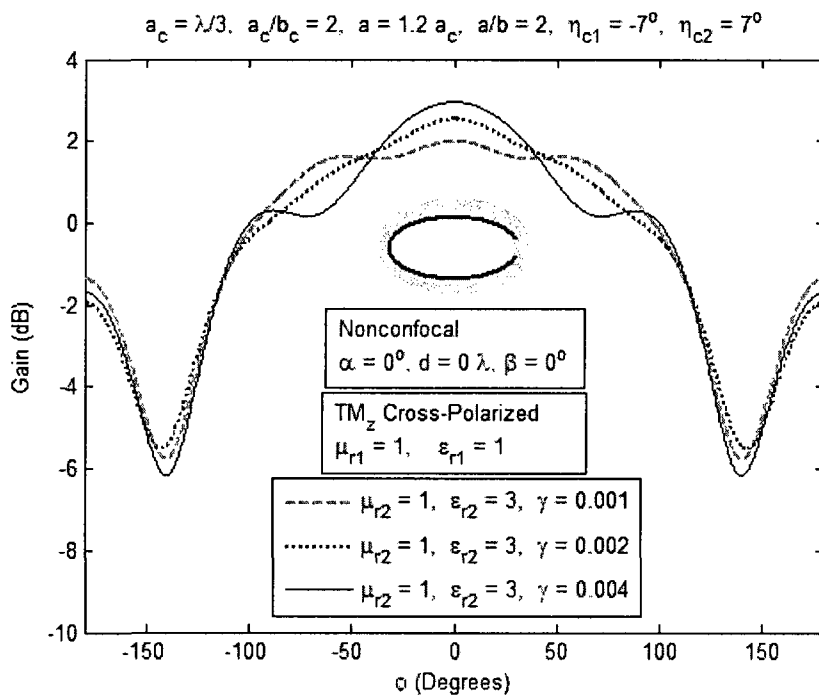


Figure 4.8 – Effect of chirality on antenna gain in TM_z cross-polarized.

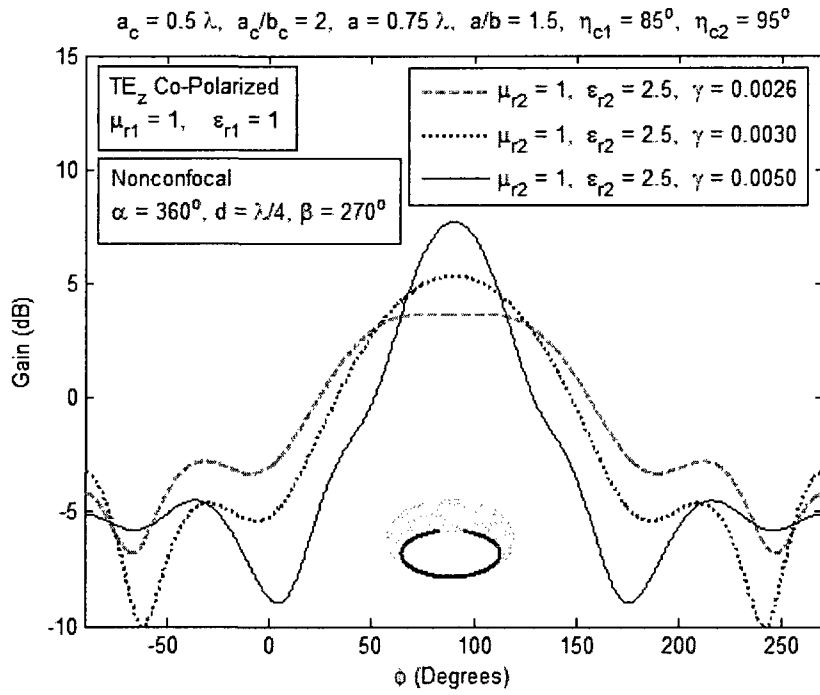


Figure 4.9 – Effect of chirality on antenna gain in TE_z co-polarized.

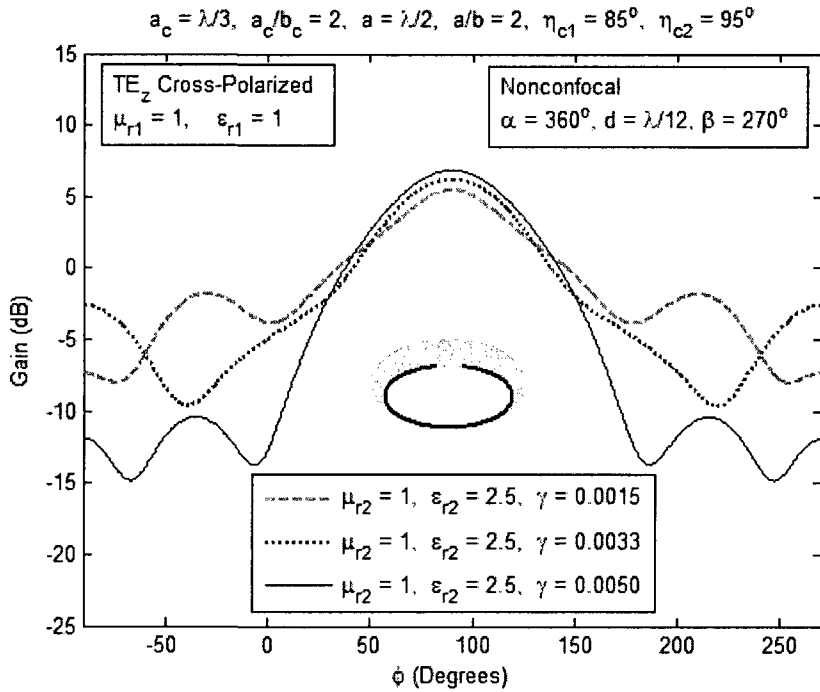


Figure 4.10 – Effect of chirality on antenna gain in TE_z cross-polarized.

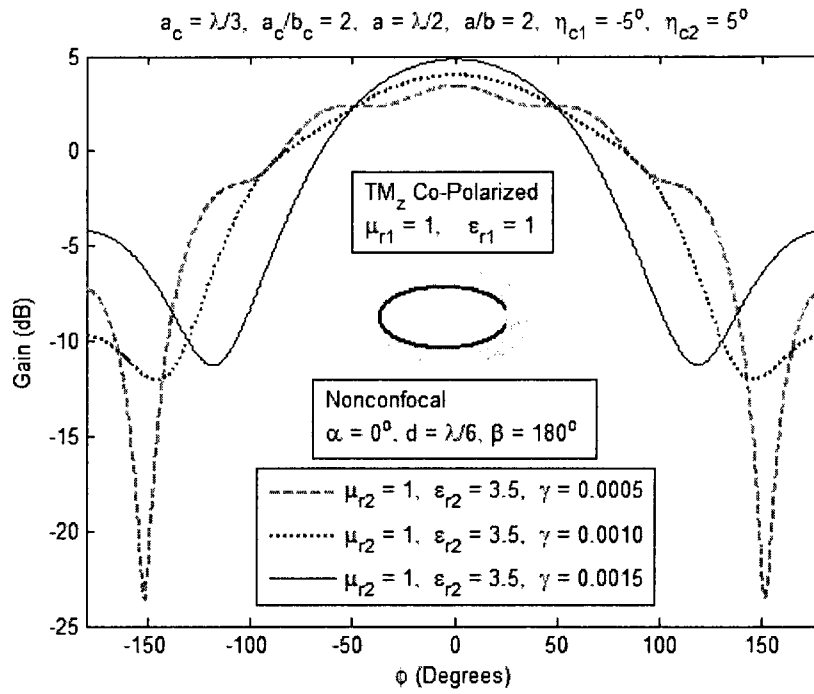


Figure 4.11 – Effect of chirality on antenna gain in TM_z co-polarized.

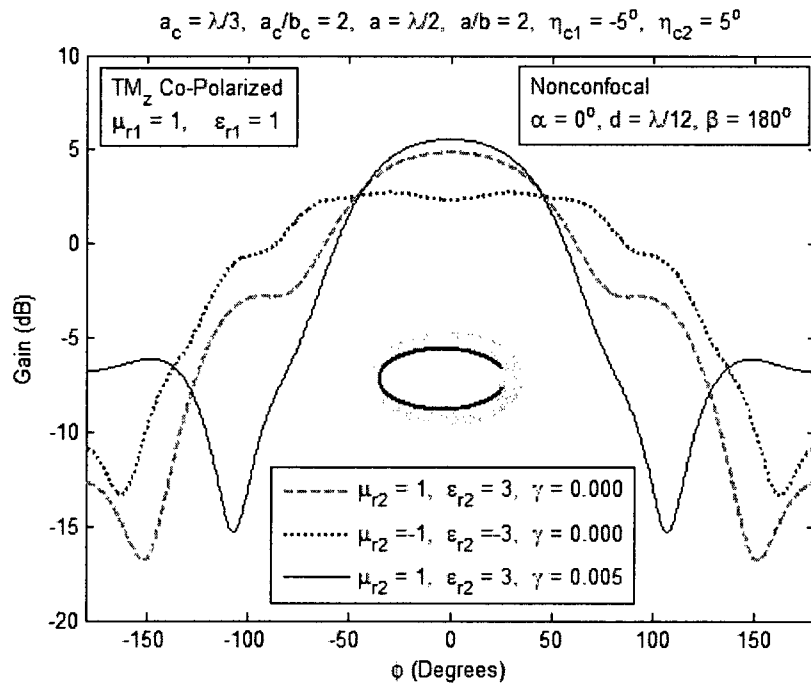


Figure 4.12 – Effect of material parameters on antenna gain in TM_z co-polarized.

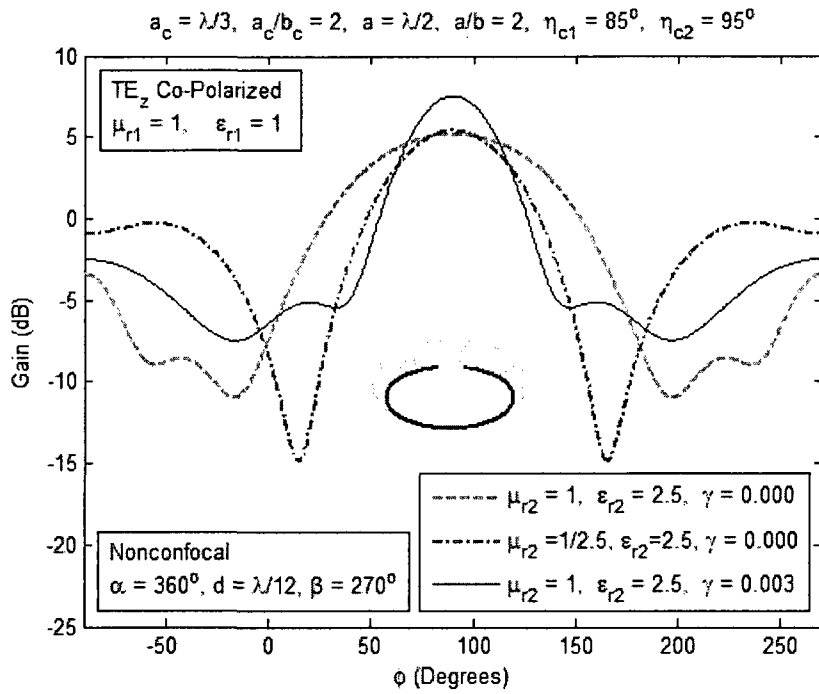


Figure 4.13 – Effect of material parameters on antenna gain in TE_z co-polarized.

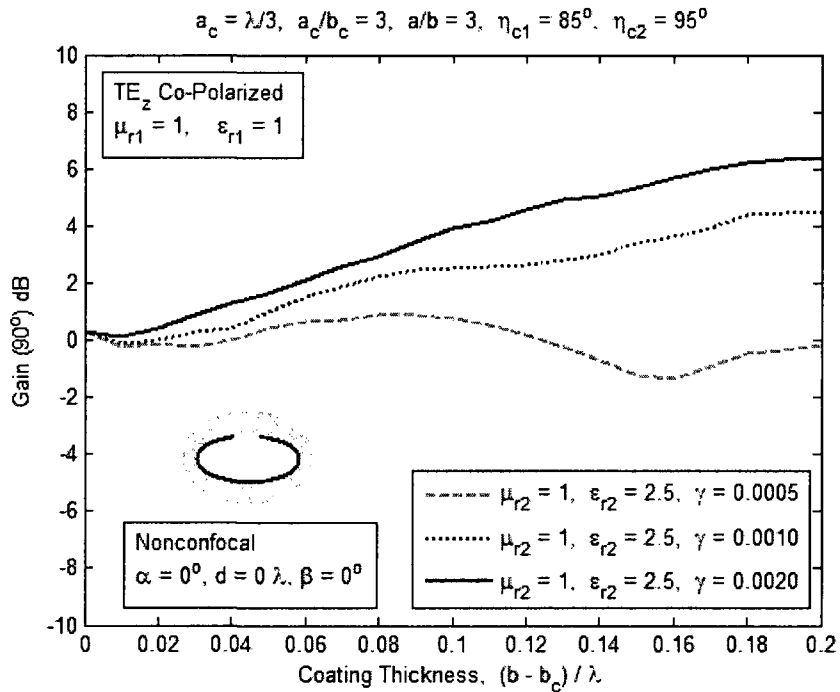


Figure 4.14 – Effect of coating thickness on antenna gain in TE_z co-polarized.

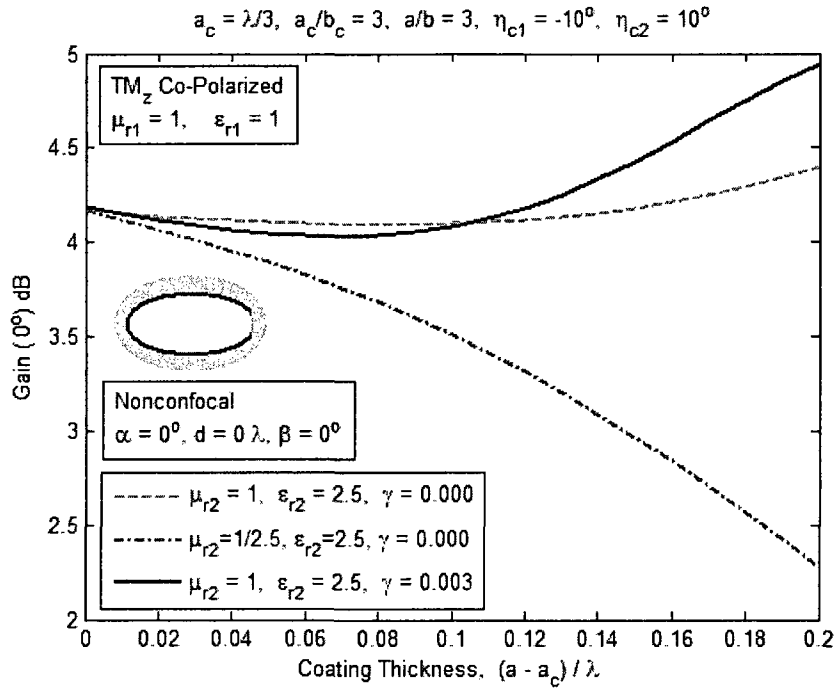


Figure 4.15 – Effect of coating thickness on antenna gain in TM_z co-polarized.

4.2.2 Aperture Conductance

Aperture conductance is another interesting quantity for the slot antennas. The effects of coating thickness and material parameters on aperture conductance are shown and discussed in the following examples. In each example an electric line source (located at the center of core cylinder) is considered and the excited wave is a TM polarized wave.

Figures 4.16 and 4.17 show the effect of coating thickness on aperture conductance due to chiral media coating with different chiralities. Figure 4.16 shows the results for slotted elliptic cylinder with semi-major axis $a_c = \lambda/3$, axial ratio $a_c/b_c = 2$, and slot angle width 10° ($\eta_{c1} = -5^\circ$ and $\eta_{c2} = 5^\circ$). The coating axial ratio $a/b = 2$ and coating thicknesses are calculated from the semi-major axis a_c . As shown in Figure 4.16, the

aperture conductance increases by increasing the chirality for coating thickness more than 0.11λ . Figure 4.17 shows the results for slotted elliptic cylinder with semi-major axis $a_c = \lambda/4$, axial ratio $a_c/b_c = 2$, and slot angle width 10° ($\eta_{c1} = 85^\circ$ and $\eta_{c2} = 95^\circ$). The coating axial ratio $a/b = 2$ and coating thicknesses are calculated from the semi-minor axis b_c . In this figure (except for coating thicknesses more than 0.11λ and less than 0.14λ), the aperture conductance increases by increasing the chirality.

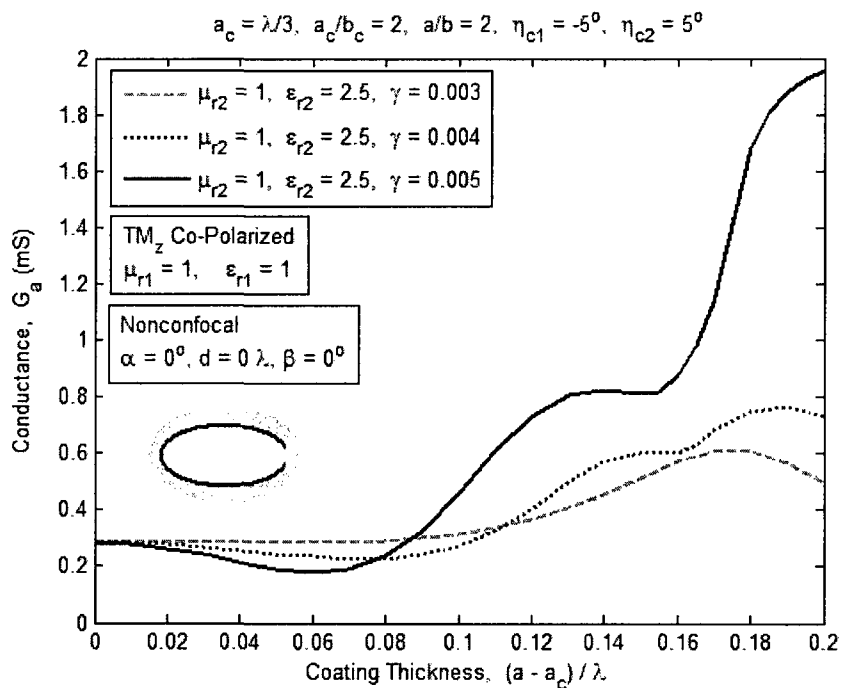


Figure 4.16 – Effect of coating thickness on aperture conductance.

The effects of coating thickness on aperture conductance due to different coating materials are shown in Figures 4.18 and 4.19. In these geometries the slotted cylinder has semi-major axis $a_c = \lambda/3$, axial ratio $a_c/b_c = 2$, and slot angle width 10° ($\eta_{c1} = -5^\circ$ and $\eta_{c2} = 5^\circ$). The coating axial ratio $a/b = 2$ and coating thicknesses are calculated from the semi-

major axis a_c . Figure 4.18 shows the results for coating materials dielectric, isorefractive, and chiral media, while Figure 4.19 shows the results for coating materials dielectric, metamaterials, and chiral media. As shown in these figures the aperture conductance due to chiral media coating is more than the aperture conductance due to other coating materials for these specific geometries and material parameters. Also, among coating materials dielectric, isorefractive and metamaterial, in general, the aperture conductance due to metamaterial coating is more than the aperture conductance due to dielectric coating, while the aperture conductance due to isorefractive coating is less than the aperture conductance due to dielectric coating.

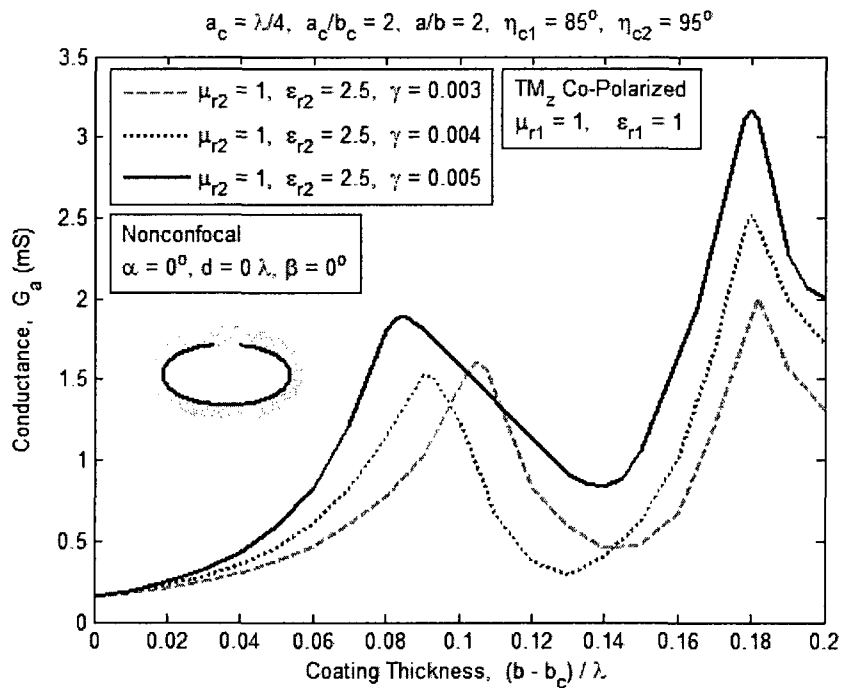


Figure 4.17 – Effect of coating thickness on aperture conductance.

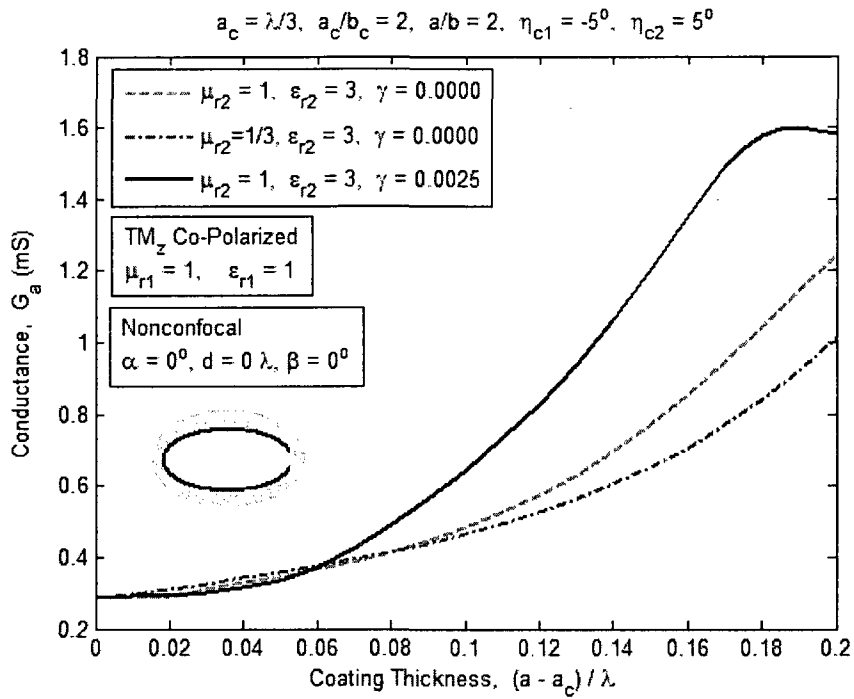


Figure 4.18 – Effect of coating thickness on aperture conductance.

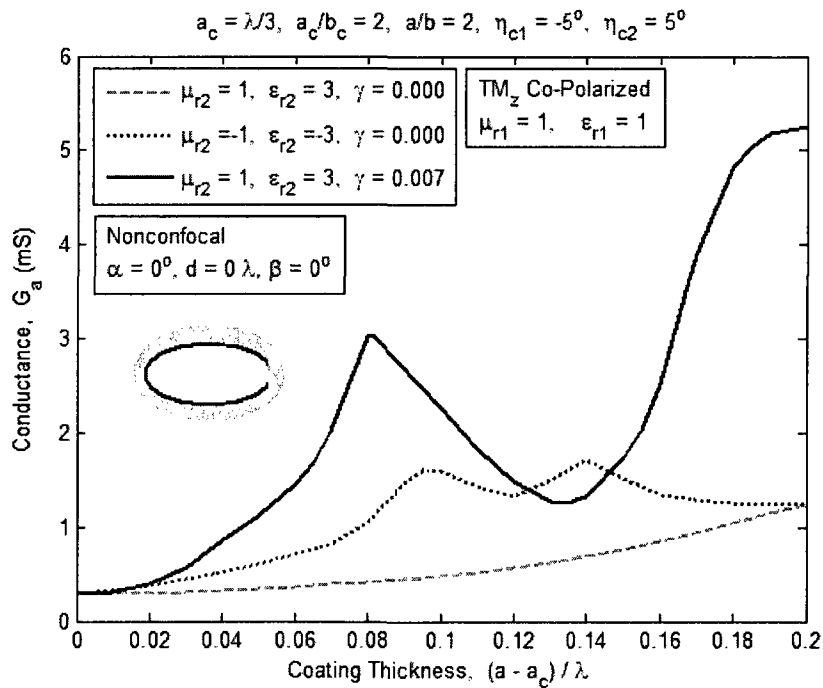


Figure 4.19 – Effect of coating thickness on aperture conductance.

4.2.3 Aperture Voltage

In this section the elliptic slot antenna is considered as the receiving antenna. The aperture voltage is one of the interesting quantities of slot antenna in receiving mode. In each of the following examples a TM polarized plane wave (located in region 3) is considered as the source. The aperture voltages are calculated for a 180-degree symmetric of geometry and incident angles. It is obvious that the maximum value of the aperture voltages is due to the incident angle which is central angle of the slot.

The effect of chirality on aperture voltage is shown in Figures 4.20 – 4.23. For all these geometries the nonconfocal coating cylinder is a chiral media with different chiralities. As shown in these figures, the aperture voltages increase by increasing the chirality. Figure 4.20 shows the aperture voltages of the slotted elliptic cylinder with semi-major axis $a_c = \lambda/3$, axial ratio $a_c/b_c = 2$, and slot angle width 10° ($\eta_{c1} = -5^\circ$ and $\eta_{c2} = 5^\circ$), coated by a cylinder with semi-major axis $a = \lambda/2$ and axial ratio $a/b = 2$. Figures 4.21 and 4.22 show the results for the geometries in which the coating thicknesses in front of slots are more than the coating thicknesses of the other parts of conducting cylinders. The results of Figure 4.21 are due to the slotted elliptic cylinder with semi-major axis $a_c = \lambda/4$, axial ratio $a_c/b_c = 2$, and slot angle width 10° ($\eta_{c1} = -5^\circ$ and $\eta_{c2} = 5^\circ$), coated by a cylinder with semi-major axis $a = \lambda/3$ and axial ratio $a/b = 2$. The core cylinder is located at $d = \lambda/12$ and $\beta = 180^\circ$ with respect to the coating cylinder. Figure 4.22 shows the aperture voltages due to the geometry same as geometry of previous example, except $\eta_{c1} = 85^\circ$, $\eta_{c2} = 95^\circ$, $a/b = 1.5$, and the core cylinder is located at $d = \lambda/24$ and $\beta = 270^\circ$ with respect to the coating cylinder. As shown in these figures, the minimum values of the aperture voltages for the results of Figure 4.20 and 4.21 are due to the incident angles which are

generally the opposite direction of the central angle of slot, while that is not correct for Figure 4.22 because of the slot location.

It is interesting to consider a conducting cylinder coated by a uniform thickness elliptic shell. This geometry is important in many applications, because it is easy to manufacture. Figures 4.23 – 4.27 show the results due to the geometries in which the coated cylinder has a uniform thickness. Each of these geometries consist of a slotted elliptic cylinder with semi-major axis $a_c = \lambda/4$, axial ratio $a_c/b_c = 3/2$, and slot angle width 10° ($\eta_{c1} = -5^\circ$ and $\eta_{c2} = 5^\circ$), coated by a cylinder with semi-major axis $a = \lambda/3$ and axial ratio $a/b = 4/3$. Figure 4.23 shows the aperture voltages of the slotted elliptic cylinder coated by a nonconfocal chiral media with different chiralities. As shown in this figure, the aperture voltages increase by increasing the chirality.

Figure 4.24 shows the comparison of the aperture voltages due to different coating materials. As shown in this figure, the aperture voltage due to chiral media coating is more than the aperture voltages due to non-coating or other coating materials (i.e., dielectric, metamaterial, or isorefractive). Also, for the incident angles around 0° , the aperture voltages due to coating materials are more than the aperture voltage due to non-coating. That means the coating materials can increase the aperture voltage. However, this effect depends on the coating materials. Figure 4.25 shows the comparison of the aperture voltages due to different materials (i.e., dielectric or metamaterial) which are loaded into conducting cylinder (in region 1) while the coated material is chiral media. As shown in this figure, the most and the least values of the aperture voltage are due to metamaterial loading and non-loading material (free space), respectively. That means the loading material can increase the aperture voltage, as well.

Since most of coating and loading materials are dielectrics, the following examples are comparison of the coating and loading dielectrics with different dielectric constants. Figure 4.26 shows the comparison of the aperture voltages due to dielectric coating with different dielectric constants. As shown in this figure, the aperture voltages increase by increasing the dielectric constant. Figure 4.27 shows the comparison of the aperture voltages due to dielectric loaded into conducting cylinder (in region 1) with different dielectric constants while the coated material is chiral media. As shown in this figure, the aperture voltages increase by increasing the dielectric constant for dielectric constant up to 3.0. However, they decrease by increasing the dielectric constant for dielectric constant more than 3.0.

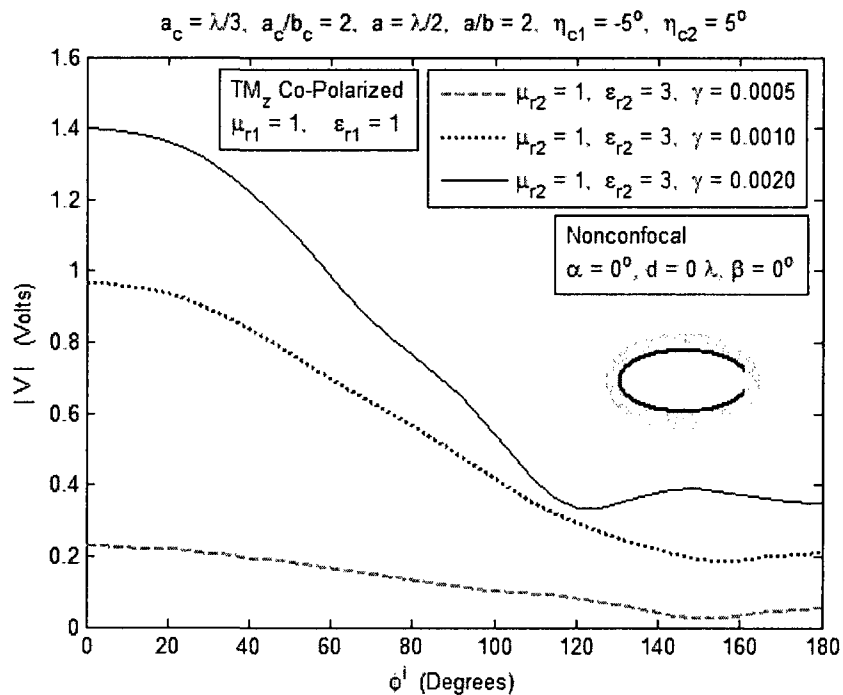


Figure 4.20 – Effect of chirality on aperture voltage.

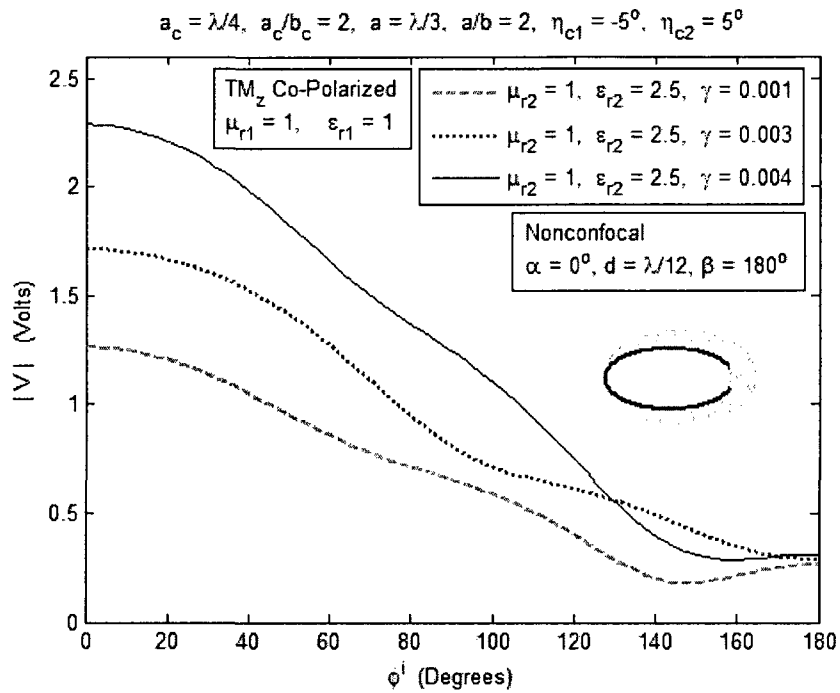


Figure 4.21 – Effect of chirality on aperture voltage.

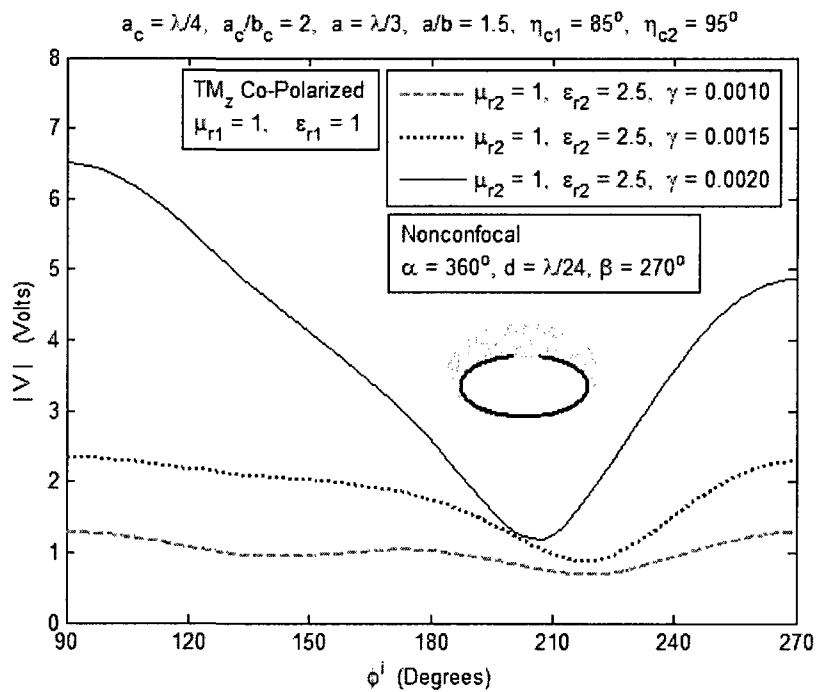


Figure 4.22 – Effect of chirality on aperture voltage.

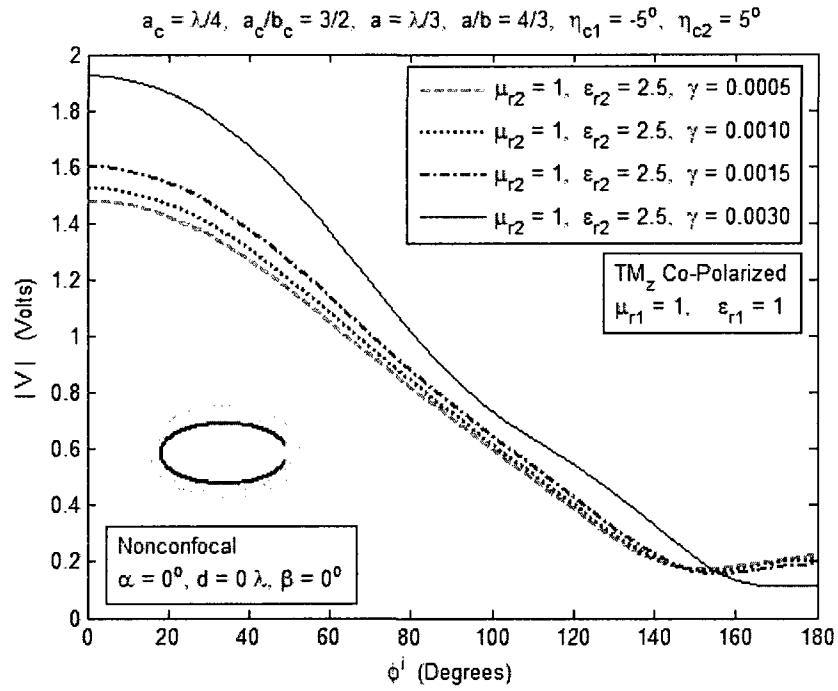


Figure 4.23 – Effect of chirality on aperture voltage.

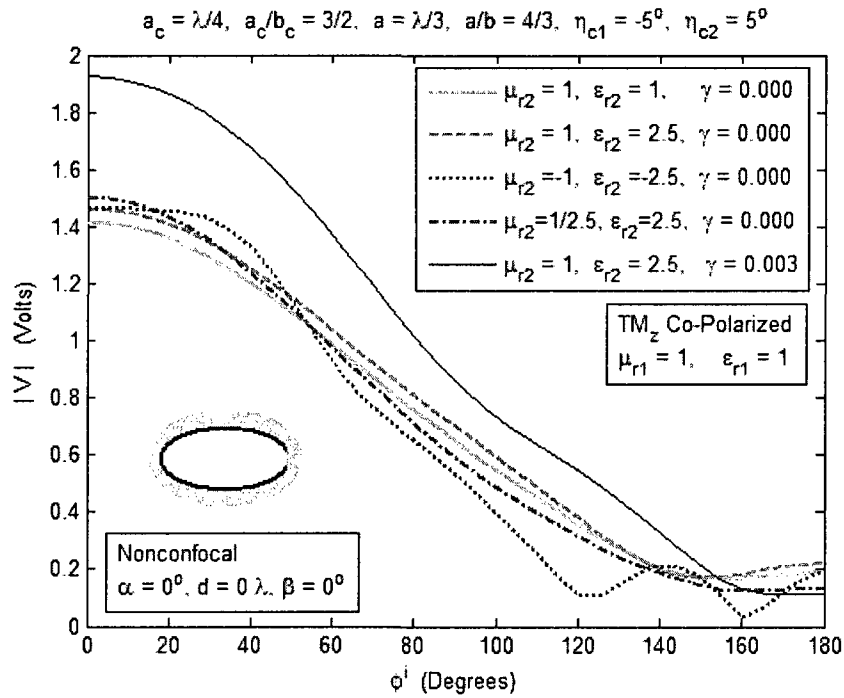


Figure 4.24 – Effect of material parameters on aperture voltage.

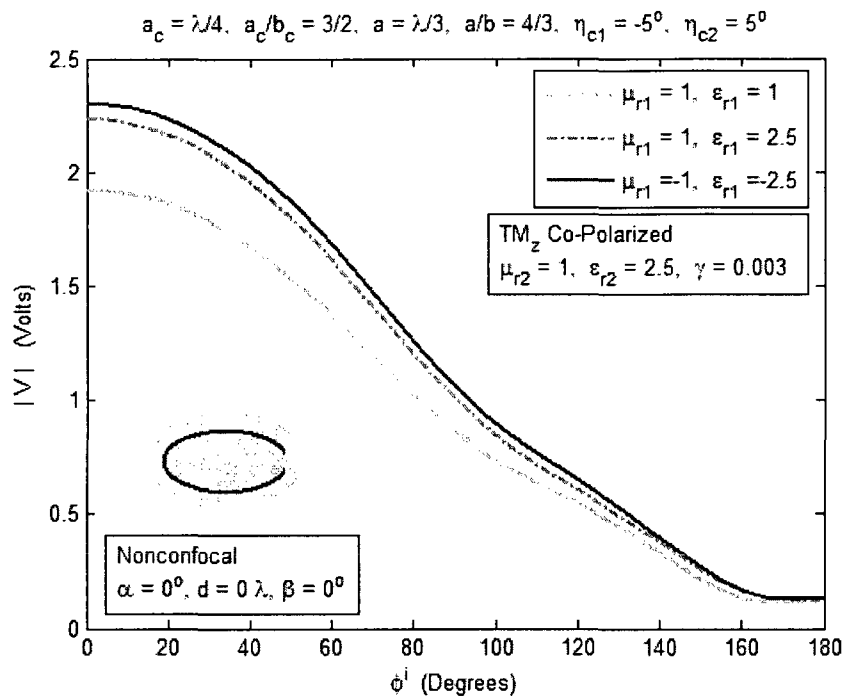


Figure 4.25 – Effect of material parameters on aperture voltage.

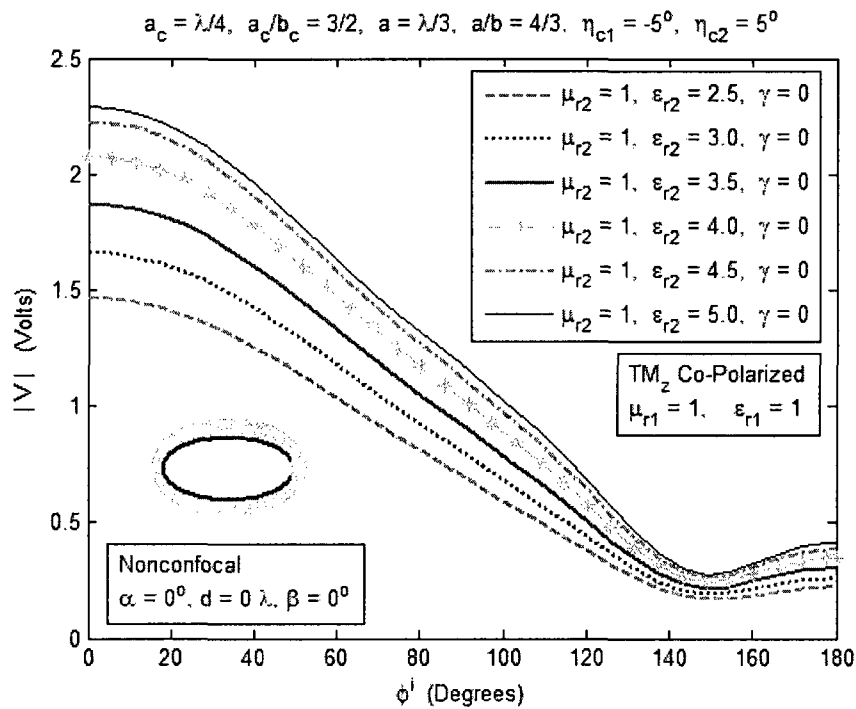


Figure 4.26 – Effect of material parameters on aperture voltage.

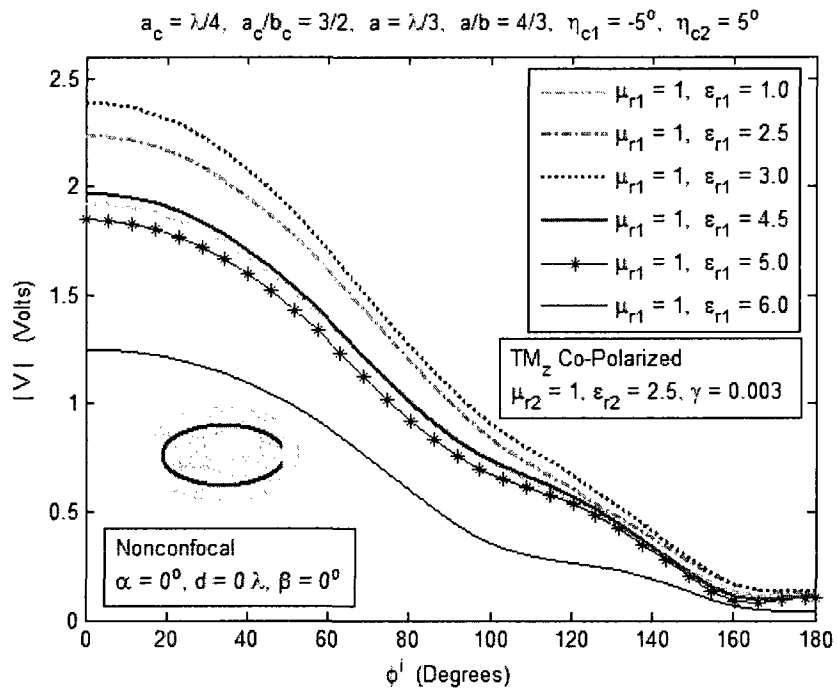


Figure 4.27 – Effect of material parameters on aperture voltage.

5. Fabrication and Testing of Elliptic Slot Antenna

The analytical solution for the characteristics of elliptic slot antenna coated by different kinds of nonconfocal materials, and the selected numerical results of this antenna are given in Chapters 3 and 4, respectively. In this chapter, first, some experimental works from feeding point of view are reviewed. Then, design, fabrication and testing of non-coated and dielectric-coated elliptic slot antennas are presented and discussed.

5.1 Feeding of Cylindrical Slot Antenna

There are many kinds of slot antennas. However, in here, only the cylindrical (i.e., rectangular, circular, and elliptic cylinders) slot antennas are considered. From feeding point of view, the cylindrical slot antennas can be divided in three categories for design and fabrication. In this section, some of them in each category are reviewed.

In the first category, the cylindrical slot antennas are fed by connecting to an open end waveguide in which electromagnetic waves flow. For examples, a slotted circular cylinder antenna with 3.5 inches diameter and 22 inches length, surrounded by a thin plasma sheath, and fed by X-band waveguide is made and experimented by Smith and Golden [1]. Six separate single-slot antennas with slot dimensions of 0.9 inches by 0.4 inches are constructed by Tetenbaum [147]. They fed by a constant-length section of X-band waveguide whose open end was shaped to conform to the curvature of the

terminating copper circular cylinder. The cylinders had 8 inches axial length with various diameters. As a final example for this category, a millimeter wave slotted rectangular waveguide antenna is fabricated and tested by Wasim and her group [148] in 2007 as shown in Figure 5.1.

In the second category, the slots (i.e., slotted conducting sheets) are center-fed by a balanced transmission line directly connected across the slot, with one side connecting to each edge of the slot. Kraus [149] bends a slotted sheet into a U-shape, with the bend parallel to the long dimension of the slot, then, joined the ends of the U-shape to form a slotted cylinder. The result is a slotted circular cylinder antenna as shown in Figure 5.2.



Figure 5.1 – Slotted rectangular waveguide antenna [148].

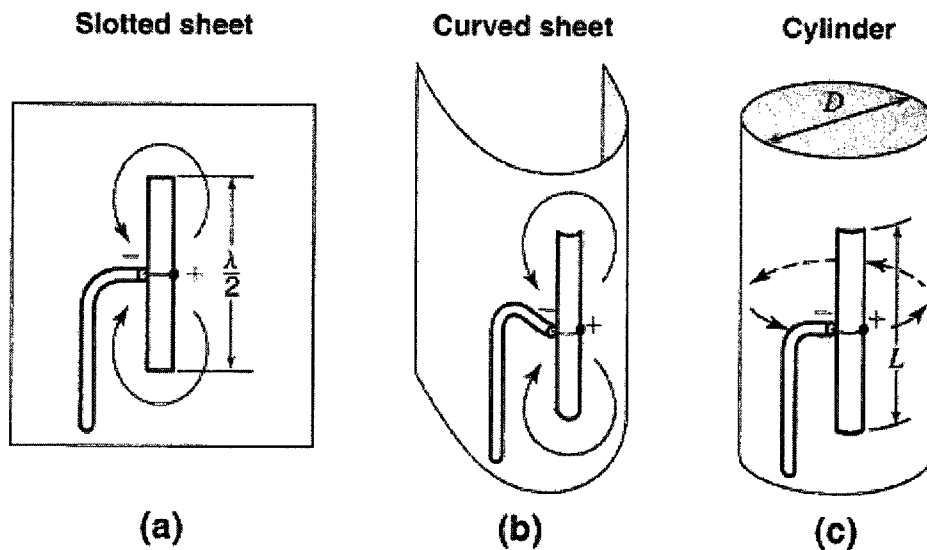


Figure 5.2 – Evolution of slotted cylinder from slotted sheet [149].

In the third category, the cylindrical slot antennas are fed by a coaxial line. The open-ended inner conductor of a coaxial line is located inside the cylinder as a monopole, and the outer conductor is connected to the cylinder. A circumferential wide slot cut on a thin circular cylinder is designed and experimented by Hirokawa and his group [150]. In this design, the open-ended inner conductor of coaxial line is located at the center of the slot to get the symmetrical radiation pattern in the horizontal plane. As a second example for this category, an X-band slot array antenna with 10 circumference slots is fabricated by Shin and Eom [151] in 2005. The fabricated antenna consists of a coaxially fed monopole, slotted circular cylinder, and SMA termination as shown in Figure 5.3. The coaxially fed monopole, which has a protruding inner conductor of 6 millimeters length, radiates the TM mode into the slotted circular cylinder. The SMA termination used in the measurements has SWR below 1.1 at X-band.

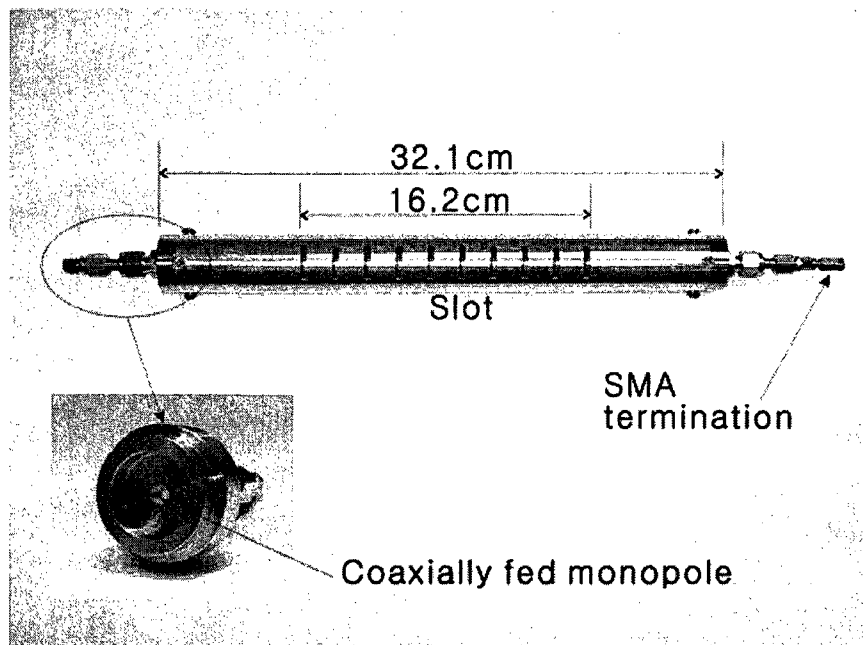


Figure 5.3 – Photograph of a circular slot antenna [151].

5.2 Analytical and Experimental Solutions

In the analytical solutions of Chapters 3, it is assumed that the line source and cylinders have infinite length (i.e., in z direction), and they are uniform along this direction. Thus, their analysis is a two-dimensional analysis (no z variations). For a line (i.e., a wire) with infinite length and a current directed along it, the radiated wave is a cylindrical wave [140]. In addition, for analytical solution of the problems with such geometries the feeding lines (or ports) are not directly involved.

In practice, we deal with the limited dimensions of geometries. Thus, the infinite length can be reduced to a few times of λ (same as Figure 4.4), so that, the obtained results due to this length are very good agreement with the results due to infinite length (Figures 4.5 and 4.6). Another problem for such experimental works is feeding lines. To have a cylindrical wave, a sufficient long line with a current directed along it, is needed. To do that, we have to use a conductor, i.e., a single straight wire, and connect two ends of this wire to a power supply by two other single lines, so that, only the straight wire (as a load) can radiate while two other lines are isolated (no effect on radiation). Using this line source and a slotted conducting cylinder, we can fabricate a sample of slotted antennas which are analyzed and discussed in Chapter 3 and 4. However, because of isolation parts, its fabrication and measurement are not easy.

Therefore, for experimental work we have to use one of categories which are discussed in Section 5.1. The third category is more compatible to our analytical solutions. According to this category, the cylindrical slot antenna is fed by a coaxial line, so that, its open-ended inner conductor is located inside the cylinder as a monopole, and the outer one is connected to the cylinder as a ground. This geometry is very different

with the geometries which are considered for analytical solutions in Chapters 3 and 4. Consequently, it is clear that the experimental results can not be comparable with the analytical results.

5.3 Simulation and Design

Before prototype construction, simulation can be used to find an accurate design and reduce the costs of fabrication. The Ansoft's high frequency structure simulator (HFSS) is an effective tool for modeling electromagnetic structures. HFSS employs the finite element method (FEM) which is a very powerful tool for solving complex engineering problems. The basic approach of this method is to divide a complex structure into smaller sections of finite dimensions known as elements. These elements are connected to each other via joints called nodes. Each unique element is then solved independently of the others thereby drastically reducing the solution complexity. The final solution is then computed by reconnecting all the elements and combining their solutions.

Using HFSS, Figure 5.4 shows the simulated geometry of an elliptic slot antenna according to the third category of slot antenna discussed in Section 5.1. In this simulation, two perfect electric conductor sheets are used for top and bottom of the cylinder. The open-ended inner conductor of a coaxial line is located inside the cylinder as a monopole, and the outer conductor is connected to the sheet. To have a matched load or a very low reflection power, many designs (same as Figure 5.4) are simulated by changing the length of cylinder, the major and minor axes, the slot width and its location,

and the length of monopole and its location. However, a good solution is not found for the limited dimensions of this geometry.

In theory, there is a solution for an infinite electric line source which is parallel placed at distance d an infinite flat electric conductor [140]. We use this theory to simulate geometry with a limited length of line source parallel to the limited dimensions of a perfect electric conductor (a flat plate) as shown in Figure 5.5. It is found that there is a good solution for this geometry. Now, we can bend the plate to have an elliptic cylinder as shown in Figure 5.6. By doing that, some questions can be asked. Is there any effect on the results? If so, why we have to make the elliptic cylinder? Why not the circular one as shown in Figure 5.7?

To answer to these questions, the mentioned geometries (Figures 5.5 – 5.7) are simulated at 10 GHz and their results are compared to each other. For these geometries the same dimensions of plate, monopole, and coaxial line are considered. The elliptic and circular cylinders (Figures 5.6 and 5.7) have same slot widths. After many simulations, the sizes and parameters are chosen so that, to have good results for elliptic cylinder slot antenna (Figure 5.6). Figures 5.8 and 5.9 show the simulation results of S11 and radiation pattern for these three geometries (Figures 5.5 – 5.7). The results show that, with these parameters (i.e., dimensions of plate) we can not have a circular cylinder slot antenna, or a good monopole antenna with flat ground plane. However, these parameters may be appropriate for an elliptic cylinder slot antenna.

Therefore, these parameters can be used to design a non-coated elliptic slot antenna at 10 GHz. Two conductors (cylinders) are considered to simulate a coaxial line. The characteristic impedance of the coaxial line is defined [152] as

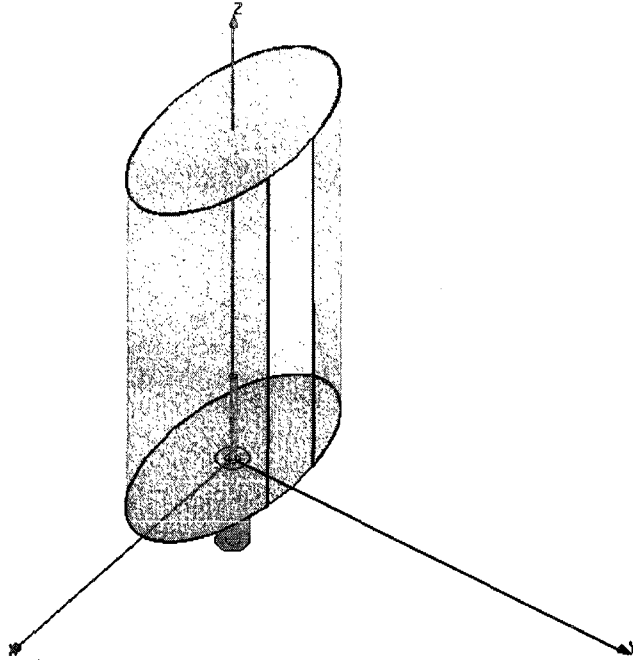


Figure 5.4 – Geometry of an elliptic cylinder slot antenna with perfect electric conductor sheets at top and bottom of cylinder.

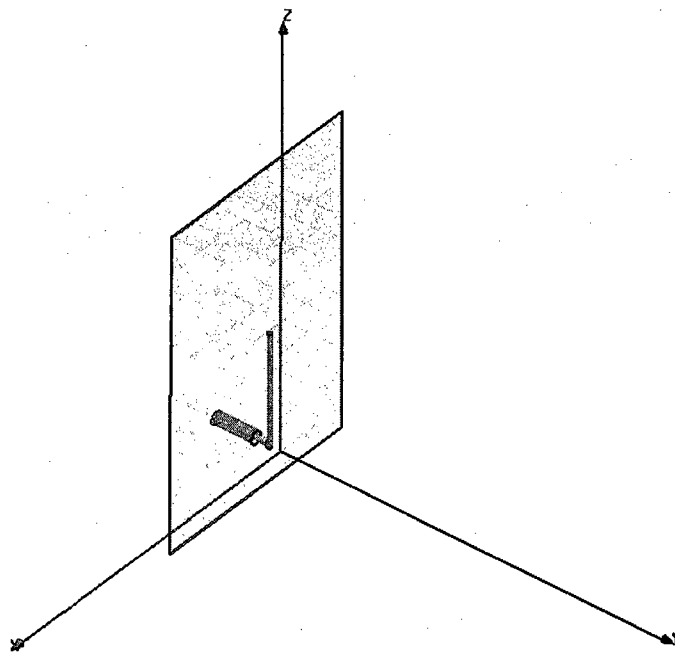


Figure 5.5 – Geometry of an electric line source parallel with a flat electric conductor.

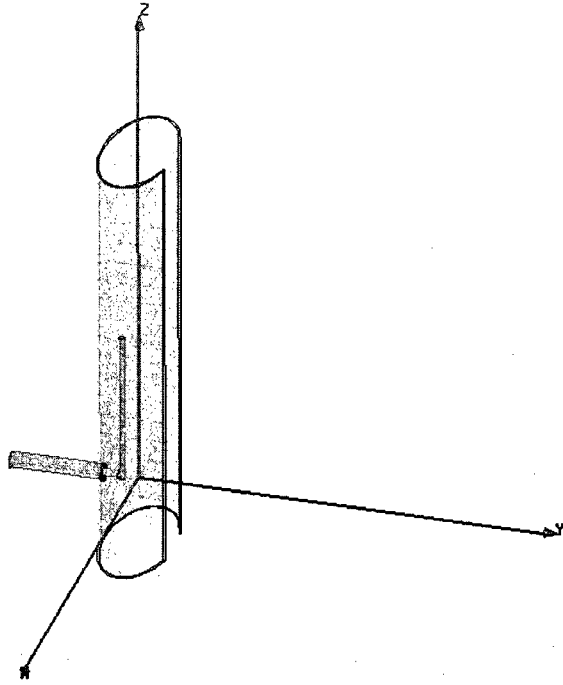


Figure 5.6 – Geometry of an elliptic cylinder slot antenna.

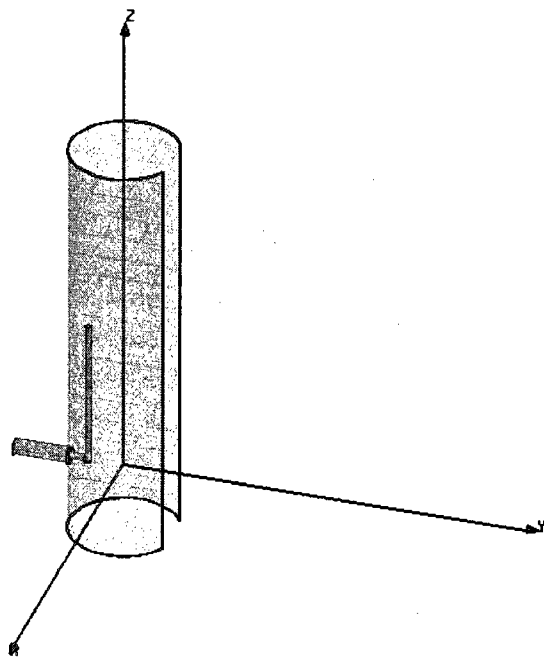


Figure 5.7 – Geometry of a circular cylinder slot antenna.

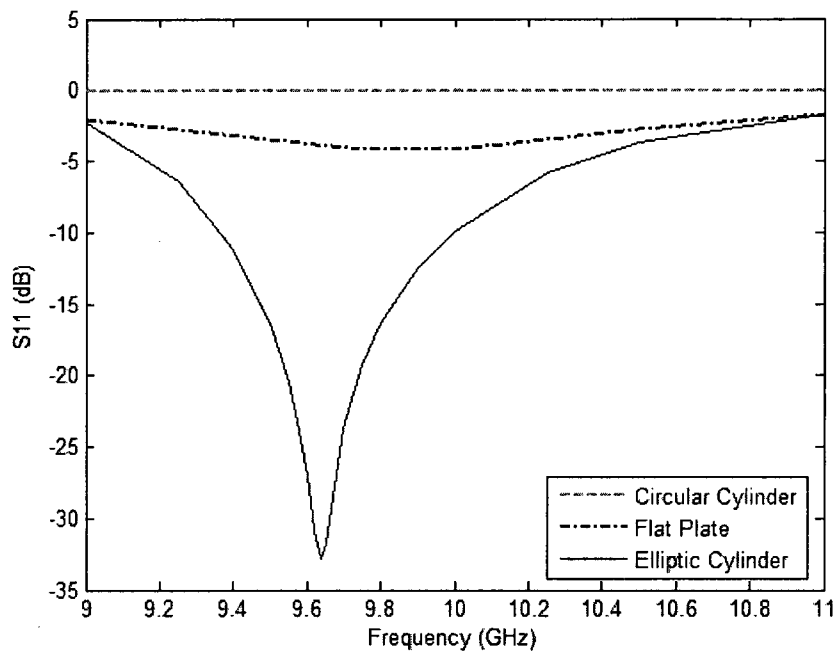


Figure 5.8 – Comparison of S_{11} for three different geometries.

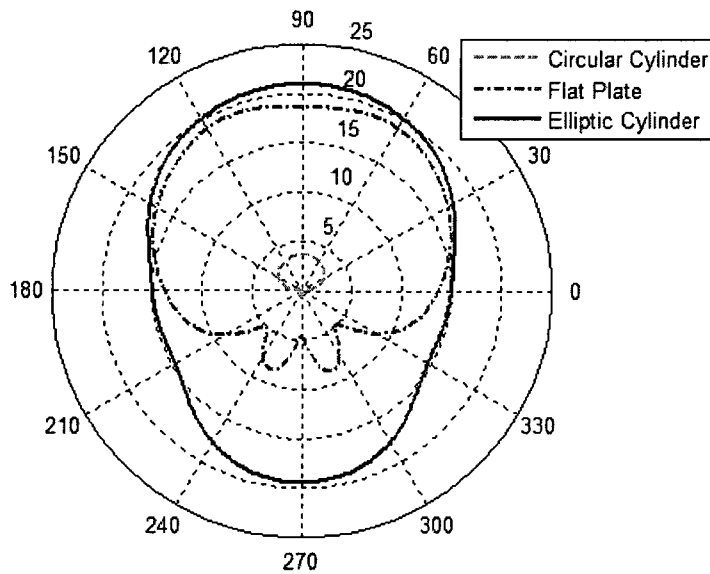


Figure 5.9 – Comparison of radiation patterns (in dB) for three different geometries.

$$Z_0 = \frac{1}{2\pi} \sqrt{\mu/\epsilon} \ln(D/d), \quad (5.1)$$

where μ and ϵ are permeability and permittivity for dielectric of coaxial cable, d is the outer diameter of inner conductor, and D is the inner diameter of outer conductor. For a 50- Ω standard coaxial line with free space between two conductors, we have

$$\frac{D}{d} = e^{\frac{50 \times 2\pi}{120\pi}} = 2.30 \quad (5.2)$$

Using a wave port and relation (5.2), a coaxial fed line can be simulated, so that, the inner conductor connected to the monopole and the outer one connected to the cylinder. The coaxial line is located at distance 10 mm from the bottom of cylinder. The monopole is placed on minor axis parallel to the cylinder at distance 2 mm of its inner surface. The feed point and monopole locations are optimized after many simulations to find the minimum reflection power (or S11). More details of this design are given in Table 5.1.

Table 5.1 – Design parameters for a non-coated elliptic slot antenna at 10 GHz.

	Millimeter (mm)	Free Space Wavelength (λ)
Wavelength	30.00	1.000
Length of Monopole	21.50	0.717
Diameter of Monopole	0.80	0.027
Thickness of Plate for Cylinder	0.25	0.008
Length of Cylinder	60.00	2.000
Outer Major Axis	20.00	0.667
Outer Minor Axis	10.00	0.333
Slot Width	7.50	0.250

The results of a non-coated elliptic slot antenna are shown in Figures 5.8 and 5.9. The effect of coating material on radiation pattern is another subject that we are interested to simulate it. Figure 5.10 shows the simulated geometry of an elliptic slot antenna coated by a nonconfocal material. That is nonconfocal because the thickness of material around the cylinder is uniform. The effect of coating material on radiation pattern for different coating thicknesses is shown in Figure 5.11. The material is a dielectric with dielectric constant, $\epsilon_r = 2.20$. As shown in this figure, by increasing the coating thickness, the radiation patterns become more directed to a desire angle (at 90°) and their back lobes decrease.

In practice, fabrication of geometry like the one shown in Figure 5.10 coated with a thick dielectric may not be easy. Instead, the nonconfocal coating material can cover only part of cylinder, i.e., front of slot. Figure 5.12 shows the geometry in which the coated dielectric covers slot and extends almost $\lambda/4$ both sides of slot. The effect of partial coated dielectric on radiation pattern for different coating thickness is shown in Figure 5.13. By comparison between this figure and Figure 5.11, it can be concluded that the radiation patterns due to partial coating become much more directed to desire angle. However, the back lobes due to partial coating are more than the back lobes due to full coating for coating thicknesses 0.787 mm and 1.575 mm.

Therefore, based on simulations and results discussed in this section, the geometry shown in Figure 5.6 is an appropriate geometry for a non-coated elliptic slot antenna at 10 GHz. Its design parameters are given in Table 5.1. To investigate the effect of material properties on radiation pattern and simplify the fabrication, a partial coating by dielectric may be used as shown in Figure 5.12.

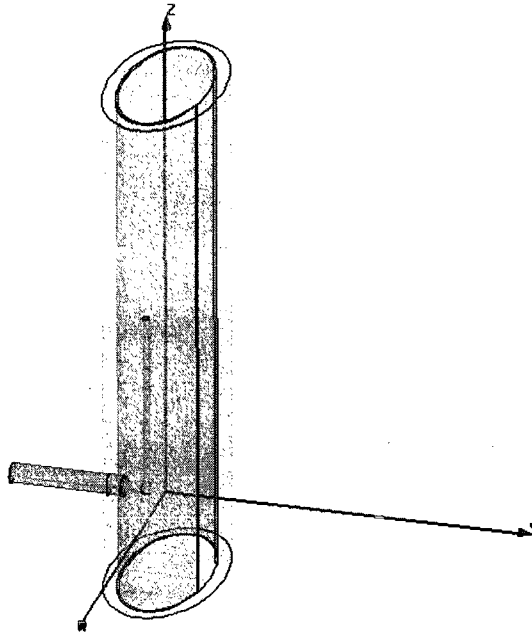


Figure 5.10 – Geometry of an elliptic cylinder slot antenna coated by a nonconfocal dielectric.

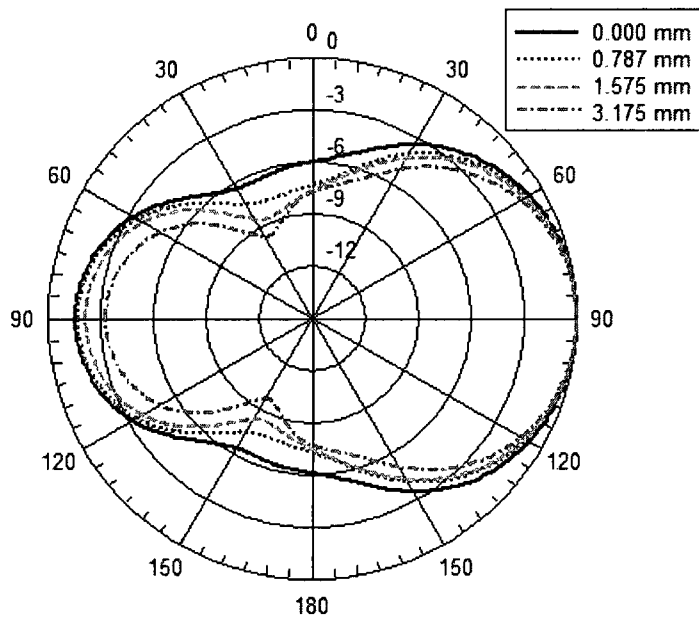


Figure 5.11 – Radiation patterns of an elliptic slot antenna coated by different thicknesses of a nonconfocal dielectric.

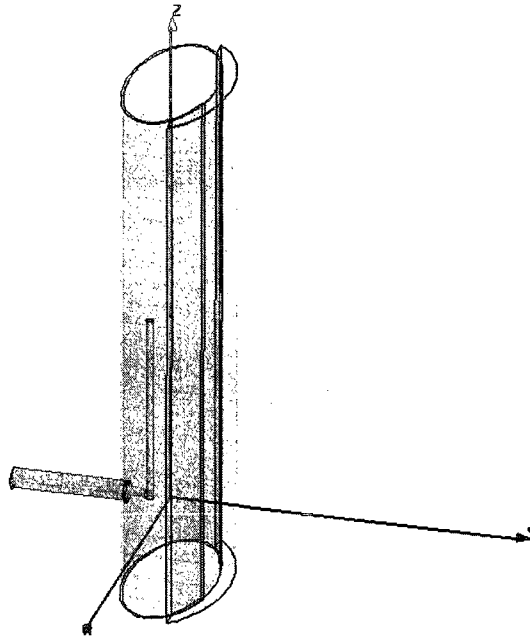


Figure 5.12 – Geometry of an elliptic cylinder slot antenna partial coated by dielectric.

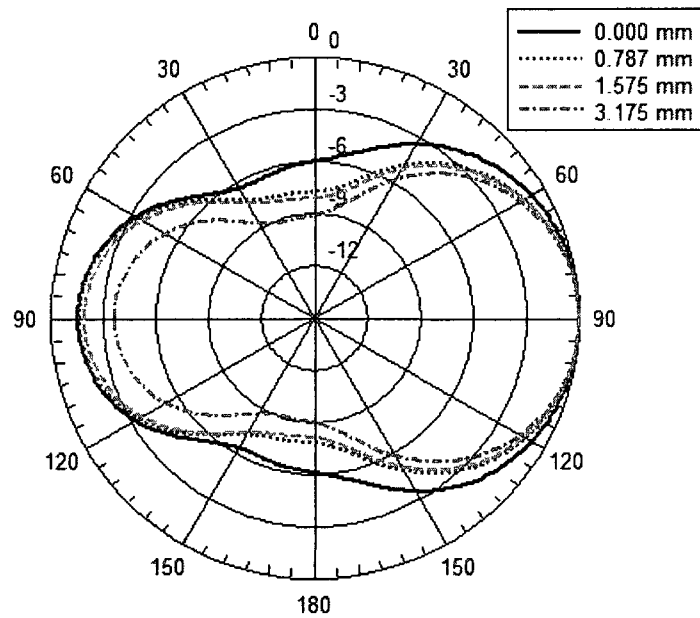


Figure 5.13 – Radiation patterns of an elliptic slot antenna partial coated by different thicknesses of a nonconfocal dielectric.

5.4 Fabrication and Measurement

As discussed in Section 5.1, a waveguide or cylindrical slot antenna can have rectangular, circular, or elliptic cylinder shape. Different materials can be used for fabrication of these antennas (Figure 5.14). A rectangular cylinder slot antenna can be made by a rectangular aluminium waveguide. Also, different circular cylinder slot antennas can be produced using different sizes of copper pipes. However, finding a metal with elliptic cylinder shape is not easy due to lack of machine shop. Therefore, we have to use the copper sheet for fabrication of elliptic cylinder slot antenna.

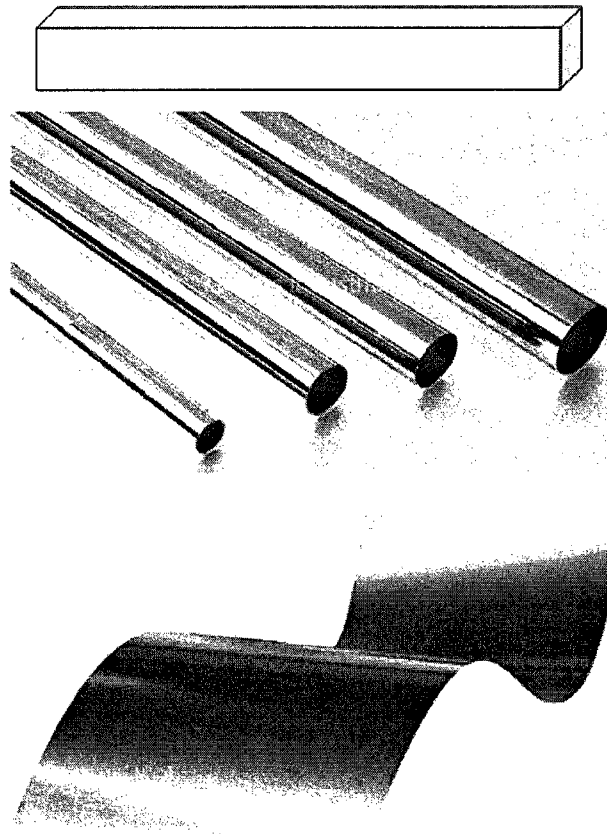


Figure 5.14 – The materials which may be used to make rectangular, circular, and elliptic cylinder slot antenna.

After many simulations which are discussed in Section 5.3, the design parameters for a non-coated elliptic slot antenna at 10 GHz are found and given in Table 5.1. We use these parameters and some simple tools (Figure 5.15) to fabricate this antenna. The thickness of copper sheet is chosen so that, it must be soft enough and flexible to make an elliptic cylinder, and it must be enough hard to keep its shape. Thus, the copper sheet with thickness 0.25 mm is used for this purpose. The ellipse formula and MatLab program are used to draw and print an ellipse on a paper sheet with the exact design size. Using a piece of hard metal, an elliptic ring is made so that, the inner diameter of ring equals to outer diameter of ellipse which is drawn on the paper sheet.

Considering the design sizes, a rectangular piece of copper sheet is cut. A hole is made in this rectangular piece which is located at the width center and 10 mm to the length end. Then, the rectangular sheet is bended to make a slotted elliptic cylinder. This is done step by step and its shape controlled by passing from the elliptic ring, so that, the outer surface of cylinder be exactly tangent to inner surface of ring (Figure 5.15).

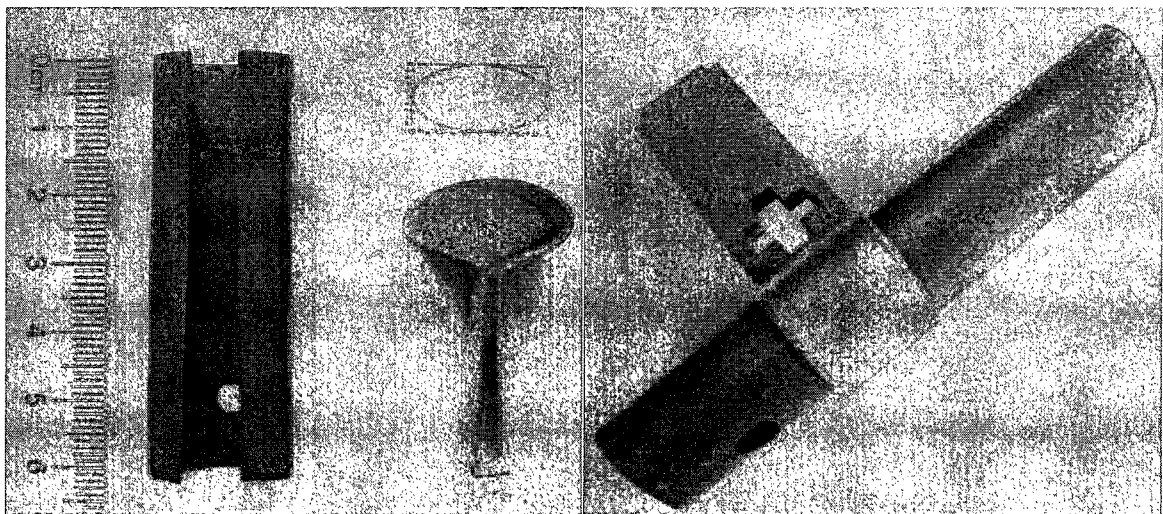


Figure 5.15 – Photographs to show how the slotted elliptic cylinder is made.

The next step is installation of monopole and connector. A 90-degree connector is used and its inner conductor connected to the monopole and outer one connected to the cylinder. The connector is placed at the same hole location, so that, its inner conductor passed from the hole. The monopole is installed on minor axis and parallel of cylinder at distance of 2 mm from inner surface of cylinder and 10 mm from the bottom of cylinder. The feed point and monopole locations are optimized using many simulations. Figure 5.16 shows photographs of the fabricated non-coated elliptic slot antenna. After fabrication of slot antenna some measurements are done and compared to the simulation results.

Figure 5.17 shows the simulation and measurement results for S11 of the non-coated elliptic slot antenna. As shown in this figure the minimum value of simulation result is almost -32.9 dB at frequency 9.64 GHz, while the minimum value of measurement result is almost -18.6 dB at frequency 9.59 GHz. However, both results have almost same -10 dB bandwidth.

For measurement of radiation pattern, the non-coated elliptic slot antenna is installed in anechoic chamber (Figure 5.18). The provided systems (i.e., synthesized oscillator, horn transmitter antenna, spectrum analyzer, and positioner) in this room are used to measure the radiation pattern, and transfer data into a text file by a computer and a specific software. Using this data and a MatLab program, the radiation pattern can be plot. Figure 5.19 shows the simulation and measurement radiation patterns of the non-coated elliptic slot antenna. The main lobe of measurement result is in very good agreement with the main lobe of simulation result. However, there are some disagreements for side lobes and back lobe.

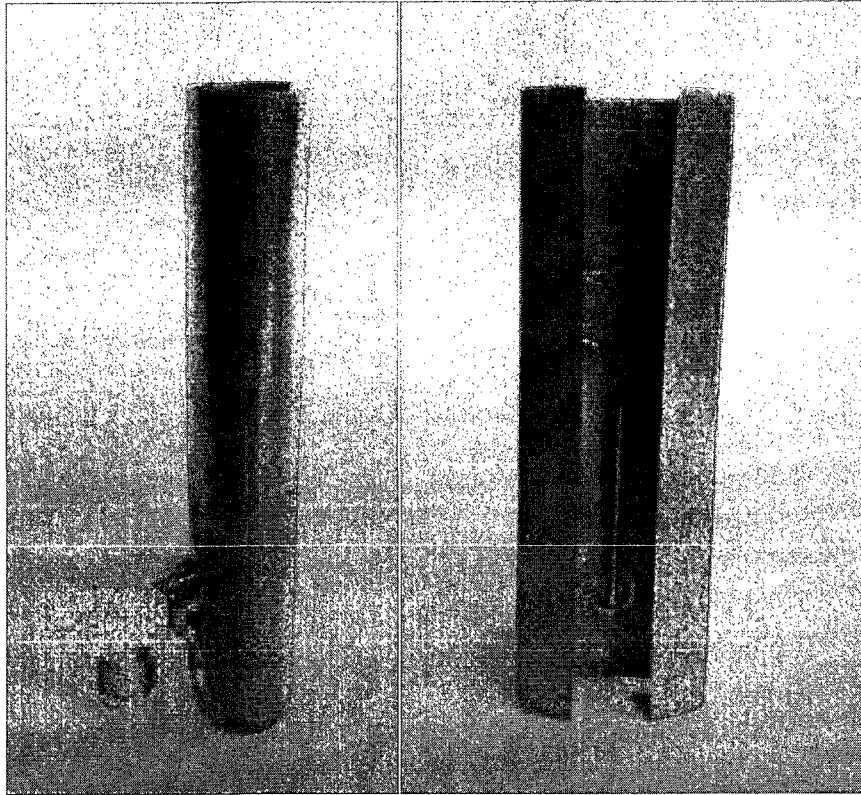


Figure 5.16 – Photographs of fabricated non-coated elliptic slot antenna.

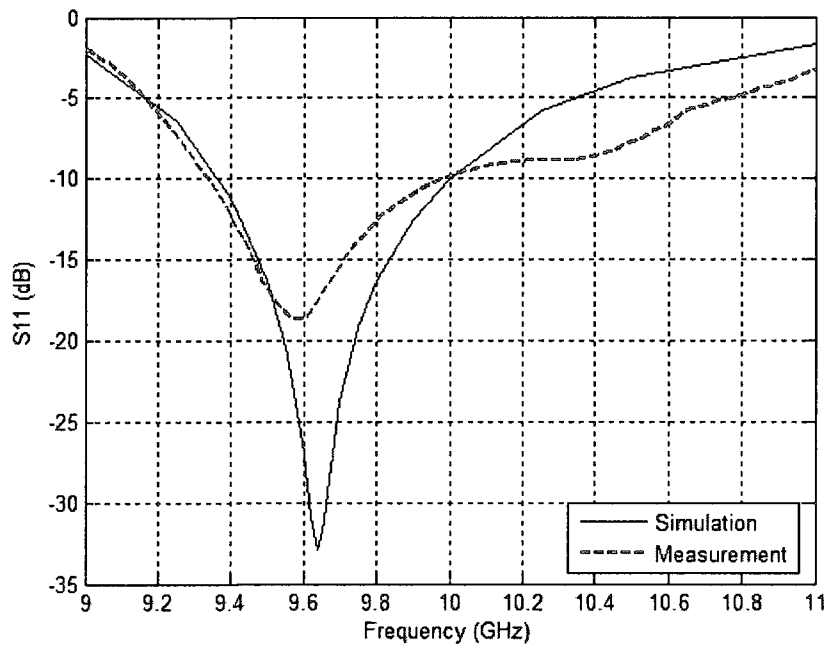


Figure 5.17 – The simulation and measurement results of non-coated elliptic slot antenna.

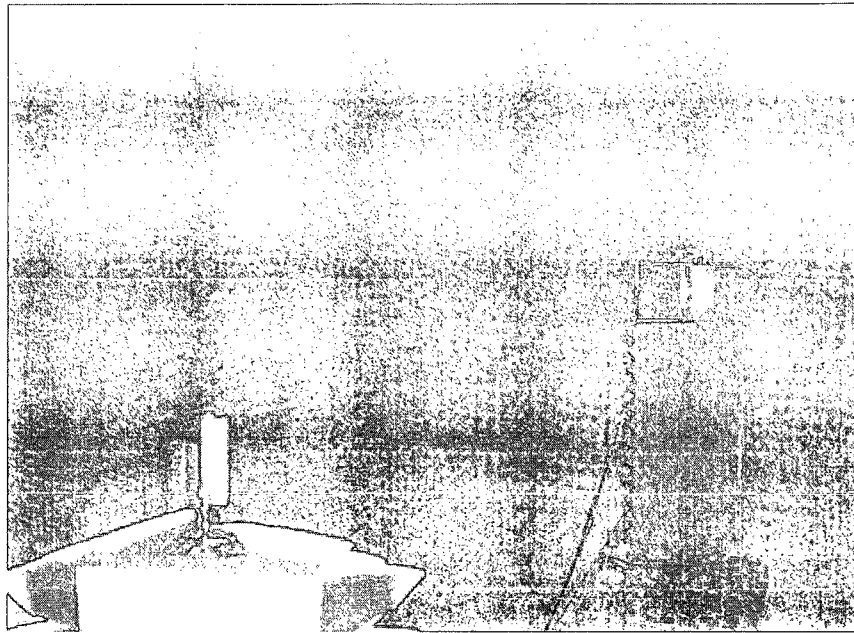


Figure 5.18 – Photograph of non-coated elliptic slot antenna under measurement.

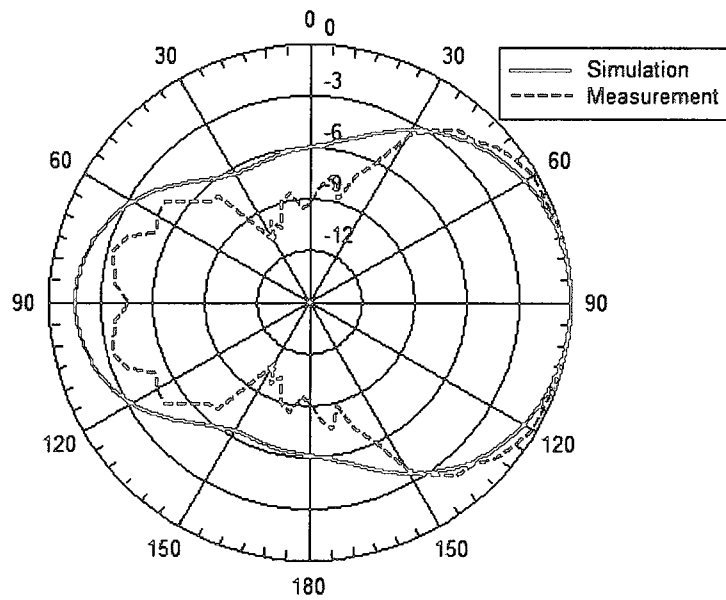


Figure 5.19 – Radiation patterns of non-coated elliptic slot antenna.

The effect of coating material on radiation pattern is measured using partial coating geometry (same as Figure 5.12) where Rogers' standard RT/duroid 5880 high frequency laminate is used. That is a double-side copper clad laminate with thickness 1.575 mm and dielectric constant, $\epsilon_r = 2.20$. A piece of this laminate is installed on elliptic slot antenna by tape, after removing the copper from both sides. Figure 5.20 shows the photograph of fabricated elliptic slot antenna partial coated by this dielectric. The coated dielectric covered slot and extended almost $\lambda/4$ both sides of slot.

Figure 5.21 shows the simulation and measurement results for S11 of the partial coated elliptic slot antenna. As shown in this figure the minimum value of simulation result is almost -24.4 dB at frequency 9.51 GHz, while the minimum value of measurement result is almost -14.9 dB at frequency 9.56 GHz. We can see the effect of coating material on S11 by comparison of the simulations and measurements results due to non-coated and partial coated elliptic slot antenna as shown in Figures 5.17 and 5.21. It is observable that the minimum values of the results due to coated elliptic slot antenna occur at lower frequencies. This shift for simulation result is more than the shift for measurement result.

The partial coated elliptic slot antenna is installed in anechoic chamber to measure the radiation pattern (Figure 5.22). Figure 5.23 shows the corresponding simulation and measurement radiation patterns. Again, the main lobe of measurement result is in very good agreement with the main lobe of simulation result, and there are some disagreements for side lobes and back lobe. By comparison of the results in Figures 5.19 and 5.23, it is observable that the radiation patterns due to partial coating become more

directed to desire angle. The simulations results show that the coated dielectric more affects on side lobes, while the measurements results show it more affects on back lobe.

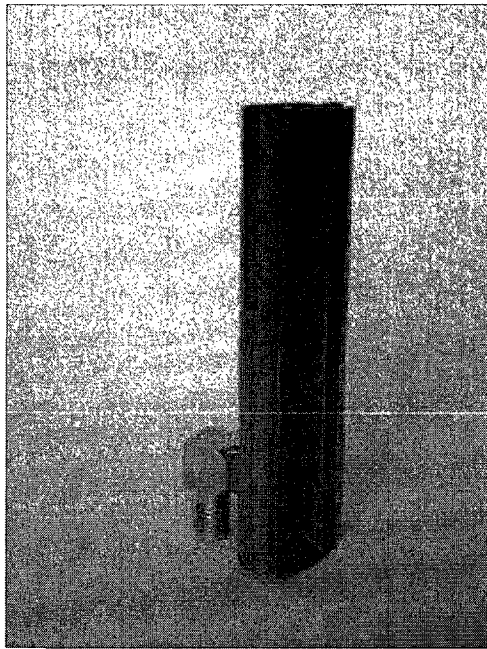


Figure 5.20 – Photograph of fabricated elliptic slot antenna partial coated by dielectric.

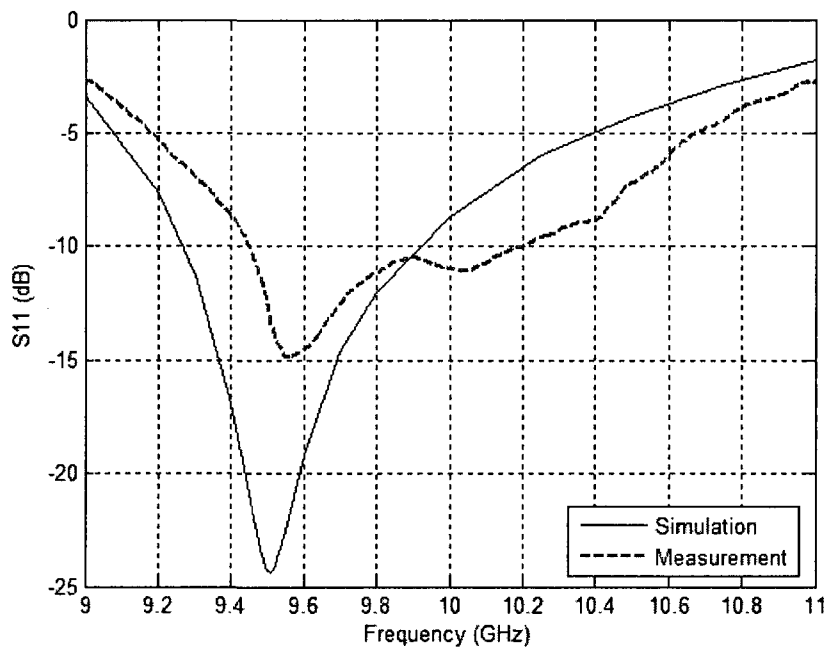


Figure 5.21 – The simulation and measurement results of coated elliptic slot antenna.

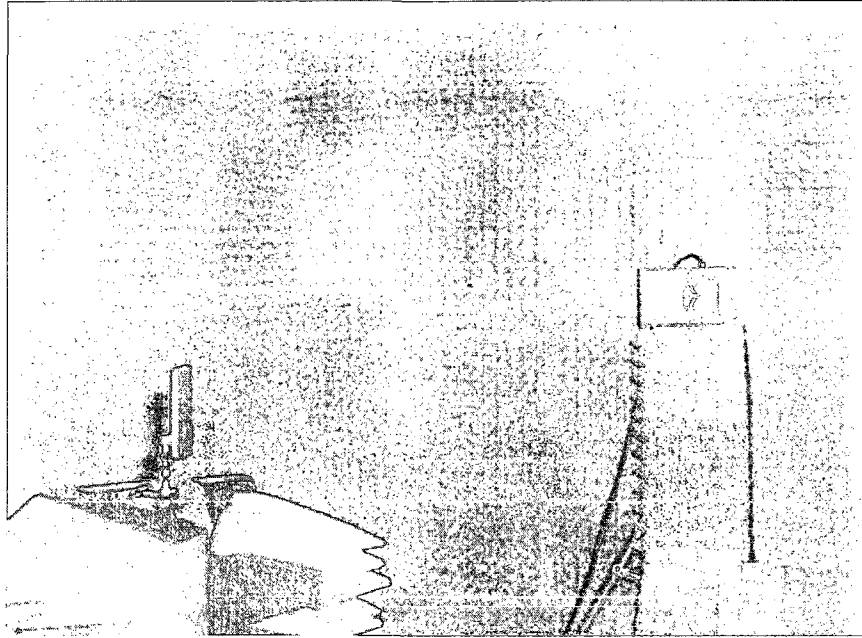


Figure 5.22 – Photograph of partial coated elliptic slot antenna under measurement.

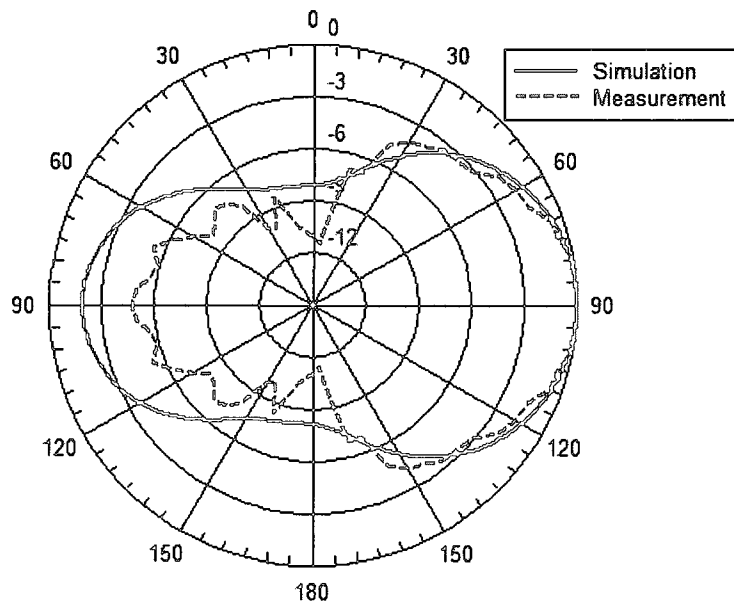


Figure 5.23 – Radiation patterns of partial coated elliptic slot antenna.

As shown in this section, there are some disagreements between the simulations and measurements results. One reason for these disagreements is the shape of elliptic cylinder. The elliptic cylinder is hand made using copper sheet and some simple tools trying to make an exact shape. However, it is not made as a perfect elliptic cylinder. A second reason is the installation of monopole. The location of monopole inside the cylinder is very important. By many simulations it is found that the results are very sensitive to the location of monopole. Also, it must be exactly parallel to the cylinder. The monopole is installed by a 90-degree connector. Since the surface of cylinder is not flat, installation of connector was not an easy task. Therefore, the location and orientation of monopole were not easily controllable. The third reason which may applicable for dielectric-coated antenna is the installation of coating material. The coating dielectric is installed by a tape which may result in a small gap between the cylinder and dielectric.

There are some other reasons that may affect measured results while in simulation, perfect conditions are considered. For example, for feeding the antenna a coaxial line is simulated while in fabrication a 90-degree connector is used.

6. Conclusions and Future Works

6.1 Conclusions

The characteristics of a slot antenna on a perfectly conducting elliptic cylinder coated by different kinds of materials have been investigated. To realistically model some practical geometries and environmental conditions, as well as, to increase the number of design degrees of freedom, the geometry with nonconfocal coating is considered. The chiral media is considered for the coating region in order to develop a general solution that is applicable to different coating types. Two elliptic cylindrical coordinate systems (local and global) are considered. The analysis is carried out by expressing the fields in and around the cylinder in terms of Mathieu and modified Mathieu functions using the separation of variables and exact boundary value technique. The expansion coefficients are found by applying the boundary conditions and employing the addition theorem and orthogonality properties of the Mathieu functions.

The analytical technique is used for exact formulation, generating accurate numerical results, and studying the effects of different geometries and materials parameters. Prototypes of non-coated and dielectric-coated elliptic slot antennas are designed and fabricated. The measurement results for non-coated and dielectric-coated elliptic slot antennas are compared to the results which are simulated using the commercial software Ansoft's HFSS.

In Chapter 2, background of slot antennas and some materials (i.e., dielectric, isorefractive, metamaterials, and chiral media) and details of the electromagnetic

behaviors and applications of these materials are reviewed. Also, idea technique to produce an artificial material in general form with soft and flexible host media is presented.

In Chapter 3, wave equations and eigenfunction expansions are expressed for different regions of the slotted elliptic cylinder loaded and coated with nonconfocal chiral media. The unknown expansion coefficients and other required quantities are determined after applying the boundary conditions and transformation of the field components (inside the coating area) in terms of the global coordinate system.

In Chapter 4, the accuracy and validation of formulations and associated software program are verified in two ways. Some generated numerical results for special cases are compared to the generated numerical results by other researchers, and some other ones are compared to the simulated results by HFSS. The analytical results for antenna gain and aperture conductance (in transmitting mode), and for aperture voltage (in receiving mode) are also presented and discussed.

Details of the simulation, design, fabrication, and measurement of the elliptic slot antenna are given in Chapter 5. The non-coated and dielectric-coated elliptic slot antennas are fabricated and the measured and simulated results are compared and discussed.

The formulation for slot antennas mounted on elliptic cylinder geometry coated by different kinds of nonconfocal materials offers a general solution with many parameters to control the radiated power and other characteristics of the antenna. This solution can be used for many applications which need circular or elliptic cylinder geometry with many design parameters, i.e. geometry size, materials parameters, location

and orientation of core and coated cylinders. Based on the properties of materials and geometries used in this work and the analytical and experimental results, the following conclusions are summarized:

- **Antenna Gain and Coating Materials:** The generated numerical results due to the elliptic cylinder coated by chiral media show that the antenna gain increases by increasing the chirality. For the considered cases, this behaviour is demonstrated for both TM and TE cases, and for co- and cross-polarized waves. In addition, the generated numerical results corresponding different kinds of coating materials (i.e., dielectric, isorefractive, metamaterial, and chiral media) show that the antenna gain due to chiral media coating is more than the gains due to other coating materials for both TM and TE cases.
- **Antenna Gain and Coating Thickness:** The generated numerical results show that the antenna gain due to chiral media coating increases by increasing the chirality and by increasing the coating thickness. Also, by increasing the coating thickness, the gains due to dielectric coating increases while the gain due to isorefractive coating decreases.
- **Aperture Conductance and Coating Thickness:** The results show that, in general, the aperture conductance due to chiral media coating increases by increasing the chirality. Also, the aperture conductance due to chiral media coating is more than the aperture conductance due to other coating materials.
- **Aperture Voltage and Incident Angles:** As maybe expected, the generated numerical results show that the maximum value of aperture voltage is when the incident wave angle is directed towards the centre of the slot. Also, the aperture

voltage decreases when the incident angle gets far away from the centre of the slot in either direction.

- **Aperture Voltage and Coating Materials:** The results due to the elliptic cylinder coated by chiral media show that the aperture voltage increases by increasing the chirality. Also, the generated numerical results of the aperture voltages due to different coating materials show that the aperture voltage due to chiral media coating is more than the aperture voltages due to non-coating or other coating materials. The results also show that the aperture voltage due to dielectric coating increases by increasing the dielectric constant.
- **Aperture Voltage and Loading Materials:** The generated numerical results show that (while the coated material is a chiral media) the most and the least values of the aperture voltage are due to metamaterial loading and non-loading material (free space), respectively.
- **Measured and Simulated Results:** It is observable that the minimum values of S_{11} for the measured and simulated results due to dielectric-coated elliptic slot antenna occur at lower frequencies than the expected value. This shift for simulated results is more than the shift for measured results. Also, the radiation patterns due to dielectric-coated elliptic slot antenna are more directed to desire angle. The simulated results show that the coated dielectric has more affects on side lobes, while the measured results show it affects more the back lobe.
- **Comparison of the Measured and Simulated Results:** Comparison of the measured and simulated results shows some disagreements between these results. Some reasons for these disagreements can be summarized as follow. The first

reason is the shape of elliptic cylinder which is handmade and not made as a perfect elliptic cylinder. The second reason is the installation of monopole. From the simulations it is found that the results are very sensitive to the location of monopole. Also, it must be exactly parallel to the cylinder. Since the surface of cylinder is not flat, installation of a connector was not easy. Therefore, the location and orientation of monopole may not exactly correct. The third reason which may applicable for dielectric-coated antenna is the installation of coating material. The coating dielectric is installed by a tape which may results in a small gap between the cylinder and dielectric.

- **Slot Location and Back Lobe:** From the generated numerical results it is observed that in general, elliptic slot antennas with slot located on the minor axis (centered at 90°) have larger back lobe compared to antennas with slot located on the major axis (centered at 0°). However, to simplify the fabrication, the fabricated antenna is an elliptic slot antenna with the slot located on the minor axis. Therefore, the measured and simulated results show a large back lobe.

6.2 Contributions

The main research contributions of these theoretical and experimental works are given as follows,

- Slot antenna on elliptic cylinder geometry, with unknown aperture fields, coated by materials is proposed for the first time in studying of the coupling properties of slotted elliptic cylinder coated by dielectric/metamaterials [16]. The effect of

loaded and coated materials (i.e., dielectric and metamaterials) on the electric fields is investigated using line and plane wave sources.

- A general solution for the problem of slotted conducting elliptic cylinder coated by chiral media is given and the effects of geometrical and material parameters on antenna gain for different kinds of confocal [153] and nonconfocal [154] coating materials are studied. The problem formulation for chiral medium is more complicated but can be used for other materials as well.
- The general formulation has also been extended and applied to scattering problems involving parallel elliptic cylinders where the addition theorem for Mathieu function is used. The exact solutions to the multiple scattering by M parallel two-layer elliptic cylinders are developed and presented in [75] and [77]. The effect of different geometrical and materials parameters on the monostatic and bistatic echo widths (radar cross sections) are investigated and discussed.
- The general solution for the slotted elliptic cylinder loaded and coated with nonconfocal materials is applied to studying the characteristics of slot antennas in the receiving mode using different geometrical and materials parameters. The aperture field distribution on the slot is obtained as part of the general solution [16], [153], [154]. For the proposed geometry and to the best of our knowledge, other works in open literature assume the aperture field without taken into account the coupling between the interior and exterior fields of the slot antenna.
- Design, fabrication and testing of two prototypes: non-coated and dielectric-coated elliptic slot antennas. The simulated and measured results are reasonably in good agreement. This contribution is in the process of submission for publication.

- Furthermore, efficient algorithms for calculating the elliptic cylinder wave functions are developed using the software package MATLAB. The algorithm developed here for calculating the Mathieu functions is compact, fast, and efficient, and compared well with other results in the literature.

6.3 Future Works

To extend the work reported in this thesis, future works can be divided into two categories. The first category is investigating a new geometry of slot antenna coated by different kinds of materials and the second category is to study implementation techniques of artificial materials.

Investigating the characteristics of an antenna with N axial slots on a perfectly conducting elliptic cylinder loaded and coated with different kinds of materials, is an interesting topic for cylindrical slot antennas that may be used as base station antennas. The locations of the slots can be varied in a general solution to control both the direction and strength of the radiated field. The solution can be considered for confocal or nonconfocal coatings.

According to the technique presented in Chapter 2, a study to make artificial materials in a soft and flexible host media is another interesting subject. Producing artificial materials in a general form by embedding a three-dimensional array of objects in a soft host media (i.e. soft plastic) may need an advanced fabrication technology. However, it could be made easier using layers of foam and embedding arrays of objects in each layer. The objects can be wires and ring resonators for metamaterial or helices for chiral media.

References

1. T. M. Smith and K. E. Golden, "Radiation Patterns from a Slotted Cylinder Surrounded by a Plasma Sheath," *IEEE Transactions on Antennas and Propagation*, pp. 775-780, Sep. 1965.
2. L. Shafai, "Radiation from an Axial Slot Antenna Coated with a Homogeneous Material," *Canadian J. Phys.*, Vol. 50, pp. 23-27, 1972.
3. J. H. Richmond and M. C. Gilreath, "Flush-Mounted Dielectric-Loaded Axial Slot on Circular Cylinder," *IEEE Transactions on Antennas and Propagation*, Vol. AP-23, No. 3, pp. 348-351, May 1975.
4. J. Chalupa, "Asymptotic Surface Field of Slot Antenna on Coated Cylindrical Conductor," *IEEE Electronics Letters*, Vol. 25, No. 24, pp. 1657-1659, 1989.
5. X. B. Wu and W. Ren, "Axial Slot Antenna on an Anisotropic Dielectric-Coated Circular Cylinder," *IEE Proceeding Microwave Antennas Propagation*, Vol. 141, No. 6, pp. 527-530, Dec. 1994.
6. H. A. Ragheb and E. E. Hassan, "Radiation Characteristic of Slots on Conducting Circular Cylinder Covered by Eccentric Dielectric Cylinder," *IEE Proceeding Microwave Antenna Propagation*, Vol. 142, No. 2, pp. 168-172, April 1995.
7. O. Aydin and A. Hizal, "Radiation Characteristics of Slot Excited Cylindrical Antenna Coated by Layered Anisotropic Material," *IEEE, MELECON '96*, 8th Mediterranean, Vol. 3, pp. 1404-1406, May 13-16, 1996.

8. M. A. Mushref, "TM Radiation from an Eccentric Dielectric Coated Cylinder with Two Axial Slots," *Journal of Electromagnetic Waves and Applications*, Vol. 19, No. 5, pp. 577–590, 2005.
9. M. Hussein, A. Sebak, and M. Hamid, "Scattering and coupling properties of a Slotted Elliptic Cylinder," *IEEE Transaction on Electromagnetic Compatibility*, Vol. 36, No. 1, pp. 76-81, Feb. 1994.
10. T. Hinata and H. Hosono, "Scattering of Electromagnetic Waves by an Axially Slotted Conducting Elliptic Cylinder," *MMET'96 Proceedings*, Ukraine, pp. 28-31, Sep. 10-13, 1996.
11. J. H. Richmond, "Axial Slot Antenna on Dielectric-Coated Elliptic Cylinder," *IEEE Transactions on Antennas and Propagation*, Vol. 37, No. 10, pp. 1235-1241, Oct. 1989.
12. H. A. Ragheb, A. Sebak, and L. Shafai, "Radiation by Axial Slots on a Dielectric-Coated Nonconfocal Conducting Elliptic Cylinder," *IEE Proc. Microwave Antennas Propagation*, Vol. 143, No 2, pp. 124-130, April 1996.
13. M. I. Hussein and A. K. Hamid, "Radiation by Axial Slot Elliptical Antenna Coated by a Lossy Dielectric Material," *IEEE International Symposium on Electromagnetic Compatibility, EMC'03*, Istanbul, pp. 146-149, May 16-16, 2003.
14. M. I. Hussein and A. K. Hamid, "Radiation Characteristics of N Axial Slot Antenna on a Lossy Dielectric-Coated Elliptic Cylinder," *Can. J. Phys.* 82, pp. 141-149, 2004.
15. A. K. Hamid, "Study of Lossy Effects on the Characteristics of Axially Slotted Circular or Elliptical Cylindrical Antennas Coated with Metamaterials," *IEE Proceedings Mic. Antennas Propagation*, Vol. 152, No. 6, pp. 485-490, Dec. 2005.

16. B. N. Khatir and A. Sebak, "Coupling Properties of Slotted Elliptic Cylinder Coated by Dielectric/Metamaterials," *URSI GA08*, Chicago, USA, August 7-16, 2008.
17. Ansoft's HFSS, Version 10.1.2, *Ansoft Corporation*, Pittsburg, PA, Build 28, September 2006.
18. A. Alford. "Long Slot Antennas," *Proc. Nat. Elect. Conf.*, Vol. 2, 1946.
19. G. Sinclair, "The Patterns of Slotted-Cylinder Antennas," *Proc. IRE*, Vol. 36, pp. 1487-1492, Dec. 1946.
20. G. Sinclair, E. C. Jordan, and E. W. Vaughan. "Measurement of Aircraft-Antenna Patterns Using Models," *Proc. IRE*, Vol. 35, pp. 1451-1452, Dec. 1947.
21. S. Silver and W. K. Saunders, "The External Field Produced by a Slot in an Infinite Circular Cylinder," *Jour. Appl. Phys.* Vol. 21, pp. 745-749, Aug. 1950.
22. J. R. Wait, *Electromagnetic Radiation from Cylindrical Structures*, Pergamon Press, Inc., New York, NY, 1959.
23. E. W. Wolff, *Antenna Analysis*, John Wiley & Sons, Inc., USA, 1966.
24. N. Engheta and R. W. Ziolkowski, *Metamaterials: Physics and Engineering Explorations*, John Wiley & Sons, Inc., USA, 2006.
25. J. C. Bose, "On the Rotation of Plane of Polarisation of Electric Waves by a Twisted Structure," *Proc. Roy. Soc.*, Vol. 63, pp. 146-152, 1898.
26. I. V. Lindell, A. H. Sihvola, and J. Kurkijarvi, "Karl F. Lindman: The last Hertzian, and a Harbinger of electromagnetic chirality," *IEEE Antennas Propagation Magazine*, Vol. 34, No. 3, pp. 24-30, June 1992.
27. W. E. Kock, "Metallic delay lenses," *Bell Sys. Tech. J.*, Vol. 27, pp. 58-82, 1948.

28. J. Daintith, *Biographical Encyclopedia of Scientists*, CRC Press, ISBN 0750302879, page 943, 1994.
29. A. R. V. Hippel, *Dielectric Materials and Applications*, Technology Press of MIT and John Wiley, NY, 1954.
30. P. L. E. Uslenghi and S. Roy, "Waveguiding Structures Containing Isorefractive Materials," *Asia Pacific Microwave Conference*, pp. 581-583, 1997.
31. P. L. E. Uslenghi, "Exact Scattering by Isorefractive Bodies," *IEEE Transactions on Antennas and Propagation*, Vol. 45, No. 9, pp. 1382-1385, Sep. 1997.
32. P. L. E. Uslenghi and R. E. Zich, "Radiation and Scattering from Isorefractive Bodies of Revolution," *IEEE Transaction on Antennas and Propagation*, Vol. 46, No. 11, pp. 1606-1611, Nov. 1998.
33. P. L. E. Uslenghi, "Exact Penetration, Radiation, and Scattering for a Slotted Semielliptical Channel Filled with Isorefractive Material," *IEEE Transactions on Antennas and Propagation*, Vol. 52, No. 6, pp. 1473-1480, June 2004.
34. C. Berardi, D. Erricolo, and P. L. E. Uslenghi, "Exact Dipole Radiation for an Oblate Spheroidal Cavity Filled with Isorefractive Material and Aperture-Coupled to a Half Space," *IEEE Trans. on Ant. and Propag.*, Vol. 52, No. 9, pp. 2205-2213, Sep. 2004.
35. D. Erricolo and P. L. E. Uslenghi, "Exact Radiation and Scattering for an Elliptic Metal Cylinder at the Interface between Isorefractive Half-Spaces," *IEEE Trans. on Antennas and Propagation*, Vol. 52, No. 9, pp. 2214-2225, Sep. 2004.
36. D. Erricolo and P. L. E. Uslenghi, "Penetration, Radiation, and Scattering for a Cavity-Backed Gap in a Corner," *IEEE Transactions on Antennas and Propagation*, Vol. 53, No. 8, pp. 2738-2748, Aug. 2005.

37. D. Erricolo and P. L. E. Uslenghi, "Exact Radiation for Dipoles on Metallic Spheroids at the Interface between Isorefractive Half-Spaces," *IEEE Transactions on Antennas and Propagation*, Vol. 53, No. 12, pp. 3974-3981, Dec. 2005.
38. J. Liang and P. L. E. Uslenghi, "Exact Scattering by Isorefractive Paraboloidal Radomes," *IEEE Transactions on Antennas and Propagation*, Vol. 55, No. 6, pp. 1546-1553, June 2007.
39. D. Erricolo, M. D. Lockard, C. M. Butler, and P. L. E. Uslenghi, "Currents on Conducting Surfaces of a Semielliptical-Channel-Backed Slotted Screen in an Isorefractive Environment," *IEEE Transactions on Antennas and Propagation*, Vol. 53, No. 7, pp. 2350-2356, July 2005.
40. L. W. Li, H. G. Wee, T. S. Yeo, and M. S. Leong, "Analysis of Scattering by a Dielectric Elliptical Cylinder Using Radiation-To-Scattering Transform," *IEEE*, pp. 2348-2351, 2000.
41. S. Caorsi and M. Pastorino, "Scattering by Multilayer Isorefractive Elliptic Cylinders," *IEEE Transactions on Antennas and Propagation*, Vol. 52, No. 1, pp. 189-196, Jan. 2004.
42. L. W. Li, H. G. Wee, and M. S. Leong, "Dyadic Green's Functions Inside/Outside a Dielectric Elliptical Cylinder: Theory and Application," *IEEE Transactions on Antennas and Propagation*, Vol. 51, No. 3, pp. 564-574, March 2003.
43. J. S. Tyo, "A Class of Artificial Materials Isorefractive with Free Space," *IEEE Trans. on Antennas and Propagation*, Vol. 51, No. 5, pp. 1093-1099, May 2003.
44. R. M. Walser, in: W. S. Weiglhofer and A. Lakhtakia, *Introduction to Complex Mediums for Electromagnetics and Optics*, SPIE Press, Bellingham, WA, USA, 2003.

45. V. G. Veselago, "The electrodynamics of substances with simultaneously negative values of ϵ and μ ," *Sov. Phys. Uspekhi*, Vol. 10, No. 4, pp. 509–514, 1968.
46. D. R. Smith, W. J. Padilla, D. C. Vier, S. C. N. Nasser, and S. Schultz, "Composite medium with simultaneously negative permeability and permittivity," *Physical Review Letters*, Vol. 84, No. 18, pp. 4184–4187, May 2000.
47. R. A. Shelby, D. R. Smith, S. C. N. Nasser, and S. Schultz, "Microwave Transmission through a Two-Dimensional, Isotropic, Left-Handed Metamaterial," *Applied Physics Letters*, Vol. 78, No. 4, pp. 489-491, Jan. 2001.
48. R. A. Shelby, D. R. Smith, and S. Schultz, "Experimental verification of a negative index of refraction," *Science*, Vol. 292, No. 5514, pp. 77–79, April 2001.
49. N. Engheta, "An Idea for Thin Subwavelength Cavity Resonators Using Metamaterials with Negative Permittivity and Permeability," *IEEE Antennas and Wireless Propagation Letters*, Vol. 1, pp. 10-13, 2002.
50. R. W. Ziolkowski, "Double Negative Metamaterial Design, Experiments, and Applications," *IEEE Antennas and Propagation Society International Symposium*, Vol. 2, pp. 396-399, June 16-21, 2002.
51. A. Alu and N. Engheta, "Pairing an Epsilon-Negative Slab With a Mu-Negative Slab: Resonance, Tunneling and Transparency," *IEEE Transactions on Antennas and Propagation*, Vol. 51, No. 10, pp. 2558-2571, Oct. 2003.
52. M. Caiazzo, S. Maci, and N. Engheta, "A Metamaterial Surface for Compact Cavity Resonators," *IEEE Antennas and Wireless Prop. Letters*, Vol. 3, pp. 261-264, 2004.
53. A. Alù and N. Engheta, "Guided Modes in a Waveguide Filled With a Pair of Single-Negative (SNG), Double-Negative (DNG), and/or Double-Positive (DPS) Layers,"

- IEEE Transactions on Microwave Theory and Techniques*, Vol. 52, No. 1, pp. 199-210, Jan. 2004.
54. A. Erentok, P. L. Luljak, and R. W. Ziolkowski, "Characterization of a Volumetric Metamaterial Realization of an Artificial Magnetic Conductor for Antenna Applications," *IEEE Transactions on Antennas and Propagation*, Vol. 53, No. 1, pp. 160-172, Jan. 2005.
55. S. Arslanagic, R. W. Ziolkowski, and O. Breinbjerg, "Line Source Excitation of Multilayered Metamaterial Cylinders: Source and Scattering Results," *IEEE*, pp. 676-679, 2006.
56. A. Alù, F. Bilotti, N. Engheta, and L. Vegni, "Metamaterial Covers Over a Small Aperture," *IEEE Transactions on Antennas and Propagation*, Vol. 54, No. 6, pp. 1632-1643, June 2006.
57. S. Arslanagic, R. W. Ziolkowski, and O. Breinbjerg, "Excitation of an Electrically Small Metamaterial-Coated Cylinder by an Arbitrarily Located Line Source," *Microwave and Optical Technology Letters*, Vol. 48, No. 12, pp. 2598-2606, Dec. 2006.
58. A. Alù, F. Bilotti, N. Engheta, and L. Vegni, "Subwavelength, Compact, Resonant Patch Antennas Loaded with Metamaterials," *IEEE Transactions on Antennas and Propagation*, Vol. 55, No. 1, pp. 13-25, Jan. 2007.
59. A. Alù, F. Bilotti, N. Engheta, and L. Vegni, "Subwavelength Planar Leaky-Wave Components with Metamaterial Bilayers," *IEEE Transactions on Antennas and Propagation*, Vol. 55, No. 3, pp. 882-891, March 2007.

60. C. Li and Z. Shen, "Electromagnetic Scattering by a Conducting Cylinder Coated with Metamaterials," *Progress In Electromag. Research*, PIER 42, pp. 91–105, 2003.
61. J. D. Baena, R. Marques, J. Martel, and F. Medina, "Experimental Results on Metamaterial Simulation Using SRR-Loaded Waveguides," *IEEE Antennas and Propag. Society International Symposium*, Vol. 1, pp. 106-109, June 22-27, 2003.
62. Y. Xu, "Wave Propagation in Rectangular Waveguide Filled with Single Negative Metamaterial Slab," *Electronics Letters*, Vol. 39, No. 25, Dec. 2003.
63. A. Akyurtlu and D. H. Werner, "A Novel Dispersive FDTD Formulation for Modeling Transient Propagation in Chiral Metamaterials," *IEEE Transactions on Antennas and Propagation*, Vol. 52, No. 9, pp. 2267-2276, Sep. 2004.
64. J. Huangfu, L. Ran, H. Chen, X. Zhang, K. Chen, T. M. Grzegorzcyk, and J. A. Kong, "Experimental Confirmation of Negative Refractive Index of a Metamaterial Composed of Ω -Like Metallic Patterns," *App. Phy. Let.*, Vol. 84, No. 9, pp. 1537-1539, March 2004.
65. H. Cory and C. Zach, "Wave Propagation in Metamaterial Multi-Layered Structures," *Microwave and Optical Technology Letters*, Vol. 40, No. 6, pp. 460-465, March 2004.
66. S. Hrubar, J. Bartolic, and Z. Sipus, "Waveguide Miniaturization Using Uniaxial Negative Permeability Metamaterial," *IEEE Transactions on Antennas and Propagation*, Vol. 53, No. 1, pp. 110-119, Jan. 2005.
67. F. Zhu, Q. Lin, and J. Hu, "A Directive Patch Antenna with a Metamaterial Cover," *IEEE-APMC2005 Proceedings*, 2005.

68. X. Dardenne and C. Craeye, "ASM Based Method for the Study of Periodic Metamaterials Excited by a Slotted Waveguide," *IEEE Antennas and Propagation Society International Symposium*, Vol. 1A,, pp. 692-695, July 3-8, 2005.
69. J. Sun, W. Sun, T. Jiang, and Y. Feng, "Directive Electromagnetic Radiation of a Line Source Scattered by a Conducting Cylinder Coated with Left-handed Metamaterial," *Microwave and Optical Technology Letters*, Vol. 47, No. 3, pp. 274-279, Nov. 2005.
70. I. A. Eshrah, A. A. Kishk, A. B. Yakovlev, and A. W. Glisson, "Rectangular Waveguide With Dielectric-Filled Corrugations Supporting Backward Waves," *IEEE Transactions on Microwave Theory and Techniques*, Vol. 53, No. 11, pp. 3298-3304, Nov. 2005.
71. I. A. Eshrah, A. A. Kishk, A. B. Yakovlev, and A. W. Glisson, "Spectral Analysis of Left-Handed Rectangular Waveguides With Dielectric-Filled Corrugations," *IEEE Transactions on Antennas and Propagation*, Vol. 53, No. 11, pp. 3673-3683, Nov. 2005.
72. S. Hrabar, J. Bartolic and Z. Sipus, "Waveguide Miniaturization Using Uniaxial Negative Permeability Metamaterial," *IEEE Transactions on Antennas and Propagation*, Vol. 53, No. 1, pp. 110-119, Jan. 2005.
73. A. Shooshtari and A. R. Sebak, "Electromagnetic Scattering by Parallel Metamaterial Cylinders," *Progress In Electromagnetics Research*, PIER 57, pp. 165–177, 2006.
74. H. Y. Yao, L. W. Li, and C. W. Qiu, "Electromagnetic Scattering Properties in a Multilayered Metamaterial Cylinder," *IEEE MELECON - Spain*, pp. 246-249, May 2006.

75. B. N. Khatir and A. Sebak, "Transverse Electric Wave Scattering by Parallel Two-Layer Elliptic Cylinders," *EMTS*, Ottawa, Canada, July 26-28, 2007.
76. M. A. Mushref, "Closed solution to electromagnetic scattering of a plane wave by an eccentric cylinder coated with metamaterials," *Optics Com.* 270, pp. 441–446, 2007.
77. B. N. Khatir and A. R. Sebak, "Electromagnetic Wave Scattering by Parallel Dielectric/Metamaterial Coated Elliptic Cylinders," *International Review on Modelling and Simulations (IREMOS)*, Vol. 0, No. 0, pp. 41-48, August 2008.
78. J. D. Wilson, Z. D. Schwartz, C. T. Chevalier, A. N. Downey, and K. R. Vaden, "Flat Lens Focusing Demonstrated With Left-Handed Metamaterial," *National Aeronautics and Space Administration (NASA)*, Jan. 2005.
79. F. A. Cotton and G. Wilkinson, *Advanced Inorganic Chemistry: a Comprehensive Text*, Forth Edition, John Wiley & Sons, Inc., NY, p. 47, 1980.
80. <http://www.mi.sanu.ac.yu/vismath/schulze/metaeder/metaeder1/geometrie/chiral>
81. A. Bessette, "Hands on Chemistry: Chirality," *Bryn Mawr Alumnae Bulletin*, Bryn Mawr College, Sep. 2001.
82. J. Applequist, "Optical Activity: Biot's Bequest," *Amer. Scientist*, Vol. 75, pp. 58-68, 1987.
83. M. H. Winkler, "An experimental investigation of some models for optical activity," *J. Phys. Chem.*, Vol. 60, pp. 1656-1659, Dec. 1956.
84. I. Tinoco and M. P. Freeman, "The optical activity of oriented copper helices: I. Experimental," *J. Phys. Chem.*, Vol. 61, p. 1196, 1957.
85. I. Tinoco and R. W. Woody, "Optical rotation of oriented helices 11. Calculation of the rotatory dispersion of the α helix," *J. Phys. Chem.*, Vol. 32, p. 461, 1960.

86. T. Guire, V. V. Varadan, and V. K. Varadan, "Influence of Chirality on the Reflection of EM Waves by Planar Dielectric Slabs," *IEEE Transactions on Electromagnetic Compatibility*, Vol. 32, No. 4, pp. 300-303, Nov. 1990.
87. J. Svigelj, E. Michielssen, and R. Mittra, "Numerical Study of Chiral Properties of the Wire Helix," *IEEE Antennas and Propagation Society International Symposium*, Vol. 2, pp. 695-698, July 18-25, 1992.
88. I. V. Lindell and A. J. Viitanen, "Plane Wave Propagation in Uniaxial Bianisotropic Medium," *Electronics Letters*, Vol. 29, No. 2, pp. 150-152, Jan. 1993.
89. A. J. Viitanen and I. V. Lindell, "Uniaxial Chiral Quarter-Wave Polarisation Transformer," *Electronics Letters*, Vol. 29, No. 12, pp. 1074-1075, June 1993.
90. A. J. Bahr and K. R. Clausing, "An Approximate Model for Artificial Chiral Material," *IEEE Trans. on Antennas and Propagation*, Vol. 42, No. 12, pp. 1592-1599, Dec. 1994.
91. K. W. Whites, "Full-Wave Computation of Constitutive Parameters for Lossless Composite Chiral Materials," *IEEE Transactions on Antennas and Propagation*, Vol. 43, No. 4, pp. 376-384, April 1995.
92. M. Zhang and W. X. Zhang, "The Chirality from Microstructure of Conductive Twist Strips," *IEEE Antennas and Propagation Society International Symposium*, Vol. 1, pp. 414-417, June 18-23, 1995.
93. S. A. Tretyakov, T. G. Kharina, A. A. Sochava, and S. Bolioli, "Measurements and Theory of Reflection and Transmission in Bianisotropic Omega Composites," *IEEE Antennas and Propagation Society International Symposium*, Vol. 4, pp. 1864-1867, June 18-23, 1995.

94. I. V. Lindell and A. H. Sihvola, "Plane-Wave Reflection from Uniaxial Chiral Interface and Its Application to Polarization Transformation," *IEEE Transactions on Antennas and Propagation*, Vol. 43, No. 12, pp. 1397-1404, Dec. 1995.
95. F. Mariotte, S. A. Tretyakov, B. Sauviac, "Modeling Effective Properties of Chiral Composites," *IEEE Antennas and Propagation Magazine*, Vol. 38, No. 2, pp. 22-32, April 1996.
96. S. A. Tretyakov, F. Mariotte, C. R. Simovski, T. G. Kharina, and J. P. Heliot, "Analytical Antenna Model for Chiral Scatterers: Comparison with Numerical and Experimental Data," *IEEE Transactions on Antennas and Propagation*, Vol. 44, No. 7, pp. 1006-1014, July 1996.
97. M. Bingle, J. H. Cloete and D. B. Davidson, "Microwave Absorption by Chiral, Racemic and Non-Chiral Unit Cells: The Role of Chirality in Absorbing Materials," *IEEE COMSIG '98, Proceedings of the 1998 South African Symposium*, pp. 441-444, Sep. 7-8, 1998.
98. S. Prosvirnin and T. Vasilyeva, "Moment-Method Analysis of Electromagnetic Wave Scattering by Plane Array of Chiral Strip Elements," *MMET 98 Proceedings*, 1998.
99. G. Busse, J. Reinert, and A. F. Jacob, "Waveguide Characterization of Chiral Material: Experiments," *IEEE Transactions on Microwave Theory and Techniques*, Vol. 47, No. 3, pp. 297-301, March 1999.
100. C. R. B. Taylor, P. G. Lederer, F. C. Smith, and S. Haq, "Measurement and Prediction of Helix-Loaded Chiral Composites," *IEEE Transactions on Antennas and Propagation*, Vol. 47, No. 4, pp. 692-700, April 1999.

101. S. Zouhdi, G. E. Couenon, and A. F. Lamer, "Scattering from a Periodic Array of Thin Planar Chiral Structures - Calculations and Measurements," *IEEE Transactions on Antennas and Propagation*, Vol. 47, No. 6, pp. 1061-1065, June 1999.
102. C. A. Moses and N. Engheta, "An Idea for Electromagnetic "Feedforward-Feedbackward" Media," *IEEE Transactions on Antennas and Propagation*, Vol. 47, No. 5, pp. 918-928, July 1999.
103. C. R. Simovski, M. S. Kondratjev, P. A. Belov, and S. A. Tretyakov, "Interaction Effects in Two-Dimensional Bianisotropic Arrays," *IEEE Transactions on Antennas and Propagation*, Vol. 47, No. 9, pp. 1429-1439, Sep. 1999.
104. V. N. Apletalin, P. A. Malyshkin, A. D. Shatrov, and V. S. Solosin, "Back-Scattering from a Chiral Anisotropic Conducting Cylinder with a Longitudinal Slot," *MSMW 2001 Symposium Proceedings - Ukraine*, June 2001.
105. I. V. Semchenko and S. A. Khakhornov, "Artificial Anisotropic Chiral Structures with Dielectric and Magnetic Properties at Oblique Incidence of Electromagnetic Waves," *SBMO/IEEE MTT-S IMOC 2001 Proceedings*, 2001.
106. S. R. Cloude, "Helicity in Radar Remote Sensing," *IEEE Geoscience and Remote Sensing Symposium*, Vol. 1, pp. 411-413, June 24-28, 2002.
107. B. R. Long and D. H. Werner, "Equivalent Circuit Models for Canonical Chiral Elements," *IEEE Antennas and Propagation Society International Symposium*, Vol. 1, pp. 752-755, June 16-21, 2002.
108. B. J. Hu, E. K. N. Yung, and Y. F. Wang, "Resonant Behavior of Scattering by Conducting Infinite Helix," *IEEE Antennas and Propagation Society International Symposium*, Vol. 4, pp. 460-463, June 22-27, 2003.

109. A. Ishimaru, S. W. Lee, Y. Kuga, and V. Jandhyala, "Generalized Constitutive Relations for Metamaterials Based on the Quasi-Static Lorentz Theory," *IEEE Transactions on Antennas and Propagation*, Vol. 51, No. 10, pp. 2550-2557, Oct. 2003.
110. S. G. Lukishova, A. W. Schmid, A. J. McNamara, R. W. Boyd, and C. R. Stroud, "Room Temperature Single-Photon Source: Single-Dye Molecule Fluorescence in Liquid Crystal Host," *IEEE Journal of Selected Topics in Quantum Electronics*, Vol. 9, No. 6, pp. 1512-1518, Nov./Dec. 2003.
111. S. Prosvirnin, "Reciprocity Principle and Electromagnetic Wave Scattering by Plano-Chiral Double-Periodic Array," *IEEE Mathematical Methods in Electromagnetic Theory, 10th International Conference*, pp. 88-93, Sep. 14-17, 2004.
112. P. L. Mladyonov, "Electromagnetic Wave Diffraction by the Microstrip Two-periodic Grating of Chiral Metal Strips," *IEEE Mathematical Methods in Electromagnetic Theory, 10th International Conference*, pp. 513-515, Sep. 14-14, 2004.
113. J. Psilopoulos, C. Meiners, and A. F. Jacob, "A Scattering Approach for the Characterization of Composite Materials," *IEEE Transactions on Antennas and Propagation*, Vol. 53, No. 4, pp. 1507-1513, April 2005.
114. M. Zang, "Band Theory of Single-Walled Carbon Nanotubes," *IEEE Transactions on Nanotechnology*, Vol. 4, No. 4, pp. 452-459, July 2005.
115. C. Meiners and A. F. Jacob, "On the Scattering Properties of Composite Materials," *IEEE Geoscience and Remote Sensing Symposium*, Vol. 1, pp. 566-569, July 25-29, 2005.

116. M. G. Silveirinha, "Linear to Circular Polarization Conversion Using a Metamaterial with Helical Inclusions," *IEEE Antennas and Propagation Society International Symposium*, Vol. 1B, pp. 619-622, 2005.
117. B. K. Canfield, S. Kujala, K. Laiho, and M. Kauranen, "Robust Nonlinear Chiral Responses from Gold Nanoparticle Arrays," *Quantum Electronics and Laser Science Conference (QELS)*, 2005.
118. A. K. Bhattacharyya, "Control of Radar Cross-Section and Cross Polarisation Characteristics of an Isotropic Chiral Sphere," *Electronics Letters*, Vol. 26, No. 14, pp. 1066-1067, July 1990.
119. D. L. Jaggard, N. Engheta, and J. Liu, "Chiroshield: a Salisbury/Dallenbach Shield Alternative," *Electronics Letters*, Vol. 26, No. 17, pp. 1332-1334, Aug. 1990.
120. M. S. Kluskens and E. H. Newman, "Scattering by a Chiral Cylinder of Arbitrary Cross Section," *IEEE Trans. on Antennas and Propag.*, Vol. 38, No. 9, pp. 1448-1455, Sep. 1990.
121. D. L. Jaggard, J. C. Liu, and X. Sun, "Spherical Chiroshield," *Electronics Letters*, Vol. 27, No. 1, pp.77-79, Jan. 1991.
122. M. S. Kluskens and E. H. Newman, "Scattering by Multilayer Chiral Cylinder," *IEEE Transactions on Antennas and Propagation*, Vol. 39, No. 1, pp. 91-96, Jan. 1991.
123. D. J. Hoppe and Y. R. Samii, "Higher Order Impedance Boundary Conditions for Anisotropic and Nonreciprocal Coatings," *IEEE Antennas and Propagation Society International Symposium*, Vol. 4, pp. 1993-1996, July 18-25, 1992.

124. D. L. Jaggard, J. C. Liu, and P. Pelet, "Radiation and Scattering from Thin Wires in Chiral Media," *IEEE Transactions on Antennas and Propagation*, Vol. 40, No. 11, pp. 1273-1282, Nov. 1992.
125. M. Tanaka and A. Kusunoki, "Depolarization Properties of a Chiral Coated Dielectric Cylinder with Application to RCS Reduction," *APMc 93*, Vol. 2, 1993.
126. S. F. Mahmoud, "Characteristics of a Chiral-Coated Slotted Cylindrical Antenna," *IEEE Transactions on Antennas and Propagation*, Vol. 44, No. 7, pp. 814-821, July 1996.
127. Z. Chen, W. Hong, and W. X. Zhang, "Electromagnetic Scattering from a Chiral Cylinder – General Case," *IEEE Transactions on Antennas and Propagation*, Vol. 44, No. 7, pp. 912-917, July 1996.
128. M. A. Al-Kanhal and E. Arvas, "Electromagnetic Scattering from a Chiral Cylinder of Arbitrary Cross Section," *IEEE Transactions on Antennas and Propagation*, Vol. 44, No. 7, pp. 1041-1048, July 1996.
129. J. Reinert, G. Busse, and A. F. Jacob, "Waveguide Characterization of Chiral Material: Theory," *IEEE Transactions on Microwave Theory and Techniques*, Vol. 47, No. 3, pp. 290-296, March 1999.
130. W. Y. Yin, L. W. Li, Z. Z. Wei, and M. S. Leong, "Scattering from Strip-Loaded Composite Chiral Cylindrical Structure," *IEEE Microwave Conference, 1999 Asia pasific*, pp. 920-923, Nov. 30-Dec. 03, 1999.
131. F. Bilotti and L. Vegni, "Chiral Cover Effects on Microstrip Antennas," *IEEE Transactions on Antennas and Propagation*, Vol. 51, No. 10, pp. 2891-2898, Oct. 2003.

132. C. N. Chiu and C. I. G. Hsu, "Scattering and Shielding Properties of a Chiral-Coated Fiber-Reinforced Plastic Composite Cylinder," *IEEE Transactions on Electromagnetic compatibility*, Vol. 47, No. 1, pp. 123-130, Feb. 2005.
133. B. N. Khatir and A. Sebak, "Transverse Electric Wave Scattering by Elliptic Chiral Cylinder," *ANTEM/URSI*, Montreal, Canada, July 17-19, 2006.
134. C. I. G. Hsu, C. N. Chiu, C. M. Wu, and Y. C. Kang, "Numerical Analysis of Scattering from a General Bi-Isotropic Cylindrical Shell with an Interior Metal Coating," *17th International Zurich Symposium on Electromag. Compatibility*, 2006.
135. B. N. Khatir, M. Al-Kanhal, A. Sebak, "Electromagnetic Wave Scattering by Elliptic Chiral Cylinder," *Journal of Electromagnetic Waves and Applications*, Vol. 20, No. 10, pp. 1377-1390, 2006.
136. D. X. Wang, E. K. N. Yung, and R. S. Chen, "A Coupled Integral Equation Solution of Chirally Coated Conducting Bodies," *IEEE Antennas and Propagation Society International Symposium*, pp. 2843-2846, July 9-14, 2006.
137. M. Schneider and J. Marquardt, "Fast Computation of Modified Mathieu Functions Applied to Elliptical Waveguide Problems," *IEEE Transactions on Microwave Theory and Techniques*, Vol. 47, No 4, pp. 513-515, April 1999.
138. N. W. McLachlan, *Theory and Application of Mathieu Functions*, Dover Publications, Inc., New York, 1964.
139. C. F. Bohren, "Scattering of Electromagnetic Waves by an Optically Active Cylinder," *Journal of Colloid and Interface Science*, Vol. 66, No 1, pp. 105-109, Aug. 1978.

140. C. A. Balanis, *Advanced Engineering Electromagnetics*, John Wiley & Sons, New York, 1989.
141. K. Saermark, "A Note on Addition Theorems for Mathieu Functions," *Z. Math. Phys.*, Vol. 10, pp. 426-428, 1959.
142. H. A. Ragheb, L. Shafai, and M. Hamid, "Plane Wave Scattering by a Conducting Elliptic Cylinder Coated by a Nonconfocal Dielectric," *IEEE Transactions on Antennas and Propagation*, Vol. 39, No 2, pp. 218-223, Feb. 1991.
143. A. Sebak, "Transverse Magnetic Scattering by Parallel Conducting Elliptic Cylinders," *Can. J. Phys.*, Vol. 69, No 10, pp. 1233-1241, 1991.
144. A. Sebak, H. A. Ragheb, and L. Shafai, "Plane Wave Scattering by a Dielectric Elliptic Cylinder Coated with Nonconfocal Dielectric," *Radio Science*, Vol. 29, No 6, pp. 1393-1401, Nov.-Dec. 1994.
145. P. M. Morse and H. Feshbach, *Methods of Theoretical Physics*, Vols. I and II, McGraw-Hill, New York, 1953.
146. A. Sebak and L. Shafai, "Generalized Solutions for Electromagnetic Scattering by Elliptical Structures," *Computer Physics Communications*, 68, pp. 315-330, 1991.
147. S. J. Tetenbaum, "Experimental VSWR's and Radiation Patterns of an Axial Rectangular Slot on Conducting Cylinders of Varying Curvature," *IEEE Transactions on Antennas and Propagation*, pp. 835-837, November 1974.
148. Z. Wasim, R. A. Bhatti, and J. K. Kayani, "Design, Fabrication and Testing of a Millimeter Wave Slotted Waveguide Antenna," *Proceedings of International Bhurban Conference on Applied Sciences & Technology*, Islamabad, Pakistan, Jan. 8-11, 2007.

149. J. D. Kraus and R. J. Marhefka, *Antennas for All Applications*, Third Edition, McGraw-Hill, New York, 2002.
150. J. Hirokawa, S. I. Sumikawa, M. Ando, and N. Goto, "Analysis and Design of A Circumferential Wide Slot Cut on A Thin Cylinder for Mobile Base Station Antennas," *IEEE Antennas and Propagation Society International Symposium*, Vol. 3, pp. 1842-1845, June 28-July 02, 1993.
151. D. H. Shin and H. J. Eom, "Radiation from Narrow Circumferential Slots on a Conducting Circular Cylinder," *IEEE Transactions on Antennas and Propagation*, Vol. 53, No. 6, pp. 2081-2088, June 2005.
152. D. M. Pozar, *Microwave Engineering*, Second Edition, John Wiley & Sons Inc., New York, 1998.
153. B. N. Khatir and A. R. Sebak, "Slot Antenna on a Conducting Elliptic Cylinder Coated by Chiral Media," *Electromagnetics*, Vol. 29, No. 7, pp. 522-540, 2009.
154. B. N. Khatir and A. R. Sebak, "Slot Antenna on a Conducting Elliptic Cylinder Coated by Nonconfocal Chiral Media," *Progress In Electromagnetics Research*, PIER 93, pp. 125–143, 2009.

Appendix A

Addition Theorem for Mathieu Functions

Consider two nonconfocal elliptic cylindrical coordinate systems (ξ_q, η_q, z) and (ξ_r, η_r, z) . The following relations can be written for these systems;

$$R_{\epsilon_m}^{(s)}(c_q, \xi_q) S_{\epsilon_m}(c_q, \eta_q) = \sum_{l=0}^{\infty} WE_{\epsilon_{lm}}^{q \rightarrow r} R_{el}^{(s)}(c_r, \xi_r) S_{el}(c_r, \eta_r) + \sum_{l=1}^{\infty} WO_{\epsilon_{lm}}^{q \rightarrow r} R_{ol}^{(s)}(c_r, \xi_r) S_{ol}(c_r, \eta_r), \quad (A.1)$$

where the functions R and S are the radial Mathieu function and the angular Mathieu function, respectively,

$$WE_{\epsilon_{lm}}^{q \rightarrow r} = \frac{\pi(j)^{l-m}}{N_{el}(c_r)} \sum_i \sum_p (-j)^{i+p} D_{\epsilon_i}^m(c_q) D_{\epsilon_p}^l(c_r) X_{\epsilon_{ip}}^{q \rightarrow r}, \quad (A.2)$$

$$WO_{\epsilon_{lm}}^{q \rightarrow r} = \mp \frac{\pi(j)^{l-m}}{N_{ol}(c_r)} \sum_i \sum_p (-j)^{i+p} D_{\epsilon_i}^m(c_q) D_{\epsilon_p}^l(c_r) Y_{\epsilon_{ip}}^{q \rightarrow r}, \quad (A.3)$$

the sum (\sum) is over only even or odd values of $i(p)$ depending whether $m(l)$ is even or odd. The coefficients $D_{\epsilon_i}^n$ and $D_{\epsilon_i}^m$ are the Fourier series coefficients of the Mathieu functions,

$$X_{\epsilon_{ip}}^{q \rightarrow r} = J_{p-i}(kd_{qr}) \begin{bmatrix} \cos \psi^- \\ \sin \psi^- \end{bmatrix} + (-1)^i J_{p+i}(kd_{qr}) \begin{bmatrix} \cos \psi^+ \\ \sin \psi^+ \end{bmatrix}, \quad (A.4)$$

$$Y_{\epsilon_{ip}}^{q \rightarrow r} = J_{p-i}(kd_{qr}) \begin{bmatrix} \sin \psi^- \\ \cos \psi^- \end{bmatrix} - (-1)^i J_{p+i}(kd_{qr}) \begin{bmatrix} \sin \psi^+ \\ \cos \psi^+ \end{bmatrix}, \quad (A.5)$$

$$\psi^\pm = i\psi_{qr} \pm p\psi_{rq}, \quad (A.6)$$

and $J_p(u)$ is the Bessel function of the order of p and argument u . Also k is the wave number, d_{qr} is the distance between the centers of two coordinate systems, and ψ_{rq} is the angle between the x -axis of cylinder r and the distance line of two centers, measured from the x -axis of cylinder r .

Appendix B

G's Matrices for TM Case

The expansion coefficients for the TM case (Equations (3.85) – (3.101)) are given in terms of the matrices $T1$ through $T146$, and matrices $G1$ through $G48$. The matrices $G1$ through $G48$ are given in this appendix.

$$G1_{\epsilon} = 1 \quad (B.1)$$

$$G2_{\epsilon nm} = \frac{1}{N_{\epsilon n}(c_1)J'_{\epsilon n}(c_1)} \sum_m Q_{\epsilon nm}(c_1) \quad (B.2)$$

$$G3_{\epsilon nm} = \begin{cases} \frac{H_{\epsilon n}(c_1)}{J'_{\epsilon n}(c_1)}, & n = m \\ 0, & n \neq m \end{cases} \quad (B.3)$$

$$G4_{\epsilon} = 1 \quad (B.4)$$

$$G5_{\epsilon nm} = \frac{1}{N_{\epsilon n}(c_1)J'_{\epsilon n}(c_1)} \sum_m Q_{\epsilon nm}(c_1) \quad (B.5)$$

$$G6_{\epsilon} = 1 \quad (B.6)$$

$$G7_{\epsilon nm} = \begin{cases} \frac{K'_{\epsilon n}(c_R)}{J'_{\epsilon n}(c_R)}, & n = m \\ 0, & n \neq m \end{cases} \quad (B.7)$$

$$G8_{\epsilon nm} = \frac{k_R}{k_L} \frac{1}{N_{\epsilon n}(c_R)J'_{\epsilon n}(c_R)} \sum_m M_{\epsilon nm}(c_R, c_L) J'_{\epsilon m}(c_L) \quad (B.8)$$

$$G9_{\epsilon nm} = \frac{k_R}{k_L} \frac{1}{N_{\epsilon n}(c_R)J'_{\epsilon n}(c_R)} \sum_m M_{\epsilon nm}(c_R, c_L) K'_{\epsilon m}(c_L) \quad (B.9)$$

$$G10_{\epsilon nm} = \frac{k_R}{k_1} \frac{1}{N_{\epsilon n}(c_R)J'_{\epsilon n}(c_R)} \sum_m Q_{\epsilon nm}(c_R) \quad (B.10)$$

$$G11_{\epsilon} = 1 \quad (B.11)$$

$$G12_{\epsilon nm} = \begin{cases} \frac{K_{\epsilon n}(c_R)}{J_{\epsilon n}(c_R)}, & n = m \\ 0, & n \neq m \end{cases} \quad (B.12)$$

$$G13_{\epsilon nm} = \frac{1}{N_{\epsilon n}(c_R)J_{\epsilon n}(c_R)} \sum_m M_{\epsilon nm}(c_R, c_L) J_{\epsilon m}(c_L) \quad (B.13)$$

$$G14_{\epsilon nm} = \frac{1}{N_{\epsilon n}(c_R)J_{\epsilon n}(c_R)} \sum_m M_{\epsilon nm}(c_R, c_L) K_{\epsilon m}(c_L) \quad (B.14)$$

$$G15_{\epsilon nm} = \frac{1}{N_{\epsilon n}(c_R)J_{\epsilon n}(c_R)} \sum_m Q_{\epsilon nm}(c_R) \quad (B.15)$$

$$G16_{\epsilon nm} = \sum_m Q_{\epsilon mn}(c_1) H'_{\epsilon m}(c_1) \quad (B.16)$$

$$G17_{\epsilon nm} = \sum_m Q_{\epsilon mn}(c_1) J'_{\epsilon m}(c_1) \quad (B.17)$$

$$G18_{\epsilon nm} = \frac{\omega\mu_1}{k_R\sqrt{\mu_2/\epsilon_2}} \sum_m Q_{\epsilon mn}(c_R) J'_{\epsilon m}(c_R) \quad (B.18)$$

$$G19_{\epsilon nm} = \frac{\omega\mu_1}{k_R\sqrt{\mu_2/\epsilon_2}} \sum_m Q_{\epsilon mn}(c_R) K'_{\epsilon m}(c_R) \quad (B.19)$$

$$G20_{\epsilon nm} = \frac{\omega\mu_1}{k_L\sqrt{\mu_2/\epsilon_2}} \sum_m Q_{\epsilon mn}(c_L) J'_{\epsilon m}(c_L) \quad (B.20)$$

$$G21_{\epsilon nm} = \frac{\omega\mu_1}{k_L\sqrt{\mu_2/\epsilon_2}} \sum_m Q_{\epsilon mn}(c_L) K'_{\epsilon m}(c_L) \quad (B.21)$$

$$G22_{\epsilon nm} = \frac{\sqrt{\mu_2 / \epsilon_2}}{\sqrt{\mu_1 / \epsilon_1}} \sum_m Q_{\epsilon mn}(c_1) J_{\epsilon m}(c_1) \quad (B.22)$$

$$G23_{\epsilon nm} = \sum_m Q_{\epsilon mn}(c_R) J_{\epsilon m}(c_R) \quad (B.23)$$

$$G24_{\epsilon nm} = \sum_m Q_{\epsilon mn}(c_R) K_{\epsilon m}(c_R) \quad (B.24)$$

$$G25_{\epsilon nm} = \sum_m Q_{\epsilon mn}(c_L) J_{\epsilon m}(c_L) \quad (B.25)$$

$$G26_{\epsilon nm} = \sum_m Q_{\epsilon mn}(c_L) K_{\epsilon m}(c_L) \quad (B.26)$$

$$G27_{\epsilon nm} = \frac{k_L}{k_R} \sum_l M_{\epsilon nl}(c_{L2}, c_{R2}) J'_{\epsilon l}(c_{R2}) \sum_m \begin{bmatrix} WE_{\epsilon lm} \\ WO_{\epsilon lm} \end{bmatrix} \quad (B.27)$$

$$G28_{\epsilon nm} = \frac{k_L}{k_R} \sum_l M_{\epsilon nl}(c_{L2}, c_{R2}) J'_{\epsilon l}(c_{R2}) \sum_m \begin{bmatrix} WE_{\circ lm} \\ WO_{\circ lm} \end{bmatrix} \quad (B.28)$$

$$G29_{\epsilon nm} = N_{\epsilon n}(c_{L2}) J'_{\epsilon n}(c_{L2}) \sum_m \begin{bmatrix} WE_{\epsilon nm} \\ WO_{\epsilon nm} \end{bmatrix} \quad (B.29)$$

$$G30_{\epsilon nm} = N_{\epsilon n}(c_{L2}) J'_{\epsilon n}(c_{L2}) \sum_m \begin{bmatrix} WE_{\circ nm} \\ WO_{\circ nm} \end{bmatrix} \quad (B.30)$$

$$G31_{\epsilon nm} = \frac{k_L}{k_R} \sum_l M_{\epsilon nl}(c_{L2}, c_{R2}) K'_{\epsilon l}(c_{R2}) \sum_m \begin{bmatrix} WE_{\epsilon lm} \\ WO_{\epsilon lm} \end{bmatrix} \quad (B.31)$$

$$G32_{\epsilon nm} = \frac{k_L}{k_R} \sum_l M_{\epsilon nl}(c_{L2}, c_{R2}) K'_{\epsilon l}(c_{R2}) \sum_m \begin{bmatrix} WE_{\circ lm} \\ WO_{\circ lm} \end{bmatrix} \quad (B.32)$$

$$G33_{\epsilon nm} = N_{\epsilon n}(c_{L2}) K'_{\epsilon n}(c_{L2}) \sum_m \begin{bmatrix} WE_{\epsilon nm} \\ WO_{\epsilon nm} \end{bmatrix} \quad (B.33)$$

$$G34_{\epsilon_{nm}} = N_{\epsilon_n}(c_{L2})K'_{\epsilon_n}(c_{L2})\sum_m \begin{bmatrix} WE_{\circ nm} \\ WO_{\circ nm} \end{bmatrix} \quad (B.34)$$

$$G35_{\epsilon_{nm}} = \frac{k_L}{k_3} \sum_m M_{\epsilon_{nm}}(c_{L2}, c_3) H'_{\epsilon_m}(c_3) \quad (B.35)$$

$$G36_{\epsilon_{nm}} = \sum_l M_{\epsilon_{nl}}(c_{L2}, c_{R2}) J_{\epsilon_l}(c_{R2}) \sum_m \begin{bmatrix} WE_{\epsilon lm} \\ WO_{\epsilon lm} \end{bmatrix} \quad (B.36)$$

$$G37_{\epsilon_{nm}} = \sum_l M_{\epsilon_{nl}}(c_{L2}, c_{R2}) J_{\epsilon_l}(c_{R2}) \sum_m \begin{bmatrix} WE_{\circ lm} \\ WO_{\circ lm} \end{bmatrix} \quad (B.37)$$

$$G38_{\epsilon_{nm}} = N_{\epsilon_n}(c_{L2}) J_{\epsilon_n}(c_{L2}) \sum_m \begin{bmatrix} WE_{\epsilon nm} \\ WO_{\epsilon nm} \end{bmatrix} \quad (B.38)$$

$$G39_{\epsilon_{nm}} = N_{\epsilon_n}(c_{L2}) J_{\epsilon_n}(c_{L2}) \sum_m \begin{bmatrix} WE_{\circ nm} \\ WO_{\circ nm} \end{bmatrix} \quad (B.39)$$

$$G40_{\epsilon_{nm}} = \sum_l M_{\epsilon_{nl}}(c_{L2}, c_{R2}) K_{\epsilon_l}(c_{R2}) \sum_m \begin{bmatrix} WE_{\epsilon lm} \\ WO_{\epsilon lm} \end{bmatrix} \quad (B.40)$$

$$G41_{\epsilon_{nm}} = \sum_l M_{\epsilon_{nl}}(c_{L2}, c_{R2}) K_{\epsilon_l}(c_{R2}) \sum_m \begin{bmatrix} WE_{\circ lm} \\ WO_{\circ lm} \end{bmatrix} \quad (B.41)$$

$$G42_{\epsilon_{nm}} = N_{\epsilon_n}(c_{L2}) K_{\epsilon_n}(c_{L2}) \sum_m \begin{bmatrix} WE_{\epsilon nm} \\ WO_{\epsilon nm} \end{bmatrix} \quad (B.42)$$

$$G43_{\epsilon_{nm}} = N_{\epsilon_n}(c_{L2}) K_{\epsilon_n}(c_{L2}) \sum_m \begin{bmatrix} WE_{\circ nm} \\ WO_{\circ nm} \end{bmatrix} \quad (B.43)$$

$$G44_{\epsilon_{nm}} = \sum_m M_{\epsilon_{nm}}(c_{L2}, c_3) J_{\epsilon_m}(c_3) \quad (B.44)$$

$$G45_{\epsilon_{nm}} = \sum_m M_{\epsilon_{nm}}(c_{L2}, c_3) H_{\epsilon_m}(c_3) \quad (B.45)$$

$$G46_{\epsilon_{nm}} = \frac{k_L \sqrt{\mu_2 / \epsilon_2}}{\omega \mu_3} \sum_m M_{\epsilon_{nm}}(c_{L2}, c_3) J'_{\epsilon_m}(c_3) \quad (B.46)$$

$$G47_{\epsilon_{nm}} = \frac{k_L \sqrt{\mu_2 / \epsilon_2}}{\omega \mu_3} \sum_m M_{\epsilon_{nm}}(c_{L2}, c_3) H'_{\epsilon_m}(c_3) \quad (B.47)$$

$$G48_{\epsilon_{nm}} = \frac{\sqrt{\mu_2 / \epsilon_2}}{\sqrt{\mu_3 / \epsilon_3}} \sum_m M_{\epsilon_{nm}}(c_{L2}, c_3) H_{\epsilon_m}(c_3) \quad (B.48)$$

Appendix C

T's Matrices for TM Case

The expansion coefficients for the TM case (Equations (3.85) – (3.101)) are given in terms of the matrices $T1$ through $T146$, and matrices $G1$ through $G48$. The matrices $T1$ through $T146$ are given in this appendix.

$$T1 = G35_e^{-1} G27_e \quad (C.1)$$

$$T2 = G35_e^{-1} G28_e \quad (C.2)$$

$$T3 = G35_e^{-1} G29_e \quad (C.3)$$

$$T4 = G35_e^{-1} G30_e \quad (C.4)$$

$$T5 = G35_e^{-1} G31_e \quad (C.5)$$

$$T6 = G35_e^{-1} G32_e \quad (C.6)$$

$$T7 = G35_e^{-1} G33_e \quad (C.7)$$

$$T8 = G35_e^{-1} G34_e \quad (C.8)$$

$$T9 = G36_e - G48_e T1 \quad (C.9)$$

$$T10 = G37_e - G48_e T2 \quad (C.10)$$

$$T11 = -G38_e + T9 G8_e + G48_e T3 \quad (C.11)$$

$$T12 = T11^{-1} T9 G10_e \quad (C.12)$$

$$T13 = T11^{-1}T10G10_o \quad (C.13)$$

$$T14 = T11^{-1}\{G39_e - T10G8_o - G48_e T4\} \quad (C.14)$$

$$T15 = T11^{-1}\{-G40_e + T9G7_e + G48_e T5\} \quad (C.15)$$

$$T16 = T11^{-1}\{-G41_e + T10G7_o + G48_e T6\} \quad (C.16)$$

$$T17 = T11^{-1}\{G42_e - T9G9_e - G48_e T7\} \quad (C.17)$$

$$T18 = T11^{-1}\{G43_e - T10G9_o - G48_e T8\} \quad (C.18)$$

$$T19 = G35_o^{-1}G27_o \quad (C.19)$$

$$T20 = G35_o^{-1}G28_o \quad (C.20)$$

$$T21 = G35_o^{-1}G29_o \quad (C.21)$$

$$T22 = G35_o^{-1}G30_o \quad (C.22)$$

$$T23 = G35_o^{-1}G31_o \quad (C.23)$$

$$T24 = G35_o^{-1}G32_o \quad (C.24)$$

$$T25 = G35_o^{-1}G33_o \quad (C.25)$$

$$T26 = G35_o^{-1}G34_o \quad (C.26)$$

$$T27 = G36_o - G48_o T19 \quad (C.27)$$

$$T28 = G37_o - G48_o T20 \quad (C.28)$$

$$T29 = -G38_o + T27G8_e + G48_o T21 \quad (C.29)$$

$$T30 = -G39_o + T28G8_o + T29T14 + G48_o T22 \quad (C.30)$$

$$T31 = T30^{-1}\{-T27G10_e + T29T12\} \quad (C.31)$$

$$T32 = T30^{-1}\{-T28G10_o + T29T13\} \quad (C.32)$$

$$T33 = T30^{-1} \{-G40_o + T27G7_e - T29T15 + G48_o T23\} \quad (C.33)$$

$$T34 = T30^{-1} \{-G41_o + T28G7_o - T29T16 + G48_o T24\} \quad (C.34)$$

$$T35 = T30^{-1} \{G42_o - T27G9_e - T29T17 - G48_o T25\} \quad (C.35)$$

$$T36 = T30^{-1} \{G43_o - T28G9_o - T29T18 - G48_o T26\} \quad (C.36)$$

$$T37 = G45_e^{-1} G44_e \quad (C.37)$$

$$T38 = G45_e^{-1} G36_e \quad (C.38)$$

$$T39 = G45_e^{-1} G37_e \quad (C.39)$$

$$T40 = G45_e^{-1} G38_e \quad (C.40)$$

$$T41 = G45_e^{-1} G39_e \quad (C.41)$$

$$T42 = G45_e^{-1} G40_e \quad (C.42)$$

$$T43 = G45_e^{-1} G41_e \quad (C.43)$$

$$T44 = G45_e^{-1} G42_e \quad (C.44)$$

$$T45 = G45_e^{-1} G43_e \quad (C.45)$$

$$T46 = G27_e - G47_e T38 \quad (C.46)$$

$$T47 = G28_e - G47_e T39 \quad (C.47)$$

$$T48 = G29_e + T46G8_e - G47_e T40 \quad (C.48)$$

$$T49 = G30_e + T47G8_o + T48T14 - G47_e T41 \quad (C.49)$$

$$T50 = G33_e + T46G9_e + T48T17 + T49T35 - G47_e T44 \quad (C.50)$$

$$T51 = T50^{-1} \{G46_e - G47_e T37\} \quad (C.51)$$

$$T52 = T50^{-1} \{-T46G10_e + T48T12 - T49T31\} \quad (C.52)$$

$$T53 = T50^{-1} \{-T47G10_o + T48T13 - T49T32\} \quad (C.53)$$

$$T54 = T50^{-1} \{-G31_e + T46G7_e - T48T15 - T49T33 + G47_e T42\} \quad (C.54)$$

$$T55 = T50^{-1} \{-G32_e + T47G7_o - T48T16 - T49T34 + G47_e T43\} \quad (C.55)$$

$$T56 = T50^{-1} \{-G34_e - T47G9_o - T48T18 - T49T36 + G47_e T45\} \quad (C.56)$$

$$T57 = G45_o^{-1} G44_o \quad (C.57)$$

$$T58 = G45_o^{-1} G36_o \quad (C.58)$$

$$T59 = G45_o^{-1} G37_o \quad (C.59)$$

$$T60 = G45_o^{-1} G38_o \quad (C.60)$$

$$T61 = G45_o^{-1} G39_o \quad (C.61)$$

$$T62 = G45_o^{-1} G40_o \quad (C.62)$$

$$T63 = G45_o^{-1} G41_o \quad (C.63)$$

$$T64 = G45_o^{-1} G42_o \quad (C.64)$$

$$T65 = G45_o^{-1} G43_o \quad (C.65)$$

$$T66 = G27_o - G47_o T58 \quad (C.66)$$

$$T67 = G28_o - G47_o T59 \quad (C.67)$$

$$T68 = G29_o + T66G8_e - G47_o T60 \quad (C.68)$$

$$T69 = G30_o + T67G8_o + T68T14 - G47_o T61 \quad (C.69)$$

$$T70 = G33_o + T66G9_e + T68T17 + T69T35 - G47_o T64 \quad (C.70)$$

$$T71 = G34_o + T67G9_o + T68T18 + T69T36 + T70T56 - G47_o T65 \quad (C.71)$$

$$T72 = T71^{-1} T70T51 \quad (C.72)$$

$$T73 = T71^{-1} \{G46_o - G47_o T57\} \quad (C.73)$$

$$T74 = T71^{-1} \{-T66G10_e + T68T12 - T69T31 - T70T52\} \quad (C.74)$$

$$T75 = T71^{-1} \{-T67G10_o + T68T13 - T69T32 - T70T53\} \quad (C.75)$$

$$T76 = T71^{-1} \{-G31_o + T66G7_e - T68T15 - T69T33 - T70T54 + G47_o T62\} \quad (C.76)$$

$$T77 = T71^{-1} \{-G32_o + T67G7_o - T68T16 - T69T34 - T70T55 + G47_o T63\} \quad (C.77)$$

$$T78 = G11_e G8_e + G13_e \quad (C.78)$$

$$T79 = G11_e G9_e + G14_e + T78T17 + T78T14T35 \quad (C.79)$$

$$T80 = T78T18 + T78T14T36 + T79T56 \quad (C.80)$$

$$T81 = -G11_e G7_e + G12_e + T78T15 + T78T14T33 + T79T54 + T80T76 \quad (C.81)$$

$$T82 = T81^{-1} \{-T79T51 + T80T72\} \quad (C.82)$$

$$T83 = T81^{-1} T80T73 \quad (C.83)$$

$$T84 = T81^{-1} \{-G11_e G10_e + T78T12 - T78T14T31 - T79T52 - T80T74\} \quad (C.84)$$

$$T85 = T81^{-1} \{T78T13 - T78T14T32 - T79T53 - T80T75\} \quad (C.85)$$

$$T86 = T81^{-1} G15_e \quad (C.86)$$

$$T87 = T81^{-1} \{T78T16 + T78T14T34 + T79T55 + T80T77\} \quad (C.87)$$

$$T88 = G11_o G8_o + G13_o \quad (C.88)$$

$$T89 = G11_o G9_o + G14_o + T88T36 + T88T35T56 \quad (C.89)$$

$$T90 = T88T33 + T88T35T54 + T89T76 \quad (C.90)$$

$$T91 = -G11_o G7_o + G12_o + T88T34 + T88T35T55 + T89T77 - T90T87 \quad (C.91)$$

$$T92 = T91^{-1} \{-T88T35T51 + T89T72 - T90T82\} \quad (C.92)$$

$$T93 = T91^{-1} \{-T89T73 + T90T83\} \quad (C.93)$$

$$T94 = T91^{-1} \{T88T31 + T88T35T52 + T89T74 + T90T84\} \quad (C.94)$$

$$T95 = T91^{-1} \{G11_o G10_o + T88T32 + T88T35T53 + T89T75 + T90T85\} \quad (C.95)$$

$$T96 = T91^{-1} T90T86 \quad (C.96)$$

$$T97 = T91^{-1} G15_o \quad (C.97)$$

$$T98 = G18_e G8_e + G20_e \quad (C.98)$$

$$T99 = G18_e G9_e + G21_e + T98T17 + T98T14T35 \quad (C.99)$$

$$T100 = T98T18 + T98T14T36 + T99T56 \quad (C.100)$$

$$T101 = -G18_e G7_e + G19_e + T98T15 + T98T14T33 + T99T54 + T100T76 \quad (C.101)$$

$$T102 = T98T16 + T98T14T34 + T99T55 + T100T77 + T101T87 \quad (C.102)$$

$$T103 = G17_e G5_e - T101T86 + T102T96 \quad (C.103)$$

$$T104 = T103^{-1} \{-G16_e + G17_e G3_e\} \quad (C.104)$$

$$T105 = T103^{-1} \{T99T51 - T100T72 + T101T82 + T102T92\} \quad (C.105)$$

$$T106 = T103^{-1} \{T100T73 - T101T83 + T102T93\} \quad (C.106)$$

$$T107 = T103^{-1} \{G18_e G10_e - T98T12 + T98T14T31 + T99T52 \\ + T100T74 + T101T84 - T102T94\} \quad (C.107)$$

$$T108 = T103^{-1} \{-T98T13 + T98T14T32 + T99T53 \\ + T100T75 + T101T85 - T102T95\} \quad (C.108)$$

$$T109 = T103^{-1} T102T97 \quad (C.109)$$

$$T110 = G18_o G8_o + G20_o \quad (C.110)$$

$$T111 = G18_o G9_o + G21_o + T110T36 + T110T35T56 \quad (C.111)$$

$$T112 = T110T33 + T110T35T54 + T111T76 \quad (C.112)$$

$$T113 = -G18_o G7_o + G19_o + T110T34 + T110T35T55 + T111T77 - T112T87 \quad (C.113)$$

$$T114 = T112T86 - T113T96 \quad (C.114)$$

$$T115 = G17_o G5_o - T113T97 - T114T109 \quad (C.115)$$

$$T116 = T115^{-1} T114T104 \quad (C.116)$$

$$T117 = T115^{-1} \{-G16_o + G17_o G3_o\} \quad (C.117)$$

$$T118 = T115^{-1} \{T110T35T51 - T111T72 + T112T82 + T113T92 + T114T105\} \quad (C.118)$$

$$T119 = T115^{-1} \{T111T73 - T112T83 + T113T93 + T114T106\} \quad (C.119)$$

$$T120 = T115^{-1} \{T110T31 + T110T35T52 + T111T74 \\ + T112T84 - T113T94 + T114T107\} \quad (C.120)$$

$$T121 = T115^{-1} \{G18_o G10_o + T110T32 + T110T35T53 + T111T75 \\ + T112T85 - T113T95 + T114T108\} \quad (C.121)$$

$$T122 = G23_e G8_e - G25_e \quad (C.122)$$

$$T123 = G23_e G9_e - G26_e + T122T17 + T122T14T35 \quad (C.123)$$

$$T124 = T122T18 + T122T14T36 + T123T56 \quad (C.124)$$

$$T125 = -G23_e G7_e + G24_e + T122T15 + T122T14T33 + T123T54 + T124T76 \quad (C.125)$$

$$T126 = T122T16 + T122T14T34 + T123T55 + T124T77 - T125T87 \quad (C.126)$$

$$T127 = T125T86 - T126T96 \quad (C.127)$$

$$T128 = T126T97 + T127T109 \quad (C.128)$$

$$T129 = G22_e G2_e - G23_e G10_e + T122T12 - T122T14T31 - T123T52 \\ - T124T74 - T125T84 + T126T94 - T127T107 - T128T120 \quad (C.129)$$

$$T130 = T129^{-1} \{T127T104 + T128T116\} \quad (C.130)$$

$$T131 = T129^{-1} T128T117 \quad (C.131)$$

$$T132 = T129^{-1} \{T123T51 - T124T72 + T125T82 \\ + T126T92 + T127T105 + T128T118\} \quad (C.132)$$

$$T133 = T129^{-1} \{T124T73 - T125T83 + T126T93 + T127T106 + T128T119\} \quad (C.133)$$

$$T134 = T129^{-1} \{-T122T13 + T122T14T32 + T123T53 + T124T75 \\ + T125T85 - T126T95 + T127T108 + T128T121\} \quad (C.134)$$

$$T135 = G23_o G8_o - G25_o \quad (C.135)$$

$$T136 = G23_o G9_o - G26_o + T135T36 + T135T35T56 \quad (C.136)$$

$$T137 = T135T33 + T135T35T54 + T136T76 \quad (C.137)$$

$$T138 = -G23_o G7_o + G24_o + T135T34 + T135T35T55 + T136T77 - T137T87 \quad (C.138)$$

$$T139 = T137T86 - T138T96 \quad (C.139)$$

$$T140 = T138T97 + T139T109 \quad (C.140)$$

$$T141 = T135T31 + T135T35T52 + T136T74 + T137T84 \\ - T138T94 + T139T107 + T140T120 \quad (C.141)$$

$$T142 = G22_o G2_o - G23_o G10_o - T135T32 - T135T35T53 - T136T75 \\ - T137T85 + T138T95 - T139T108 - T140T121 - T141T134 \quad (C.142)$$

$$T143 = T142^{-1} \{T139T104 + T140T116 + T141T130\} \quad (C.143)$$

$$T144 = T142^{-1} \{T140T117 + T141T131\} \quad (C.144)$$

$$T145 = T142^{-1} \{T135T35T51 - T136T72 + T137T82 + T138T92 \\ + T139T105 + T140T118 + T141T132\} \quad (C.145)$$

$$T_{146} = T_{142}^{-1} \{ T_{136} T_{73} - T_{137} T_{83} + T_{138} T_{93} + T_{139} T_{106} \\ + T_{140} T_{119} + T_{141} T_{133} \} \quad (\text{C.146})$$

Appendix D

G's Matrices for TE Case

The expansion coefficients for the TE case (Equations (3.131) – (3.147)) are given in terms of the matrices $T1$ through $T158$, and matrices $G1$ through $G48$. The matrices $G27$ through $G45$ are similar to the matrices which are given in Equations (B.27) – (B.45) of Appendix B (for the TM case). The matrices $G1$ through $G26$ and $G46$ through $G48$ are given in this appendix.

$$G1_{\epsilon_{nm}} = \sum_m Q_{\epsilon_{mn}}(c_1) J'_{\epsilon_m}(c_1) \quad (D.1)$$

$$G2_{\epsilon_{nm}} = \sum_n Q1_{\epsilon_{mn}} \quad (D.2)$$

$$G3_{\epsilon_{nm}} = \sum_m Q_{\epsilon_{mn}}(c_1) H_{\epsilon_m}(c_1) \quad (D.3)$$

$$G4_{\epsilon_{nm}} = \sum_m Q_{\epsilon_{mn}}(c_1) J_{\epsilon_m}(c_1) \quad (D.4)$$

$$G5_{\epsilon_{nm}} = G2_{\epsilon_{nm}} \quad (D.5)$$

$$G6_{\epsilon_{nm}} = \frac{k_1}{k_R} \sum_m Q_{\epsilon_{mn}}(c_R) J'_{\epsilon_m}(c_R) \quad (D.6)$$

$$G7_{\epsilon_{nm}} = \frac{k_1}{k_R} \sum_m Q_{\epsilon_{mn}}(c_R) K'_{\epsilon_m}(c_R) \quad (D.7)$$

$$G8_{\epsilon_{nm}} = \frac{k_1}{k_L} \sum_m Q_{\epsilon_{mn}}(c_L) J'_{\epsilon_m}(c_L) \quad (D.8)$$

$$G9_{\epsilon_{nm}} = \frac{k_1}{k_L} \sum_m Q_{\epsilon_{mn}}(c_L) K'_{\epsilon_m}(c_L) \quad (D.9)$$

$$G10_{\epsilon_{nm}} = G2_{\epsilon_{nm}} \quad (D.10)$$

$$G11_{\epsilon_{nm}} = \sum_m Q_{\epsilon_{mn}}(c_R) J_{\epsilon_m}(c_R) \quad (D.11)$$

$$G12_{\epsilon_{nm}} = \sum_m Q_{\epsilon_{mn}}(c_R) K_{\epsilon_m}(c_R) \quad (D.12)$$

$$G13_{\epsilon_{nm}} = \sum_m Q_{\epsilon_{mn}}(c_L) J_{\epsilon_m}(c_L) \quad (D.13)$$

$$G14_{\epsilon_{nm}} = \sum_m Q_{\epsilon_{mn}}(c_L) K_{\epsilon_m}(c_L) \quad (D.14)$$

$$G15_{\epsilon_{nm}} = G2_{\epsilon_{nm}} \quad (D.15)$$

$$G16_{\epsilon_{nm}} = \begin{cases} \frac{H'_{\epsilon_n}(c_1)}{J'_{\epsilon_n}(c_1)}, & n = m \\ 0, & n \neq m \end{cases} \quad (D.16)$$

$$G17_{\epsilon} = 1 \quad (D.17)$$

$$G18_{\epsilon_{nm}} = \frac{\omega \epsilon_1 \sqrt{\mu_2 / \epsilon_2}}{k_R N_{\epsilon_n}(c_1) J'_{\epsilon_n}(c_1)} \sum_m M_{\epsilon_{nm}}(c_1, c_R) J'_{\epsilon_m}(c_R) \quad (D.18)$$

$$G19_{\epsilon_{nm}} = \frac{\omega \epsilon_1 \sqrt{\mu_2 / \epsilon_2}}{k_R N_{\epsilon_n}(c_1) J'_{\epsilon_n}(c_1)} \sum_m M_{\epsilon_{nm}}(c_1, c_R) K'_{\epsilon_m}(c_R) \quad (D.19)$$

$$G20_{\epsilon_{nm}} = \frac{\omega \epsilon_1 \sqrt{\mu_2 / \epsilon_2}}{k_L N_{\epsilon_n}(c_1) J'_{\epsilon_n}(c_1)} \sum_m M_{\epsilon_{nm}}(c_1, c_L) J'_{\epsilon_m}(c_L) \quad (D.20)$$

$$G21_{\epsilon_{nm}} = \frac{\omega \epsilon_1 \sqrt{\mu_2 / \epsilon_2}}{k_L N_{\epsilon_n}(c_1) J'_{\epsilon_n}(c_1)} \sum_m M_{\epsilon_{nm}}(c_1, c_L) K'_{\epsilon_m}(c_L) \quad (D.21)$$

$$G22_{\epsilon} = 1 \quad (D.22)$$

$$G23_{\circ nm} = \frac{\sqrt{\mu_2 / \varepsilon_2}}{\sqrt{\mu_1 / \varepsilon_1}} \frac{1}{N_{\circ n}(c_1) J_{\circ n}(c_1)} \sum_m M_{\circ nm}(c_1, c_R) J_{\circ m}(c_R) \quad (D.23)$$

$$G24_{\circ nm} = \frac{\sqrt{\mu_2 / \varepsilon_2}}{\sqrt{\mu_1 / \varepsilon_1}} \frac{1}{N_{\circ n}(c_1) J_{\circ n}(c_1)} \sum_m M_{\circ nm}(c_1, c_R) K_{\circ m}(c_R) \quad (D.24)$$

$$G25_{\circ nm} = \frac{\sqrt{\mu_2 / \varepsilon_2}}{\sqrt{\mu_1 / \varepsilon_1}} \frac{1}{N_{\circ n}(c_1) J_{\circ n}(c_1)} \sum_m M_{\circ nm}(c_1, c_L) J_{\circ m}(c_L) \quad (D.25)$$

$$G26_{\circ nm} = \frac{\sqrt{\mu_2 / \varepsilon_2}}{\sqrt{\mu_1 / \varepsilon_1}} \frac{1}{N_{\circ n}(c_1) J_{\circ n}(c_1)} \sum_m M_{\circ nm}(c_1, c_L) K_{\circ m}(c_L) \quad (D.26)$$

The matrices $G27$ through $G45$ are similar to the matrices which are given in Equations (B.27) – (B.45) of Appendix B.

$$G46_{\circ nm} = \frac{k_L}{\omega \varepsilon_3 \sqrt{\mu_2 / \varepsilon_2}} \sum_m M_{\circ nm}(c_{L2}, c_3) J'_{\circ m}(c_3) \quad (D.27)$$

$$G47_{\circ nm} = \frac{k_L}{\omega \varepsilon_3 \sqrt{\mu_2 / \varepsilon_2}} \sum_m M_{\circ nm}(c_{L2}, c_3) H'_{\circ m}(c_3) \quad (D.28)$$

$$G48_{\circ nm} = \frac{\sqrt{\mu_3 / \varepsilon_3}}{\sqrt{\mu_2 / \varepsilon_2}} \sum_m M_{\circ nm}(c_{L2}, c_3) H_{\circ m}(c_3) \quad (D.29)$$

Appendix E

T's Matrices for TE Case

The expansion coefficients for the TE case (Equations (3.131) – (3.147)) are given in terms of the matrices $T1$ through $T158$, and matrices $G1$ through $G48$. The matrices $T1$ through $T158$ are given in this appendix.

$$T1_{\circ} = G1_{\circ}^{-1} G2_{\circ} \quad (E.1)$$

$$T2_{\circ} = G4_{\circ}^{-1} G3_{\circ} \quad (E.2)$$

$$T3_{\circ} = G4_{\circ}^{-1} G5_{\circ} \quad (E.3)$$

$$T4_{\circ} = G23_{\circ}^{-1} G22_{\circ} \quad (E.4)$$

$$T5_{\circ} = G23_{\circ}^{-1} G25_{\circ} \quad (E.5)$$

$$T6_{\circ} = G23_{\circ}^{-1} G24_{\circ} \quad (E.6)$$

$$T7_{\circ} = G23_{\circ}^{-1} G26_{\circ} \quad (E.7)$$

$$T8 = G35_e^{-1} G27_e \quad (E.8)$$

$$T9 = G35_e^{-1} G28_e \quad (E.9)$$

$$T10 = G35_e^{-1} G29_e \quad (E.10)$$

$$T11 = G35_e^{-1} G30_e \quad (E.11)$$

$$T12 = G35_e^{-1} G31_e \quad (E.12)$$

$$T13 = G35_e^{-1} G32_e \quad (E.13)$$

$$T14 = G35_e^{-1} G33_e \quad (E.14)$$

$$T15 = G35_e^{-1} G34_e \quad (E.15)$$

$$T16 = G36_e - G48_e T8 \quad (E.16)$$

$$T17 = G37_e - G48_e T9 \quad (E.17)$$

$$T18 = -G38_e + T16T5_e + G48_e T10 \quad (E.18)$$

$$T19 = T18^{-1} T16T4_e \quad (E.19)$$

$$T20 = T18^{-1} T17T4_o \quad (E.20)$$

$$T21 = T18^{-1} \{G39_e - T17T5_o - G48_e T11\} \quad (E.21)$$

$$T22 = T18^{-1} \{-G40_e + T16T6_e + G48_e T12\} \quad (E.22)$$

$$T23 = T18^{-1} \{-G41_e + T17T6_o + G48_e T13\} \quad (E.23)$$

$$T24 = T18^{-1} \{G42_e - T16T7_e - G48_e T14\} \quad (E.24)$$

$$T25 = T18^{-1} \{G43_e - T17T7_o - G48_e T15\} \quad (E.25)$$

$$T26 = G35_o^{-1} G27_o \quad (E.26)$$

$$T27 = G35_o^{-1} G28_o \quad (E.27)$$

$$T28 = G35_o^{-1} G29_o \quad (E.28)$$

$$T29 = G35_o^{-1} G30_o \quad (E.29)$$

$$T30 = G35_o^{-1} G31_o \quad (E.30)$$

$$T31 = G35_o^{-1} G32_o \quad (E.31)$$

$$T32 = G35_o^{-1} G33_o \quad (E.32)$$

$$T33 = G35_o^{-1} G34_o \quad (E.33)$$

$$T34 = G36_o - G48_o T26 \quad (E.34)$$

$$T35 = G37_o - G48_o T27 \quad (E.35)$$

$$T36 = -G38_o + T34T5_e + G48_o T28 \quad (E.36)$$

$$T37 = -G39_o + T35T5_o + T36T21 + G48_o T29 \quad (E.37)$$

$$T38 = T37^{-1} \{-T34T4_e + T36T19\} \quad (E.38)$$

$$T39 = T37^{-1} \{-T35T4_o + T36T20\} \quad (E.39)$$

$$T40 = T37^{-1} \{-G40_o + T34T6_e - T36T22 + G48_o T30\} \quad (E.40)$$

$$T41 = T37^{-1} \{-G41_o + T35T6_o - T36T23 + G48_o T31\} \quad (E.41)$$

$$T42 = T37^{-1} \{G42_o - T34T7_e - T36T24 - G48_o T32\} \quad (E.42)$$

$$T43 = T37^{-1} \{G43_o - T35T7_o - T36T25 - G48_o T33\} \quad (E.43)$$

$$T44 = G45_e^{-1} G44_e \quad (E.44)$$

$$T45 = G45_e^{-1} G36_e \quad (E.45)$$

$$T46 = G45_e^{-1} G37_e \quad (E.46)$$

$$T47 = G45_e^{-1} G38_e \quad (E.47)$$

$$T48 = G45_e^{-1} G39_e \quad (E.48)$$

$$T49 = G45_e^{-1} G40_e \quad (E.49)$$

$$T50 = G45_e^{-1} G41_e \quad (E.50)$$

$$T51 = G45_e^{-1} G42_e \quad (E.51)$$

$$T52 = G45_e^{-1} G43_e \quad (E.52)$$

$$T53 = G27_e - G47_e T45 \quad (E.53)$$

$$T54 = G28_e - G47_e T46 \quad (E.54)$$

$$T55 = G29_e + T53T5_e - G47_e T47 \quad (E.55)$$

$$T56 = G30_e + T54T5_o + T55T21 - G47_e T48 \quad (E.56)$$

$$T57 = G33_e + T53T7_e + T55T24 + T56T42 - G47_e T51 \quad (E.57)$$

$$T58 = T57^{-1} \{G46_e - G47_e T44\} \quad (E.58)$$

$$T59 = T57^{-1} \{-T53T4_e + T55T19 - T56T38\} \quad (E.59)$$

$$T60 = T57^{-1} \{-T54T4_o + T55T20 - T56T39\} \quad (E.60)$$

$$T61 = T57^{-1} \{-G31_e + T53T6_e - T55T22 - T56T40 + G47_e T49\} \quad (E.61)$$

$$T62 = T57^{-1} \{-G32_e + T54T6_o - T55T23 - T56T41 + G47_e T50\} \quad (E.62)$$

$$T63 = T57^{-1} \{-G34_e - T54T7_o - T55T25 - T56T43 + G47_e T52\} \quad (E.63)$$

$$T64 = G45_o^{-1} G44_o \quad (E.64)$$

$$T65 = G45_o^{-1} G36_o \quad (E.65)$$

$$T66 = G45_o^{-1} G37_o \quad (E.66)$$

$$T67 = G45_o^{-1} G38_o \quad (E.67)$$

$$T68 = G45_o^{-1} G39_o \quad (E.68)$$

$$T69 = G45_o^{-1} G40_o \quad (E.69)$$

$$T70 = G45_o^{-1} G41_o \quad (E.70)$$

$$T71 = G45_o^{-1} G42_o \quad (E.71)$$

$$T72 = G45_o^{-1} G43_o \quad (E.72)$$

$$T73 = G27_o - G47_o T65 \quad (E.73)$$

$$T74 = G28_o - G47_o T66 \quad (E.74)$$

$$T75 = G29_o + T73T5_e - G47_o T67 \quad (E.75)$$

$$T76 = G30_o + T74T5_o + T75T21 - G47_o T68 \quad (E.76)$$

$$T77 = G33_o + T73T7_e + T75T24 + T76T42 - G47_o T71 \quad (E.77)$$

$$T78 = G34_o + T74T7_o + T75T25 + T76T43 + T77T63 - G47_o T72 \quad (E.78)$$

$$T79 = T78^{-1} T77T58 \quad (E.79)$$

$$T80 = T78^{-1} \{G46_o - G47_o T64\} \quad (E.80)$$

$$T81 = T78^{-1} \{-T73T4_e + T75T19 - T76T38 - T77T59\} \quad (E.81)$$

$$T82 = T78^{-1} \{-T74T4_o + T75T20 - T76T39 - T77T60\} \quad (E.82)$$

$$T83 = T78^{-1} \{-G31_o + T73T6_e - T75T22 - T76T40 - T77T61 + G47_o T69\} \quad (E.83)$$

$$T84 = T78^{-1} \{-G32_o + T74T6_o - T75T23 - T76T41 - T77T62 + G47_o T70\} \quad (E.84)$$

$$T85 = G18_e T5_e + G20_e \quad (E.85)$$

$$T86 = G18_e T7_e + G21_e + T85T24 + T85T21T42 \quad (E.86)$$

$$T87 = T85T25 + T85T21T43 + T86T63 \quad (E.87)$$

$$T88 = G18_e T6_e - G19_e - T85T22 - T85T21T40 - T86T61 - T87T83 \quad (E.88)$$

$$T89 = T88^{-1} G16_e \quad (E.89)$$

$$T90 = T88^{-1} \{T86T58 - T87T79\} \quad (E.90)$$

$$T91 = T88^{-1}T87T80 \quad (E.91)$$

$$T92 = T88^{-1}\{G18_e T4_e - T85T19 + T85T21T38 + T86T59 + T87T81\} \quad (E.92)$$

$$T93 = T88^{-1}\{-T85T20 + T85T21T39 + T86T60 + T87T82\} \quad (E.93)$$

$$T94 = T88^{-1}G17_e \quad (E.94)$$

$$T95 = T88^{-1}\{T85T23 + T85T21T41 + T86T62 + T87T84\} \quad (E.95)$$

$$T96 = G18_o T5_o + G20_o \quad (E.96)$$

$$T97 = G18_o T7_o + G21_o + T96T43 + T96T42T63 \quad (E.97)$$

$$T98 = T96T40 + T96T42T61 + T97T83 \quad (E.98)$$

$$T99 = G18_o T6_o - G19_o - T96T41 - T96T42T62 - T97T84 - T98T95 \quad (E.99)$$

$$T100 = T99^{-1}T98T89 \quad (E.100)$$

$$T101 = T99^{-1}G16_o \quad (E.101)$$

$$T102 = T99^{-1}\{T96T42T58 - T97T79 + T98T90\} \quad (E.102)$$

$$T103 = T99^{-1}\{T97T80 + T98T91\} \quad (E.103)$$

$$T104 = T99^{-1}\{T96T38 + T96T42T59 + T97T81 + T98T92\} \quad (E.104)$$

$$T105 = T99^{-1}\{G18_o T4_o + T96T39 + T96T42T60 + T97T82 + T98T93\} \quad (E.105)$$

$$T106 = T99^{-1}T98T94 \quad (E.106)$$

$$T107 = T99^{-1}G17_o \quad (E.107)$$

$$T108 = G11_e T5_e + G13_e \quad (E.108)$$

$$T109 = G11_e T7_e + G14_e + T108T24 + T108T21T42 \quad (E.109)$$

$$T110 = T108T25 + T108T21T43 + T109T63 \quad (E.110)$$

$$T111 = -G11_e T6_e + G12_e + T108T22 + T108T21T40 + T109T61 + T110T83 \quad (E.111)$$

$$T112 = T108T23 + T108T21T41 + T109T62 + T110T84 + T111T95 \quad (E.112)$$

$$T113 = T111T94 + T112T106 \quad (E.113)$$

$$T114 = T113T3_e + G15_e \quad (E.114)$$

$$T115 = T114^{-1} \{-T111T89 - T112T100 + T113T2_e\} \quad (E.115)$$

$$T116 = T114^{-1} \{-T112T101 - T112T107T2_o\} \quad (E.116)$$

$$T117 = T114^{-1} \{T109T58 - T110T79 + T111T90 + T112T102\} \quad (E.117)$$

$$T118 = T114^{-1} \{T110T80 - T111T91 + T112T103\} \quad (E.118)$$

$$T119 = T114^{-1} \{G11_e T4_e - T108T19 + T108T21T38 + T109T59 \\ + T110T81 + T111T92 - T112T104\} \quad (E.119)$$

$$T120 = T114^{-1} \{-T108T20 + T108T21T39 + T109T60 \\ + T110T82 + T111T93 + T112T105\} \quad (E.120)$$

$$T121 = T114^{-1} T112T107T3_o \quad (E.121)$$

$$T122 = G11_o T5_o + G13_o \quad (E.122)$$

$$T123 = G11_o T7_o + G14_o + T122T43 + T122T42T63 \quad (E.123)$$

$$T124 = T122T40 + T122T42T61 + T123T83 \quad (E.124)$$

$$T125 = -G11_o T6_o + G12_o + T122T41 + T122T42T62 + T123T84 + T124T95 \quad (E.125)$$

$$T126 = T124T94 + T125T106 \quad (E.126)$$

$$T127 = T125T107T3_o - T126T3_e T121 + G15_o \quad (E.127)$$

$$T128 = T127^{-1} \{-T124T89 - T125T100 + T126T2_e - T126T3_e T115\} \quad (E.128)$$

$$T129 = T127^{-1} \{-T125T101 + T125T107T2_o - T126T3_e T116\} \quad (E.129)$$

$$T130 = T127^{-1} \{T122T42T58 - T123T79 + T124T90$$

$$+ T_{125}T_{102} - T_{126}T_{3_e}T_{117}\} \quad (E.130)$$

$$T_{131} = T_{127}^{-1} \{T_{123}T_{80} + T_{124}T_{91} + T_{125}T_{103} - T_{126}T_{3_e}T_{118}\} \quad (E.131)$$

$$T_{132} = T_{127}^{-1} \{T_{122}T_{38} + T_{122}T_{42}T_{59} + T_{123}T_{81} + T_{124}T_{92} \\ + T_{125}T_{104} - T_{126}T_{3_e}T_{119}\} \quad (E.132)$$

$$T_{133} = T_{127}^{-1} \{G_{11_o}T_{4_o} + T_{122}T_{39} + T_{122}T_{42}T_{60} + T_{123}T_{82} \\ + T_{124}T_{93} + T_{125}T_{105} - T_{126}T_{3_e}T_{120}\} \quad (E.133)$$

$$T_{134} = G_{6_e}T_{5_e} - G_{8_e} \quad (E.134)$$

$$T_{135} = G_{6_e}T_{7_e} - G_{9_e} + T_{134}T_{24} + T_{134}T_{21}T_{42} \quad (E.135)$$

$$T_{136} = T_{134}T_{25} + T_{134}T_{21}T_{43} + T_{135}T_{63} \quad (E.136)$$

$$T_{137} = -G_{6_e}T_{6_e} + G_{7_e} + T_{134}T_{22} + T_{134}T_{21}T_{40} + T_{135}T_{61} + T_{136}T_{83} \quad (E.137)$$

$$T_{138} = T_{134}T_{23} + T_{134}T_{21}T_{41} + T_{135}T_{62} + T_{136}T_{84} + T_{137}T_{95} \quad (E.138)$$

$$T_{139} = T_{137}T_{94} + T_{138}T_{106} \quad (E.139)$$

$$T_{140} = -T_{138}T_{107}T_{3_o} + T_{139}T_{3_e}T_{121} \quad (E.140)$$

$$T_{141} = \{-G_{6_e}T_{4_e} + T_{134}T_{19} - T_{134}T_{21}T_{38} - T_{135}T_{59} - T_{136}T_{81} \\ - T_{137}T_{92} - T_{138}T_{104} + T_{139}T_{3_e}T_{119} - T_{140}T_{132}\}T_{1_e} + G_{10_e} \quad (E.141)$$

$$T_{142} = T_{141}^{-1} \{-T_{137}T_{89} - T_{138}T_{100} + T_{139}T_{2_e} - T_{139}T_{3_e}T_{115} + T_{140}T_{128}\} \quad (E.142)$$

$$T_{143} = T_{141}^{-1} \{-T_{138}T_{101} - T_{138}T_{107}T_{2_o} - T_{139}T_{3_e}T_{116} + T_{140}T_{129}\} \quad (E.143)$$

$$T_{144} = T_{141}^{-1} \{T_{135}T_{58} - T_{136}T_{79} + T_{137}T_{90} + T_{138}T_{102} \\ - T_{139}T_{3_e}T_{117} + T_{140}T_{130}\} \quad (E.144)$$

$$T_{145} = T_{141}^{-1} \{T_{136}T_{80} + T_{137}T_{91} + T_{138}T_{103} - T_{139}T_{3_e}T_{118} + T_{140}T_{131}\} \quad (E.145)$$

$$T_{146} = T_{141}^{-1} \{-T_{134}T_{20} + T_{134}T_{21}T_{39} + T_{135}T_{60} + T_{136}T_{82} + T_{137}T_{93}$$

$$+ T138T105 - T139T3_e T120 + T140T133\}T1_o \quad (E.146)$$

$$T147 = G6_o T5_o - G8_o \quad (E.147)$$

$$T148 = G6_o T7_o - G9_o + T147T43 + T147T42T63 \quad (E.148)$$

$$T149 = T147T40 + T147T42T61 + T148T83 \quad (E.149)$$

$$T150 = -G6_o T6_o + G7_o + T147T41 + T148T42T62 + T148T84 + T149T95 \quad (E.150)$$

$$T151 = T149T94 + T150T106 \quad (E.151)$$

$$T152 = T150T107T3_o + T151T3_e T121 \quad (E.152)$$

$$T153 = \{T147T38 + T147T42T59 + T148T81 + T149T92 + T150T104 \\ + T151T3_e T119 + T152T132\}T1_e \quad (E.153)$$

$$T154 = \{-G6_o T4_o - T147T39 - T147T42T60 - T148T82 - T149T93 \\ - T150T105 - T151T3_e T120 - T152T133\}T1_o - T153T146 + G10_o \quad (E.154)$$

$$T155 = T154^{-1} \{-T149T89 - T150T100 + T151T2_e + T151T3_e T115 \\ - T152T128 + T153T142\} \quad (E.155)$$

$$T156 = T154^{-1} \{-T150T101 + T150T107T2_o + T151T3_e T116 \\ - T152T129 + T153T143\} \quad (E.156)$$

$$T157 = T154^{-1} \{T147T42T58 - T148T79 + T149T90 + T150T102 \\ + T151T3_e T117 - T152T130 + T153T144\} \quad (E.157)$$

$$T158 = T154^{-1} \{T148T80 + T149T91 + T150T103 + T151T3_e T118 \\ - T152T131 + T153T145\} \quad (E.158)$$